Progress in Energy and Combustion Science 72 (2019) 1–31

Contents lists available at ScienceDirect

Progress in Energy and Combustion Science

journal homepage: www.elsevier.com/locate/pecs

A comparison of methodologies for the non-invasive characterisation of commercial Li-ion cells

Anup Barai[a,*], Kotub Uddin[b], Matthieu Dubarry[c], Limhi Somerville[d], Andrew McGordon[a], Paul Jennings[a], Ira Bloom[e]

[a] WMG, University of Warwick, Coventry CV4 7AL, United Kingdom
[b] OVO Energy, 33 Notting Hill Gate, Kensington, London W11 3JQ, United Kingdom
[c] Hawaii Natural Energy Institute, University of Hawaii at Mānoa, 1680 East-West Road, POST 109, Honolulu, HI 96822, United States
[d] Advanced Battery Research, Jaguar Land Rover, Banbury Road, Warwick CV35 0XJ, United Kingdom
[e] Argonne National Laboratory, 9700 South Cass Avenue, Argonne, IL 60439, United States

ARTICLE INFO

Article history:
Received 10 June 2018
Accepted 7 January 2019

Keywords:
Battery testing
Internal resistance
EIS
GITT
Incremental capacity
Differential voltage

ABSTRACT

Lithium-ion cells currently power almost all electronic devices and power tools; they are a key enabling technology for electric vehicles and are increasingly considered to be the technology of choice for grid storage. In line with this increased applicability, there is also an increase in the development of new commercial lithium-ion cell technologies that incorporate innovative functional components (electrode material compositions and electrolyte formulations) and designs, leading to a diverse range of performance characteristics. The uniqueness of each technology in-turn gives rise to unique evolutions of cell performance as the cell degrades because of usage. Non-destructively measuring and subsequently tracking the evolution of lithium-ion cell characteristics is valuable for both industrial engineers and academic researchers. To proceed in this regard, stakeholders have often devised their own procedures for characterising lithium-ion cells, typically without considering unification, comparability or compatibility. This makes the comparison of technologies complicated. This comprehensive review for the first time has analysed and discusses the various international standards and regulations for the characterisation and electrical testing of lithium-ion cells, specifically for high-power automotive and grid applications.

Contents

* Corresponding author.
E-mail address: a.barai@warwick.ac.uk (A. Barai).

https://doi.org/10.1016/j.pecs.2019.01.001

1. Introduction

The availability of affordable, cost effective energy and power-dense lithium-ion (Li-ion) cells is changing many industries. In comparison to lead-acid cells which have energy densities in the region of 33–42 Wh/kg and 50–70 Wh/L, power-densities of up to 180 W/kg and lifetimes of between 200 and 300 cycles [1,2], modern Li-ion cells have significantly better energy densities up to 250 Wh/kg (450 Wh/L for $LiCoO_2$/graphite cells) [2,3], power densities up to 3000 W/kg for lithium iron phosphate ($LiFePO_4$) (LFP)/graphite cells [2,4] and cycle life in excess of 20,000 cycles for cells with lithium titanate ($Li_4Ti_5O_{12}$) negative electrodes [5,6]. These features have driven Li-ion batteries to become the preferred solution for electrical energy storage. It is forecasted that across the automotive, consumer electronics and grid storage sectors, the demand for Li-ion batteries will grow from 61 GWh in 2015 to 124 GWh in 2020 [7].

The continuous advances in Li-ion cell technology, for example, advances in electrode material, electrolyte design and cell design, means that cell characterisation tests are necessary to compare the capability and track the evolution of performance over cell life. Such tests should provide useful and comparative data and be repeatable. In addition, it is just as important to understand their limitations. Typically, three parameters: cell capacity, resistance and open circuit voltage (OCV) are used to define the electrical performance of Li-ion cells. Cell capacity tests are used to define the maximum capacity in applications under a given load, while OCV tests provide key information on the thermodynamic properties of a cell. Resistance tests on the other hand, characterise cell dynamics. These tests are used to both characterise initial cell capabilities and quantify cell degradation through "reference performance tests' (RPT). The vast majority of battery engineers currently quantify ageing via loss of cell capacity (capacity fade) and increased cell resistance (power fade). The methods employed for capacity, resistance and OCV tests are not concurrent, i.e. there are multiple ways to measure capacity, impedance and OCV, and there is no 'one size fits-all' approach. Fundamentally, the appropriateness of a test depends on what the investigator is studying. The aim of this work is to present a comprehensive and critical review of the existing methods for cell characterisation with the objective of empowering the reader to make an informed decision on the most appropriate suite of tests for their application.

Previous works on reviewing characterisation standards, such as the work of Mulder et al. [8], focussed on the comparability of the results obtained from implementing different testing standards. In this work, the focus is on educating the reader on the subtle differences between the various methods of characterisation and to include tests relevant to commercial cells. We restrict this review to non-invasive dynamic and thermodynamic tests; readers interested in post-mortem tests are directed to the recent reviews by Waldmann et al. [9] and Lu et al. [10] and for in-situ techniques Harks et al. [11].

2. Capacity tests

In the simplest terms, capacity is a measure of the total electric charge stored in a cell. This is governed by the amount of active material available for intercalation (electrodes) [12]. As a cell loses lithium inventory and/or active material, the capacity of the cell reduces. In an automotive context, this reduction in cell capacity reflects a reduction in the maximum driving range of an electric vehicle. Cell capacity, therefore, is a convenient metric for defining the state of health (SoH) of a Li-ion cell [5,13–16].

2.1. Capacity test methodologies

The established method of measuring a cell's capacity is to first fully charge and then discharge the cell. During the discharge step, the time integration of current in Ah is recorded by Coulomb counting. The most commonly adopted method for charging a battery is via the constant-current constant-voltage profile with a low current cut-off (typically less than 10% of the constant-current value) for the constant-voltage part. Although the continuous discharge of a cell using a constant current is the most common

Acronyms and Nomenclature

BMS	Battery management system
BOL	Beginning of life
CC–CV	Constant-current-constant-voltage
CPE	Constant phase element
DV	Differential voltage analysis
ECM	Equivalent circuit models
EIS	Electrochemical impedance spectroscopy
EKF	Extended Kalman Filter
EMF	Electromotive force
EV	Electric Vehicle
EVS	Electrochemical voltage spectroscopies
GITT	Galvanostatic Intermittent Titration Technique
HEV	Hybrid electric vehicle
HPPC	Hybrid pulse power characterisation
IC	Incremental capacity analysis
IEC	International Electrotechnical Commission
INEEL	Idaho National Engineering and Environmental Laboratory
ISO	International Organization for Standardization
LAM	Loss of active material
LCO	$LiCoO_2$
LFP	$LiFePO_4$
Li-ion	Lithium-ion
LLI	Loss of lithium inventory
LTO	$Li_4Ti_5O_{12}$
NCA	$LiNiCoAlO_2$
NE	Negative electrode
NMC	$LiNiMnCoO_2$
OCV	Open circuit voltage
PE	Positive electrode
RMS	Root mean square
RPT	Reference performance tests
SEI	Solid electrolyte interface
SoC	State-of-Charge
SoH	State-of-Health

method, methods for discharging a cell can vary widely [17,18]. Beyond the simplicity of interpreting the results, this method has the advantage of less variability over other methods because: (i) the test is easily repeatable, (ii) the Coulomb counting method is subject to less current measurement errors (over constant power profiles, for example) and (iii) variability in resistive heat losses are better defined.

The measured capacity of a cell is dependent on the operational conditions under which the cell is tested; namely, the temperature and charge–discharge profile. Within the Butler–Volmer framework of Eq. (1) used to describe the reaction rates in electrodes, a higher discharge rate (which equates to a higher electrode current density, i) leads to a larger overpotential, i.e. the difference between the electrode potential and equilibrium potential, η, as expressed by

$$i = i_0\left(e^{\frac{\alpha_a F}{RT}\eta} - e^{-\frac{\alpha_c F}{RT}\eta}\right), \tag{1}$$

where i_0 is the exchange current density, α_a and α_c are the anodic and cathodic charge transfer coefficients, respectively, F is the Faraday constant and R is the universal gas constant. Since the equilibrium potential reduces with the state-of-charge (SoC) and internal resistance of the cell increases with the SoC, overpotentials at a low SoC progressively become higher causing a cell's voltage to reach the lower voltage limit before all the stored capacity in the cell is released. Therefore, the accessible capacity of a cell decreases as the current rate increases [19].

The reaction rate of lithium insertion is believed to have an Arrhenius dependence on temperature (T),

$$A_{ref} e^{\frac{E^A_{act}}{R}\left(\frac{1}{T_{ref}} - \frac{1}{T}\right)}, \tag{2}$$

where A_{ref} is a pre-exponential factor and E^A_{act} the activation energy which depends on the SoC as shown by Liaw et al. [20]. Higher temperatures cause both ion mobility and solid-state diffusion to improve, thus reducing a cell's internal impedance and overpotential. This means that a cell can discharge more capacity before the lower voltage limit is reached. The opposite is true for colder temperatures. In addition, at lower temperatures, the electrolyte is more viscous and ion transport properties are reduced [21], setting a lower limit on performance and consequently a lower capacity.

Because cell capacity is dependent on testing conditions, international cell testing standards suggest testing at different ambient conditions and discharge rates. Although this provides a guideline, the research community has pushed the boundaries of testing further, partly to cater to automotive applications. A review of constant-current capacity tests both within the academic literature and industrial standards is presented in this subsection.

Fig. 1 summarises the various continuous discharge currents and temperatures suggested for cell capacity tests. Most test standards, as well as the research community, suggest to perform a 1C or C/3 capacity test at 25 °C. C-rate is defined as the current value which will discharge a battery from a fully charged state to a fully discharged state in 1 h; in battery testing it is commonly defined as the current value equal to the rated capacity (Ah) of a cell, which may not always be true. In reality, the 1C or C/3 rate is arbitrary and has little electrical or electrochemical significance; it has likely been adopted as a baseline test rate relative to which results of other C-rates are often compared. To investigate new electrode designs in novel energy storage material research and similar research, current per unit of electrode surface area (A/cm^2) is used, which allows a direct comparison; this cannot be achieved with C-rates. However, A/cm^2 cannot be used with most commercial cells as electrode surface areas are not known; therefore, despite its advantages, the C-rate is used.

The IEC 62,660–1 standard [22] employs only one C-rate which differs depending on the application: C/3 for electric vehicles and 1C for hybrid electric vehicles. The International Organization for Standardization (ISO) published a two-part standard: the first part, ISO 12,405–1 [23] for high-power applications and the second part, ISO 12,405–2 [24] for high-energy applications. Although the main scope of these two parts are for battery packs, the ISO has suggested that they can also be used for cell testing. For high-power applications, the ISO 12,405–1 standard suggests using 1C, 10C or the maximum C-rate suggested by the manufacturer. For high-energy applications, the ISO 12,405–2 standard proposes the use of C/3, 1C, 2C or the maximum C-rate for discharge capacity tests. In the FreedomCAR battery test manual [25] prepared for the U.S. Department of Energy, a 1C current is suggested. In contrast, the most recent U.S. Department of Energy standard [26] suggests replacing the 1C-rate with a value relevant to the designed battery pack; the actual value is scaled from 10 kW constant power for a standard pack. This pack-level rate can be scaled down for cell-level testing depending on the number of cells in a pack; therefore, the actual rate is not fixed for all types of cells but depends on the pack requirement. The standard QC/T 743) proposed by the People's Republic of China advises the use of a base C/3 rate and an additional test at 1.5C for high energy and 4C for high power applications [27].

To contextualise the discharge rates suggested by the six standards, consider that analysis of motorway driving (average 70 mph) for the Tesla Model X electric vehicle (100-kWh battery pack, 295

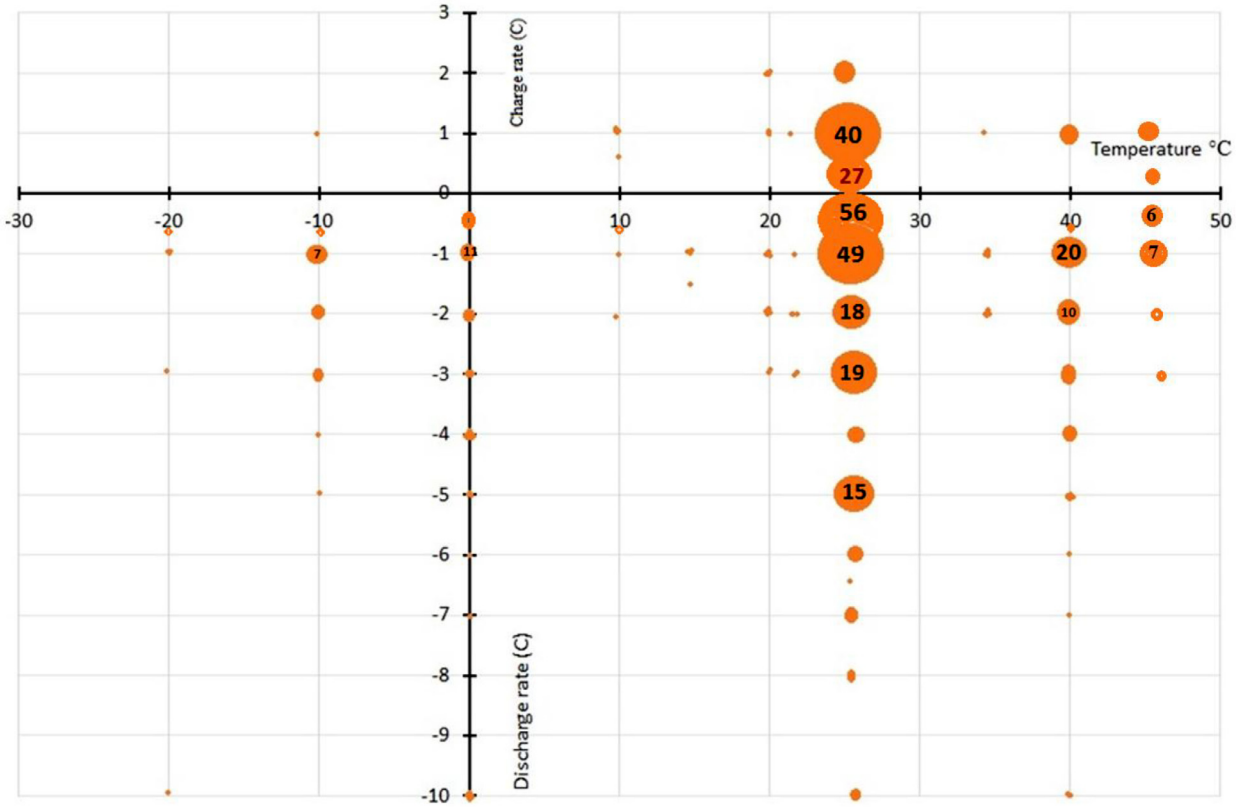

Fig. 1. Use of temperature and charge–discharge current rates for capacity tests in international standards and recent literature. Larger dots represent a higher number of standards/literature using that rate at that temperature. See supplementary file for the data sources.

EPA range) highlights an average discharge rate of around C/4; the corresponding value for the Nissan Leaf (40-kWh battery pack, 151 EPA range) is around C/2. A significant drawback of using C-rates that are different to the C-rates identified through the analysis of the application (by a factor of two or more) is the eventuality of premature/delayed labelling of end of life, even though it may not be fit for purpose. This is because of the convoluted sensitivity of capacity measurements to C-rates through cell impedance and heating [28]. Therefore, a more helpful approach for defining C-rates to be used for capacity measurements is to use the root-mean-square of cell current in an application.

There is a large variation of temperatures suggested for capacity tests in the literature. The IEC 62,660–1 standard suggests the use of 0 °C, 25 °C and 45 °C as representative of low, average and high operating temperatures of a vehicle, respectively. While both the ISO 12,405–1 and ISO 12,405–2 standards suggest measuring capacity from as low as −20 °C to a maximum of 40 °C, the QC/T 743–2006 standard [27] pushes the maximum temperature limit higher to 55 °C. In the context of electric vehicles and hybrid electric vehicles, operational temperatures can range between −30 °C and 55 °C. During operation, most thermal management systems will employ a thermal management strategy which limits the temperature to a value typically between 30 °C and 35 °C, which is assumed for all technologies to be the optimum limiting temperature for performance and lifetime [29,30]. However, the cells will be exposed to extreme temperatures while parked and not thermally managed. Therefore, testing for capacity at −30 °C and 40 °C is perhaps necessary to understand the operational limits for electric vehicle and hybrid electric vehicle applications.

As previously mentioned, colder temperatures limit ion mobility and the accessible capacity of a cell. An extreme combination of C-rate and temperature is therefore the 10C-rate at −20 °C suggested in Refs. [5,31,32]. Under these conditions, most Li-ion cells, with the exception of those containing lithium titanate oxide, $Li_4Ti_5O_{12}$, as a negative electrode, are unable to sustain large currents [33,34] for safety reasons and the risk of dendrite lithium platting at the carbonaceous negative electrode to short circuit a cell [34]. In addition, a capacity value measured with a high discharge rate at a low temperature may not represent the capacity value at that test temperature. The cell temperature will be much higher than the test temperature because of self-heating; for a 10C discharge test at −10 °C, the cell temperature can rise to 45 °C by the end of discharge [35].

It is worth highlighting that the general envelope of temperatures and currents outlined in cell testing standards coincide with the scientific literature. Key differences are that the scientific literature include tests at higher (> 1C) charging rates and have a larger concentration of tests at lower (< C/3) discharge rates. These differences reflect improvements in cell performance and the development of new analysis techniques (as discussed in later sections).

2.2. Application of constant-current capacity tests for modelling

Li-ion battery models can be divided into three broad groups: electrochemical models based on underlying electrochemical theory [36–38], semi-empirical models which exploit a combination of data and analogies with other physical systems and data-driven approaches which employ statistical techniques to learn from data directly without relying on rules-based programming. A detailed review of each modelling approach is beyond the scope of this work; readers are directed to [39].

The most established electrochemical battery model is the model proposed by Doyle, Fuller, and Newman (DFN) [36]. The framework is widely used within the battery community and has

not been significantly modified in the last two decades. Given the difficulty in measuring some of the fundamental parameters of the model for a commercial cell, many authors use parameter estimation techniques to estimate model parameters using constant-current discharge curves [40–42]. Despite the issues surrounding unique identifiability of model parameters because of the relatively large number of unknown parameters in the model discussed in [43,44], fitting data from constant-current load tests to extract model parameters for the DFN model have been effective and can lead to a relative error of $< 2\%$ [43] when validating the parametrised model with real usage cycles. It is worth noting that, under constant-current tests, there is a likely impact of 'local (electrode level) SoC' inhomogeneities [45] on identified model parameter values that has not been quantified in the literature. Beyond parametrisation, the authors of [42] claim that identifying and tracking the evolution of model parameters using constant-current capacity data unmasks the underlying mechanisms involved in battery degradation during cycling and storage.

Parametrisation of semi-empirical models by fitting constant-current load data is over-simplistic and hinders the accuracy of a model when environmental and load conditions differ from the training data set. The most notable semi-empirical model is the equivalent circuit model (ECM) which employs resistors, capacitors and a voltage source to form a circuit network that analogously describes cell behaviour [46]. Because the resistor and capacitor elements within the ECM are influenced by measurement timescale [47], using constant-current capacity tests with typical timescales of ~ 3600 s has limited scope for grid applications or other applications with similar load profiles.

Data-driven approaches have gained attention because of the increasing availability of large quantities of battery data. Data-driven techniques can be applied in various ways, and each amounts to different assumptions about the nature of the underlying processes. The simplest and most common data-driven approach is to use large look-up tables containing charge/discharge capacity measured for different constant-current rates and temperatures [48–50] which can then be used to directly map voltage to a battery SoC. The principal limitation of such empirical models is the accuracy to which the SoC and by extension, range, can be estimated under dynamic loads as is the case in real-world scenarios. The discrepancy between actual driving range and that estimated by a battery management system (BMS) employing such empirical models can be in the region of 25% [51–53].

Within the class of data-driven models are models that use statistical techniques and machine-learning techniques for time-series forecasting. These models have been used to estimate SoC and SoH and include, for example, neural networks [54,55], support vector machines [56–58], Kalman filters [59,60] and Gaussian processes [61]. There are two principal limitations to these models. First, the large amount of training data required to generate accurate predictions is often more than six months' worth [61], and second, the accuracy of the model is poor when environmental and load conditions differ from the training dataset.

2.3. Application of constant-current capacity tests for characterising degradation

The ageing of Li-ion cells involves complex electrochemical processes which encompass various ageing mechanisms [5,32,62–69]. The activation of an ageing mechanism depends on the usage conditions. The effect in systems engineering is quantified by the SoH, which is defined as a loss of cell capacity (capacity fade) and an increase in cell resistance (power fade).

To understand the causal relationship between usage profile and capacity and power fade, a number of authors have carried out ageing studies where usage has been categorised as cycling (cycle life test, i.e. long-term ageing tests where current $i \neq 0$) [5,13,14,70–74] or storage (calendar life tests, i.e. long-term ageing storage tests where $i = 0$) [75–77]. To characterise the impact of these long-term ageing tests, a plethora of characterisation tests have been performed. Specifically, constant-current capacity tests are used to define capacity fade. For example, Wang et al. [13,78] used C/20, C/2, 3C, and 6C constant-current capacity tests to characterise the effect of their ageing tests, while Kassem et al. [16] employed C/10, C/5, C/2, 1C, 2C, 3C, and 5C discharge rates. Some researchers, such as Zhang et al. [13,70], opted to measure capacity at different temperatures.

There are nuances in employing different C-rates and temperatures in capacity tests to capture degradation. For degradation studies, lower C-rates provide a more accurate valuation of thermodynamic capacity loss through loss of lithium inventory (LLI) and loss of active material (LAM). Lower C-rates $\leq$ C/10 also facilitate electrochemical voltage spectroscopy analysis [79] which has been employed to derive an understanding of degradation mechanisms involved in the ageing process [49,80,81]. At higher C-rates $\geq$ C/10, resistive effects play a more pronounced role and the kinetics can be investigated. Capacity tests employing higher C-rates will therefore include a convoluted mixture of both thermodynamically and kinetically induced changes. However, low C-rate tests have their own set of challenges; side reactions can influence the results if a test duration is very long [82], and high-precision battery cyclers with very low leakage current through voltage-sense cables are needed (details explained in Section 6). When low C-rate charge–discharge capacity is performed to high precision, the result also can be used to forecast battery life [83,84]. However, prolonged characterisation profiles introduce another potential source of cell degradation. Every charge–discharge cycle contributes to ageing as was shown by Zhang et al. [13]. In a worst-case scenario, carrying out a set of characterisation tests (capacity pulse power and electrochemical impedance spectroscopy (EIS) tests) at $-10\,^{\circ}$C, $0\,^{\circ}$C, $25\,^{\circ}$C and $45\,^{\circ}$C can reduce the cell capacity by up to 2.8%.

2.4. Discussion

A diverse range of capacity tests exists in the literature employing a wide range of C-rates and temperatures.

A pragmatic approach that yields useful relevant application data is to characterise cell capacity considering C-rates that correspond to the root mean square (RMS) current of typical usage profiles and temperatures. A number of factors should be considered when analysing typical usage profiles. These include: (1) RMS power/current demand, (2) harmonic content of the power/current demands and (3) individual user conditions. In an automotive scenario, the RMS power/current demand is directly related to the speed limit of the road, e.g. highway driving will have a higher average speed than city driving. The type of road will directly impact the variation of power/current demand. For example, while highway driving has higher average demand, it is expected that current/power fluctuations are low. In city driving, however, the average speed is low but there is a more pronounced fluctuating load profile because of frequent stop-starts and accelerations.

A lack of data around usage profiles can be estimated via tools such as AVL CRUISE or the 1-D model proposed by Taylor et al. [85] which are relevant for automotive applications. The proposed model was used to calculate the power/current demand on an individual cell within a battery and considered vehicle parameters such as mass and drag coefficient. An example of the electrical load on a cell generated from the well-established Artemis Motorway drive cycle [86] using the 1-D model presented in [85] which considered a vehicle with a 28-kWh battery pack constructed from

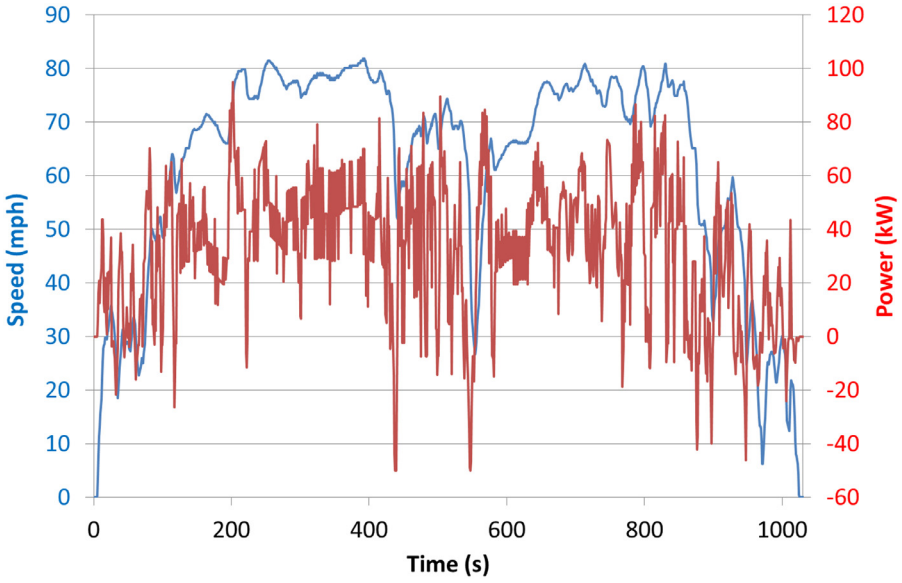

Fig. 2. Duty cycle of a vehicle's 28-kWh battery pack owing to Artemis Motorway drive cycle (positive power represents discharge). Duty cycle is generated using the 1-D model proposed by Taylor et al. [85].

20Ah LFP commercial pouch cells is shown in Fig. 2. The RMS power for this example was 31.9 kW at pack level.

If further detailed analysis on degradation modes is sought, then low C-rate ($\leq$ C/10) capacity tests can be performed which will generate thermodynamic data. In this case, when the appropriate high-precision equipment are employed and side reactions are minimised, a lower rate yields better accuracy.

3. Open-circuit voltage tests

Open-circuit voltage (OCV) tests refer to the measurement of the equilibrium voltage of a cell as a function of the SoC. At the full-cell level, the OCV vs. SoC curve is defined by the OCV curves of both active electrodes, the positive electrode (PE) and the negative electrode (NE). The specific individual electrode potential is the potential difference between an electrode and a reference, in most cases lithium metal when no external current flows and the electrode potentials are at equilibrium. As such, the electrode potential incorporates thermodynamic information about the electrode such as the number and types of phase transitions undergone by the electrode materials during charge and discharge (most battery electrodes undergo several phase transformations) and the amount of lithium intercalated in any given phase [87]. Mathematically, the potential of an electrode material during a phase transformation can be expressed via the chemical potential, which determines the change in internal energy resulting from a change in the concentration of the ionic species. At equilibrium, and for each phase, this can be calculated using the Nernst equation as [88,89]

$$E = E_0 - \frac{RT}{ze} \log \frac{a_i^+}{a_i^-} \tag{3}$$

where E_0 is the standard redox potential, R is the gas constant, T is the temperature, z is the number of electrons exchanged in the redox reaction ($z = 1$ for Li-ion systems), e is the elementary charge and a_i is the chemical activity of each electrode a_i^+ for positive and a_i^- for negative electrode. In intercalation reactions, E_0 reflects the energy of intercalated ions in specific sites within the lattice of the host material [90]. The ratio of activities is dependent on the Gibbs free energy of pure reaction of the products and the reactants [91]. However, there are cases where the electrode potential does not display Nernstian behaviour.

The full electrode thermodynamic potential/voltage signature depends on the number of phase transformations and solid solutions that the active material experiences during lithium intercalation and de-intercalation. Fig. 3 presents an example of a hypothetical material M undergoing lithiation to LiM. The phase diagram of Fig. 3(a) shows the different stable phases in the system (Greek letters) as well as their domain of stability for both composition and temperature. At a given temperature as depicted by the dotted line, the voltage variation associated with lithiation can be predicted according to the nature of the reaction, solid solution (one phase) or phase transformation (two phases). The associated voltage variation is shown in Fig. 3(c). The voltage of solid solutions varies with the composition because the Gibbs free energy of a pure reaction changes with the composition (Fig. 3(b), Region I, III and V). Phase transformations present a voltage plateau because there is a mixture of two phases which convolute, and thus ΔG_0^f remains constant (Fig. 3(b), Region II and IV).

The electrochemical response of an active material is influenced principally by the transition metals that are undergoing oxidation and reduction (e.g. $LiFePO_4$ vs. $LiCoPO_4$) and their relative proportion (e.g. $LiN_{.33}Mn_{.33}Co_{.33}O_2$ vs. $LiN_{.40}Mn_{.40}Co_{.20}O_2$). It will also be influenced by the starting atomic structure (e.g. α-V_2O_5 vs. β-V_2O_5) and the nature of the counter ions (e.g. -PO_4 vs. -AsO_4) [92–95].

At the full-cell level, the OCV vs. SoC curve is defined by the OCV curves of both active electrodes and two other significant parameters: the loading ratio that relates the capacity of the PE with respect to the NE and an offset that takes into consideration eventual SoC shifts between the electrodes, i.e. that an electrode might not be full when the other one is empty and vice versa, this is shown in Fig. 4(a) [96].

Contrary to the assertion of some authors, the OCV vs. SoC relationship of full cells changes with temperature and aging [97–100]. This is clearly identified from Nernst Eq. (3) which shows a temperature dependency; nevertheless, such changes are in most cases minimal and hence negligible. Changes in cell-level OCV with temperature can also be induced by changes in the boundaries defining regions corresponding to solid solution and phase transformation as depicted by the dotted lines in Fig. 3. In most

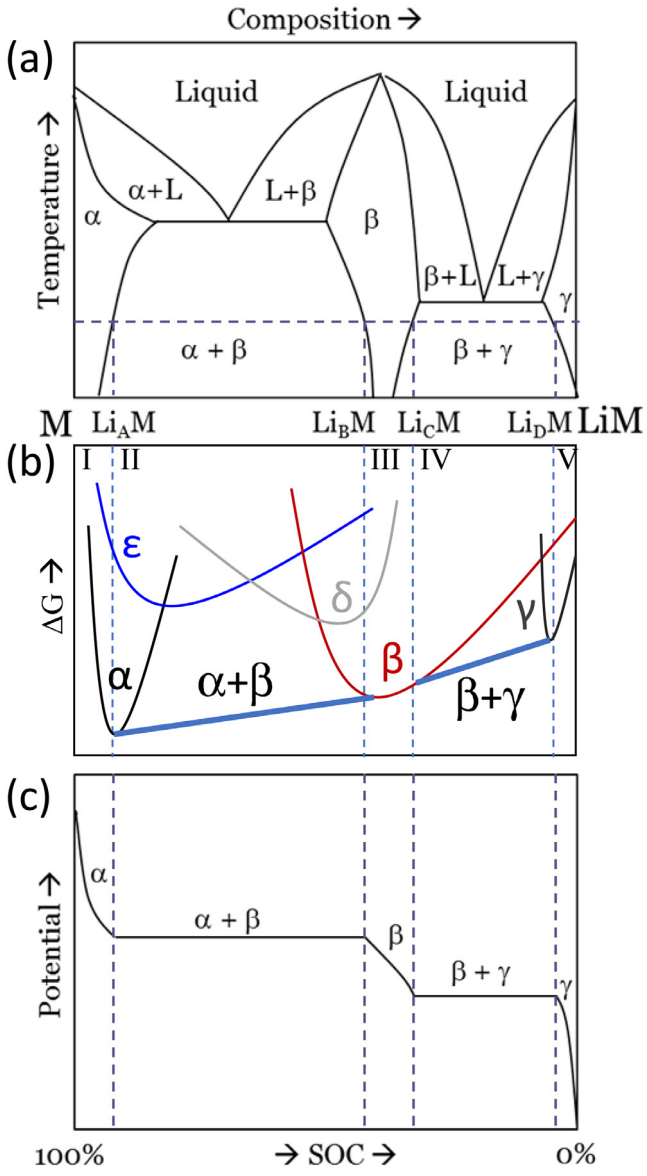

Fig. 3. Relationship between (a) phase diagram (adapted from [91]), (b) Gibbs free energy and (c) potential curve.

cases, the OCV curve of the individual electrodes will not change with aging because most materials are stable and will to intercalate/deintercalate lithium in the same way close to equilibrium. There are, however exceptions, with the best known being the voltage fade of high-energy Li-rich layered materials [101]. Even with both electrodes having stable OCV curves with aging, the OCV curve of a full cell is likely to evolve significantly upon aging because aging induces changes in the balance between the positive and negative electrodes and thus modifies the loading ratio and the offset as shown in Fig. 4(a). Changes in the loading ratio and offset not only affect the voltage response of a full cell but also its capacity retention. Fig. 4(b) presents an example of the impact of loading ratio and offset variation on capacity loss (contour plot). Further details are discussed in the electrochemical voltage spectroscopy (EVS) section.

It is essential to understand the origin of OCV and how it changes depending on the aging conditions. Of equal importance is a proper definition of SoC, a parameter that is often ill-defined in the literature. The definition of SoC is not straightforward and differs within the published literature. According to the USABC [102], SoC is defined as "*the ratio of the Ampere hours remaining in a cell at a given rate to the rated capacity under the same specified conditions*". This is often misinterpreted in a second definition where the '*rated capacity*' is replaced by the '*nominal capacity*'. These definitions differ because the "*rated capacity under the same specified conditions*" refers to the maximum capacity at the rate that was used under the same environmental conditions and not to nominal conditions. For electrochemists, SoC is a thermodynamic state function that relates to the ratio of the remaining intercalation sites for Li ions divided by the total number of sites. These three definitions are different and should not be confused. To take an analogy of a fuel tank, the true USABC definition refers to the distance that can be covered if the speed is maintained. If the speed is reduced or increased, the scale has changed, and subsequently a new estimation is necessary. The misinterpreted definition using the nominal capacity instead of the rated capacity refers to the distance that can be covered if the speed is set to a predetermined value (the rate at which the nominal capacity was determined). The thermodynamic definition refers to the distance that can be covered if the speed is reduced to the point where the fuel consumption is the lowest possible. As a fuel gauge, the USABC definition is more intuitive; nevertheless, in this case, the SoC scale changes with current and thus provides no reference to thermodynamics. The thermodynamic definition makes the least sense as a fuel gauge but offers in-depth information and thus is easier to use for modelling and degradation analysis. The misinterpreted definition serves no purpose and should never be used. The ambiguity in defining a true accepted SoC measure arises from the fact that both the USABC and thermodynamic definitions are relevant depending on the application. One solution to this problem was proposed by Dubarry et al. who used the USABC definition to calculate the depth of discharge and the thermodynamic definition to calculate the SoC [103]. In this case, depth of discharge was not equal to 1-SoC, however, a convenient fuel gauge was kept while avoiding any ambiguity. More information on SoC can be found in a recent review by Li et al. [104].

The thermodynamic definition of SoC, i.e. using the number of available intercalation sites, is not adapted to modern Li-ion cells and packs for several reasons. There are two working electrodes and, in most cases, they are each limiting at either end of the charge and discharge boundaries. That is, none of the electrodes utilise their full range of available intercalation sites and therefore their full SoC range. In the majority of cases, the NE is limiting at the end of discharge and the PE at the end of charge; this relates to the solid electrolyte interface (SEI) layer formation and the excess graphite introduced to avoid plating, respectively. This is different than $Li_4Ti_5O_{12}$-based cells, where the NE is limiting on both sides, and therefore the cell SoC is the same as that of the NE [105,106]. Another issue arises with the use of layered oxides such as $LiCoO_2$, NCA and $LiCo_{1/3}Ni_{1/3}Mn_{1/3}O_2$ (NMC), where high voltage reactions are not fully reversible. As a result, such materials are never fully delithiated, and thus, even if the PE is limiting at the end of charge the true SoC of the PE is not 100% at the end of charge. To take all of this into account, an SoC definition based on exchangeable Li ions was proposed in [49]. This definition only considered the maximum number of Li ions that could be exchanged at a really low rate for a given potential window. This definition is universal and applies to half-cells, full cells and battery packs, even if imbalanced.

$$SoC = \frac{Remaining\ exchangeable\ Li^{+}\ ions}{Total\ exchangeable\ Li^{+}\ ions} = \frac{Residual\ capacity\ @\ low\ rate}{Maximum\ capacity\ @\ low\ rate} \quad (4)$$

It is also important to note that, for every SoH, 100% of the SoC is available at low rates. The SoC scale needs to be continually ad-

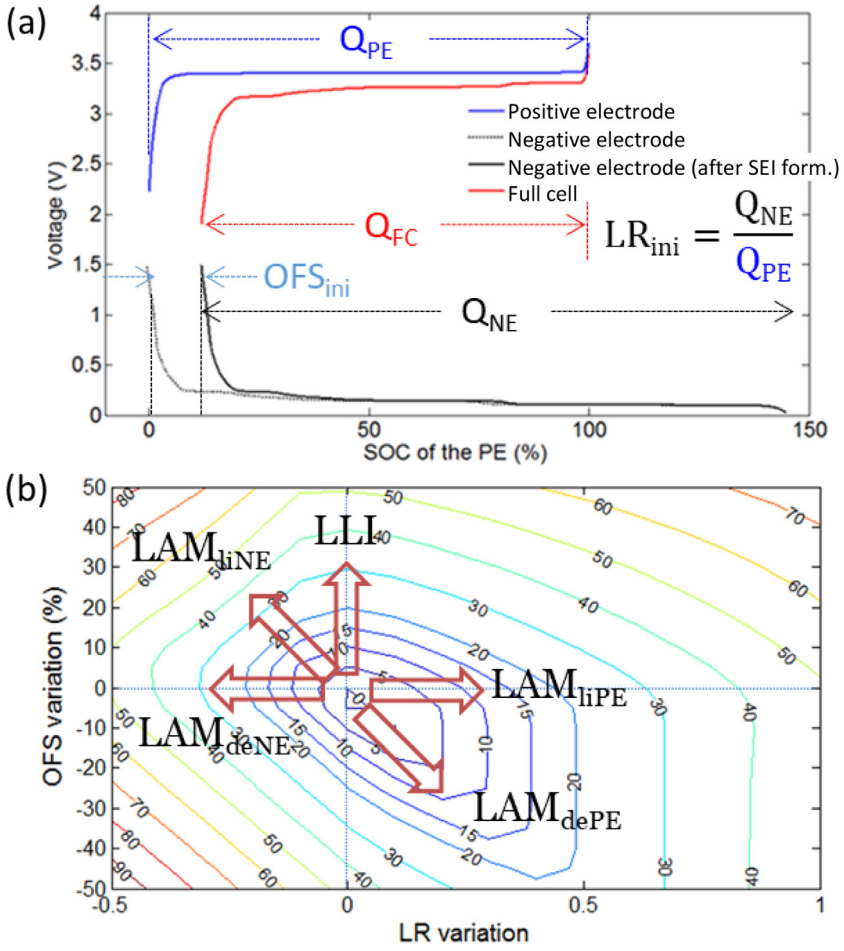

Fig. 4. (a) OCV relationship between full cell, PE and NE and (b) impact of changes of loading ratio (LR) and offset (OFS) on capacity loss.

justed with aging so that a 100% SoC corresponds to the maximum available capacity at any given time.

The most common method of measuring the OCV vs. SoC curves is based on the galvanostatic intermittent titration technique (GITT) or pseudo-OCV test. In what follows, the techniques for measuring OCV and the associated hysteresis are discussed.

3.1. Galvanostatic intermittent titration technique

Popularised in the late 1970 s [107–110], the GITT systematically adjusts a cell's SoC with prolonged relaxation periods in between. The cell voltage changes with time mainly because of the concentration gradient in the electrolyte and solid phase (diffusion) and redistribution in the solid phase. The length and current of the discharge/charge step and the duration of the relaxation is dependent on the cell temperature and the required accuracy. Since kinetic contributions are avoided in this technique, these OCV measurements are believed to be the most accurate. An alternative method to GITT is the potentiostatic intermittent titration technique which employs voltage as a control parameter instead of current to produce similar results. However, GITT has been found to be much more popular than the potentiostatic intermittent titration technique in previous studies reported in literature.

The FreedomCAR standard [25,26,111] (now attributed to USABC) outlines the measurement of OCV with periods of relaxation between charge/discharge pulses. Although this is not strictly a GITT test, it recommends discharging the cell in 10% steps and subsequently recording the voltage after 1 h of rest. This granularity of data and accuracy (considering the error that arises from assuming that a cell reaches close to thermodynamic equilibrium in 1 h) is considered sufficient for applications such as offline and online battery management system (BMS)-level modelling [112]. This is because the largest error in OCV measurements which employ the FreedomCAR approach (typically $< 0.03\%$) is significantly smaller than the smallest error of typical system-level models (typically $> 2\%$) [113]. To achieve smooth OCV curves in this case, modellers often employ spline functions [114] or other smoothing tools in their models.

More precise measurements of OCV can be informative to the scientific community interested in accurately identifying different electrochemical reactions and phases in both electrodes [115]. The obvious change to the FreedomCAR method is the introduction of more than 11 data points; i.e. to use SoC increments smaller than 10%. The second improvement is the introduction of longer relaxation periods. It has been suggested that a resting period of 1 h is acceptable for LFP batteries [116], but this is unlikely to be long enough for other Li-ion cell chemistries to reach electrochemical equilibrium [117–119], thereby leading to discrepancies between the theoretical OCV and measured OCV. Li et al. [116] showed a cell voltage change of only 2 mV after 1 h of relaxation for an LFP cell. However, in [119], it was argued that a cell including LFP may not reach electrochemical equilibrium even 40 h after a discharge/charge event. However, [118] suggests that 4 h is sufficient for cells to reach a state close to equilibrium, such that any further changes in voltage typically lower than 1 mV cannot reliably be measured with common cell characterisation equipment. Although long relaxation periods will provide voltage values very close to

theoretical, one has to weigh the improvement of the measured values against the possibility of slow chemical reactions in the cell which alter the true equilibrium state.

The authors of [118] argued that the optimal trade-off between accuracy and test duration is to measure OCV for every 1% SoC increment with a rest time of 4 h, which equates to 17 days of test time (101 rest periods, each of 4-h duration ~17 days). This is prohibitively long for investigators both within academia and industry and may not be economical or possible if time is of importance. As alluded to above, in system-modelling applications, the FreedomCAR approach is sufficient. For example, Zhang et al. [120] measured OCV according to the FreedomCAR standard. These data were then used to develop an SoC estimation algorithm which employed an extended Kalman filter to correct for state estimation errors. Using this extended Kalman filter algorithm, the SoC estimation error was found to be within 5% during the entire process of charging and discharging of a battery, which met the SoC accuracy requirements set out in that study. Furthermore, the error in SoC estimation was negligible related to OCV measurements and was linked more with errors in estimating a battery's dynamic state [120]. For tests aimed at characterising the change in OCV because of Li-ion cell degradation, Baccouche et al. found that using an SoC increment of 2.5% provided sufficient detail to study OCV evolution [121].

The systematic approach to OCV testing is to first 'weigh-up' the benefit of improved accuracy against the cost of longer rest periods and shorter SoC increments. This will then inform the investigator of the required accuracy and subsequently the SoC increments and rest time needed for their application. It is also worth noting that rather than using equidistant SoC increments, a better approach is to define a bespoke distribution of SoC points based on expected non-linearity as proposed by Nikolian et al. [122]. For regions of high non-linearity in the OCV curve, it is more informative to increase the number of data points in those regions than in regions of relative linearity.

3.1.1. Application of GITT for characterising performance

The OCV of a cell, which is analogous to electromotive force, can be used to define the performance capability of a Li-ion cell. The GITT technique has therefore been used in exploratory research to investigate the performance characteristics of cells [123–125]. Li et al. employed the GITT technique to calculate the lithium diffusion coefficient for an entire SoC range of cells incorporated with graphene sheets [126]. Their results indicated a two-fold increase in the diffusion coefficient when graphene sheets were used. Ding et al. [124] implemented GITT to measure the Li diffusion coefficient of NMC-based cathode materials coated with AlF_3. In more recent literature, researchers such as Luo et al. [127], Zhu et al. [125] and the authors of [90,128,129] relied on the GITT technique to study the diffusion coefficient of different electrode materials. Ma et al. [130] employed GITT to compare the rate capabilities of different cathode materials, i.e. $Li_4Ti_5O_{12}$, LFP, $LiCoO_2$, and NMC.

3.1.2. GITT technique for OCV hysteresis

In some cases, the GITT curves obtained during charge and discharge are slightly different and present a potential hysteresis, even if significant rest is allowed for each step. Srinivasan and Newman [131] explained this phenomenon using a high-level shrinking core model, while Dreyer et al. [132] explained it with a single-particle model. If the voltage differences are restricted to the plateaus in either charge or discharge regimes, the origin of hysteresis is likely to be structural, i.e. a phase transformation occurs either through intercalation rather than deintercalatation or vice-versa. For example, $LiMn_2O_4$ presents a 0.6-V structural hysteresis for its reaction from $LiMn_2O_4$ to $Li_2Mn_2O_4$ below 3 V [133,134]. The largest reported structural hysteresis was around 2 V for $Li_4VO(PO_4)_2$ [135], although this material is not considered for commercial Li-ion cells. It's noteworthy that studies based on Silicon anodes suggest a correlation between the mechanical stress experienced by electrodes and voltage hysteresis [136,137], although any causality is not yet established, however, indicates the requirement of further research.

If, however, most of the voltage curve is affected, a part of the measured hysteresis may be an artefact related to the issues surrounding appropriate SoC referencing. If the author's estimation of SoCs are not properly aligned when the cells are charged and discharged, a false hysteresis might be present as presented in Fig. 4 of Ref. [138]. When 0% SoC is defined as the point when a cell reaches its lowest discharge voltage $V_{min,\ dis}$ while being discharged, cells can have different relaxation voltages (different lithiated states of electrodes) depending on the discharge profile, even when discharged with the same current and at the same temperature. For example, when discharged to $V_{min,\ dis}$ with 1C constant-current without interruption, cells will have a higher relaxation voltage than when a cell is discharged to $V_{min,\ dis}$ with 1C pulsed current (as is done in GITT). This simple additional relaxation period allows for solid-state diffusion and reduces the polarisation at the electrodes, thus freeing Li sites at the surface for further intercalation and leading to the removal of a higher amount of Li from the anode before reaching the $V_{min,\ dis}$ as further explained in [138].

To eliminate this offset, Barai et al. [138] suggest performing a charge OCV test immediately after the last 4-h rest period of the discharge OCV test; therefore, the last OCV measurement of the discharge OCV test is defined as 0% SoC and becomes the first measurement for the charge OCV test and removes the mismatch at 0% SoC. To remove the mismatch at 100% SoC, it is suggested that the actual capacity data are used instead of the estimated SoC. Further details can be found in Ref [138].

This technique can provide an accurate estimation of the real OCV hysteresis for different chemistries. Employing this technique, the OCV hysteresis of an LFP cell was found [136] to be much lower than that previously shown [139–141]. To investigate OCV hysteresis, Roscher et al. [139] employed a GITT test with 5% SoC steps and 3-h intermediate rest periods. They reported an approximate 20-mV hysteresis at 50% SoC when the test was performed with C/2 charge–discharge current pulses. Interestingly, they reported that when the test was performed with a higher current pulse of 10C, the hysteresis effect was not present. This conclusion, however, was recently disputed when pulse rates between C/2 and 3C were employed to show that hysteresis was not significantly affected by charge–discharge pulse rates [142]. In [138], the authors reported the existence of a slight OCV hysteresis for different Li-ion cell chemistries when the initial conditions were correctly identified.

Beyond thermodynamic entropic effects, materials such as LFP, $Li_4Ti_5O_{12}$, and lithiated graphite (LiC_6) are subject to pronounced voltage-hysteresis arising from mechanical effects. Within the framework of phase-separation theory, which stipulates that during Li insertion in a delithiated bulk material, a lithiated phase region emerges in juxtaposition to delithiated phase regions, different lattice constants of lithiated and delithiated phases in phase separation materials like $LiFePO_4$ cause mechanical stress at the phase barrier leading to a drop in the potential inside the individual particles [143]. Moreover, lattice distortions, as a result of doping compounds, hinder the propagation of the phase barrier and thereby intensify the mechanical stress in the bulk material [144]. Accordingly, voltage hysteresis between the charge and discharge curves during galvanostatic testing is non-negligible even at low current rates. At high rates of charge and discharge, voltage hysteresis is expected to be significant. The finding of a di-

minishing voltage-hysteresis at 10C is therefore unexpected. Bai, Cogswell and Bazant [145] proposed an alternative phase-field theory. Within this framework, particle filling occurs homogeneously above a critical current density. Above this critical current density, the separation into Li-rich and Li-poor phases is suppressed, and therefore, voltage-hysteresis arising from mechanical stress is reduced.

3.1.3. Application of GITT test for modelling

The usage of GITT-based OCV profiles varies widely depending on the modelling work, from extracting model parameters for electrochemical OCV models to directly using the data in semi-empirical equivalent circuit models commonly employed for SoC and SoH estimation.

Birkl et al. [90] developed an OCV estimation model to be integrated as part of a larger cell model in a BMS. In developing their model, they measured the OCV of both half-cells and full cells using the GITT technique. Their model was reported to have an accuracy of better than 5 mV. A significant portion of this small error may be related to the relaxation period applied after each pulse in the GITT. Petzl et al. [141] reported an 8-mV discrepancy in measured OCV arising from changing the post-pulse rest in GITT from 6 min to 5 h. The OCV was found to exponentially stabilise with time. In their study, they also compared GITT test results with low-rate (C/20 and C/40) charge/discharge tests. They reported a 20-mV difference between the C/40 continuous OCV approximation compared with a GITT with 5% SoC increments and 2-h rest period between each pulse. This difference was reduced when shorter rest periods were used in the GITT. It follows that if the cells are still relaxing after 2 h, the 20-mV difference could be higher if a longer rest period was employed.

In another study, Jonghoon et al. [146] performed two GITT tests to measure OCV hysteresis, one with 10% SoC steps and another with 5% SoC steps. The data were then used to develop an online extended Kalman filter-based SoC estimation algorithm. From a comparison between the two datasets, they found that the performance of the algorithm was improved by up to 10 mV when 5% SoC-step test data were used. Similar conclusions were recently made by Mao et al. [147], who showed that shorter pulses combined with longer relaxation periods improved estimation accuracy.

Furthermore, OCV hysteresis as a function of capacity (and thus SoC), in contrast to the use of a fixed OCV hysteresis value for all SoCs as is often assumed in literature [148,149], has been shown to improve the performance of an ECM model [138] typically employed in a BMS.

To support the modelling of a layered transition metal-oxide positive electrode, Dees et al. [150,151] employed GITT to estimate Li transport within and between individual domains and the Li-diffusion parameter. In another similar study using a Li_yFeSO_4F electrode, Delacourt et al. [152] employed GITT to validate their mathematical single-particle model. The application of GITT in developing models for the electrochemical kinetics of Li ions for different electrode materials has been presented in literature [153,154].

GITT results along with OCV hysteresis can significantly improve model performance as reported by researchers. A key barrier to this method of OCV measurement is perhaps the duration of testing, up to two weeks, which is probably tolerated because of the improvement in model performance. Further research is required to reduce the GITT test duration.

3.1.4. Application of GITT tests for characterising ageing

The OCV profile measured by GITT can also provide interesting insights into cell degradation when employed along with other characterisation tests and post-mortem analysis. In a recent study, Shi et al. [129] showed that the change in cell performance characteristics, such as in a cell's polarisation properties and apparent diffusion coefficient, can be captured through a group of non-destructive tests which included GITT. They considered a cell cycled at a high temperature which led to changes in the voltage plateau of the OCV profile captured by GITT (Fig. 5). This confirmed a phase change in the graphite anode. In a similar study by Kleiner et al. [155], GITT data were used to explain how the degradation of Li-ion cells under storage ageing conditions is related to the change in the kinetics of the diffusion process within the active materials. Application of GITT to quantify ageing mechanisms has also been seen in other research [156,157]. However, as previously mentioned, the long test duration may act as a barrier for its adoption in many other degradation related research studies [14,16,78,158] where GITT could provide interesting insights for the identification and quantification of degradation mechanisms.

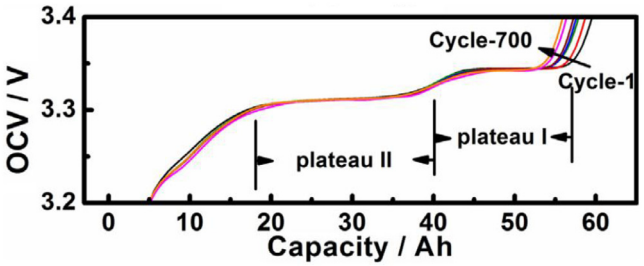

Fig. 5. Change of OCV profile (GITT) with cycling as reported by [129].

3.2. Low-rate cycling and pseudo-OCV test

3.2.1. Test methodology

Depending on the resolution required, deriving an OCV from a GITT experiment can take several weeks. To produce thermodynamic information faster, a cell can be cycled at a low rate to generate a pseudo OCV. The test is similar to a capacity test with a constant low charge/discharge rate, typically C/25 or lower. The low current is used to reduce kinetic contributions, lower the electrode polarisation and reduce ohmic heat generation. When a low driving current is used, the ohmic loss (IR_{cell}) contribution to the cell voltage (V_{cell}) is low [141]. Furthermore, ohmic heat generation is assumed to be negligible. An example of low-rate cycling is shown in Fig. 6, which illustrates the ability of low-rate cycling to capture phase information. The simplicity of this approach to capture thermodynamic information has attracted interest from a large number of researchers for both modelling and capturing degradation [13,16,49,75,78,81,98,100,141,159]. Such researchers typically employ this technique at room temperature, although repetition is usually carried out at higher and sub-zero temperatures [98,100,159]. There is, however, no standard C-rate employed in the literature for low-rate cycling, although C/25 is evidently the most utilised.

Even with low rates, cell hysteresis is convoluted with the cell overpotential, and the voltage response is different for each rate. Although close, neither the low-rate charge nor discharge curves can qualify as OCV or pseudo OCV. If it is to be used in place of OCV for modelling purposes, the charge and discharge hysteresis needs to be taken into consideration [138,160]. In low-rate regimes, even where the impact of resistance can be neglected, hysteresis is present in common electrode materials such as graphite [161], $Li_4Ti_5O_{12}$ [138], $LiMn_2O_4$ [133,162], $LiCoO_2$ [132], $LiNiMnCoO_2$ [90], $LiNiCoAlO_2$ [138], and $LiFePO_4$ [138]. Hysteresis can also be related to path dependency [131,132] of lithiation and should not be confused with the structural potential hysteresis mentioned in the previous section.

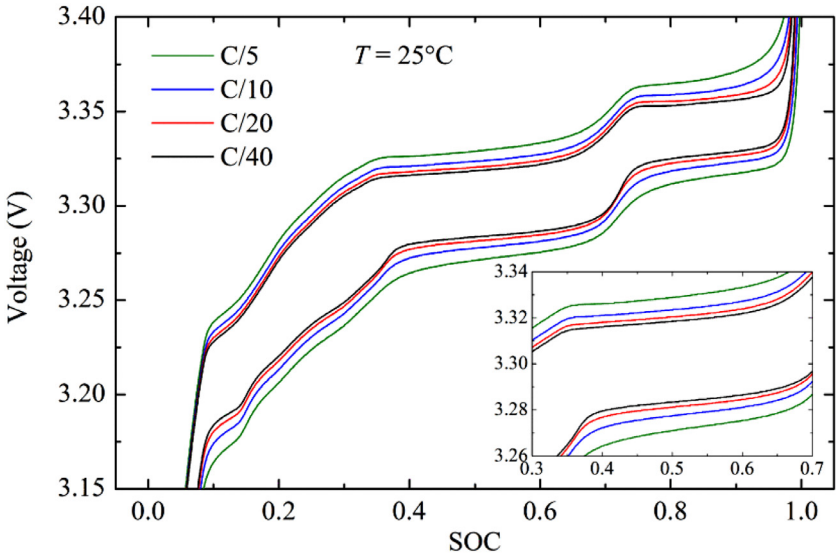

Fig. 6. Low-rate cycling profiles measured by employing different constant-current values as reported by Petzl et al. [141].

An alternative method to GITT to gather OCV data from low-rate tests is to use an average of the charge and discharge curve. The latter is known as a pseudo-OCV profile. An example of this technique can be found in Truchot et al. [49] which employed a C/25 current to measure charge–discharge voltage. They derived the single-valued OCV from these two datasets by averaging and subsequently employed this OCV for their SoC estimation algorithm. This method of OCV measurement has been adopted in earlier research by the same group of researchers for SoC estimation from voltage relaxation [81,98,99,103,163,164] and for ECM modelling [165]. To validate the accuracy of their approach, the authors often compared the SoC estimation from the pseudo-OCV curve to the real SoC obtained from measuring the residual capacity [49,81] with good results.

3.2.2. Application of low-rate cycling test for characterising performance

While the low-rate cycling test is simple to perform and provides first-hand insight into cell behaviour, it is not widely employed as a quick characterisation test in either literature or industry. The principal reasons identified for this include, first, the long test period associated with this procedure, e.g. a C/25 cycle will take more than 50 h to complete without including rest periods, which is often too long to employ as a quick characterisation tool. Second, unlike capacity tests, which provide a specific value and can be used by anyone, this test generates a voltage profile which requires detailed analysis. Nevertheless, Bloom et al. [79,166,167] and Dubarry et al. [81] popularised EVS techniques for analysing degradation mechanisms by investigating incremental changes in voltage owing to infinitesimal changes in capacity. Given the breadth of discussion needed for these techniques, Section 4 is devoted to this.

3.2.3. Application of low-rate tests and pseudo OCV for modelling

The OCV profile is a key parameter of electrical equivalent circuit models, and in this regard, there are two approaches to allow the use of low-rate cycles: the first takes hysteresis into account [138,160], while the second uses a pseudo-OCV profile [49,165]. Zhang et al. [75,168] used the C/33-rate charge/discharge voltage curves along with a single-particle electrochemical model to study the loss of cyclable Li for cells having undergone calendar ageing. Although this simplistic form is popular, it may lead to high inaccuracy in real applications, especially for cells with flatter OCV vs. voltage curves [49], where a variation of potential close to or below the resolution of voltage sensors might correspond to a significant change in the SoC. Xing et al. [159] used a C/20 current to measure both charge and discharge voltage curves and averaged these values to calculate the OCV. This OCV was later used for their SoC estimation algorithm. In this procedure, they measured OCV at intervals of 10 °C from 0 °C to 50 °C to capture the variation of OCV at different temperatures. The measured OCV showed a variation of approximately 20 mV at a particular SoC.

The dependence of OCV on temperature can be explained using the heat flow ($\dot{Q}$) within a Li-ion cell, which can be defined as

$$\dot{Q} = I(\mathrm{V} - OCV) - IT_{ref}\ \frac{\partial OCV}{\partial T}. \tag{4}$$

The first term on the right-hand side of Eq. (4) represents irreversible resistive dissipation caused by the deviation of the surface overpotential volume OCV owing to a resistance of the passage of current (I). The second term is the reversible rate of heat generation owing to the electrochemical reactions. For electrochemical reactions under fixed pressure conditions, the equilibrium potential is given by $\partial OCV/\partial T \cong \Delta S/F$. The ratio of entropy change, ΔS, to the Faraday constant, F, is in the order of 4×10^{-4} [114]. Uddin et al. [114] showed that $T_{ref}\ \frac{\partial OCV}{\partial T}$ is comparable with the term $V - OCV$ and should therefore not be neglected at small SOC values.

3.3. Discussion and future direction

There is no standardised method for performing OCV tests, which limits direct comparison of literature results. Averaging low-rate charge and discharge curves to generate a single OCV vs. SoC curve seems to be the best compromise between time and accuracy, although one has to be careful about potential OCV hysteresis and kinetic limitations which might appear upon aging [169]. Compared with alternative methods to characterise degradation, because of the relatively long test time, low-rate cycling or pseudo-OCV curves are not commonly employed for the characterisation of degradation. However, with the rise in popularity of EVS techniques (cf. Section 4), this might change for studies aiming at understanding the cell degradation mechanism.

GITT tests are commonly used to study individual electrodes; however, its use in characterising commercial cells is less common. It has been shown that GITT is a non-destructive approach that can provide beneficial insights into the identification and quantification

of ageing mechanisms, yet most cell-ageing work reported in literature does not include a GITT test. Again, the key reason for this may be the long test duration involved. Further reduction of the test duration through the integration of an OCV relaxation model with GITT tests may help reduce test times and thus promote a larger penetration of this technique in the academic literature for full-cell testing.

4. Electrochemical voltage spectroscopy tests

Tracking the changes in capacity and power retention provides an instant snapshot of the state of the cell, but it does not enable diagnosis because of the lack of accessible information on the actual degradation itself. Similarly, capacity and power tracking are not readily suited for prognosis either. Such knowledge is traditionally gathered via post-mortem analysis [9], but some authors have proved in recent years that it is also obtainable from data collected during capacity tests. With ageing, the voltage response of a cell changes, because as mentioned in Section 3, the balance between the PE and NE changes [96,170]. Voltage changes can also be associated with variations in the electrochemical reactions which occur on either electrode [101]. Therefore, tracking and studying these voltage changes will provide information on a cell's thermodynamic state and on its kinetics and thus enable diagnosis and prognosis.

The voltage changes associated with a change in electrode balance and/or a change in the electrode signature are in most cases minute, a few mV, and are therefore difficult to visualise and quantify on the classic voltage (V) vs. capacity (Q) curve in which the voltage range typically spans approximately 2 V. To enhance these changes, a derivative of the V vs. Q curve is necessary. The incremental capacity (IC), or $dQ/dV = f(V)$, was proposed by Belewski and Brenet in 1967 [171] to study the reactivity of manganese dioxide versus a standard hydrogen electrode for Leclanché battery applications. The method was later used by Clauss and Schweigart for the same application [172,173], and Thompson applied it to Li metal cells in the late 1970s [109,174,175]. Following these studies, the technique was adopted by other groups and started to become widely used with Dahn et al. [176–178] and Barker et al. [179,180] as early adopters. In the 1990s, much attention was given to potential electrodes for Li-ion cells with reports of the IC signature for graphite by several groups [181–183] and on positive electrode materials notably by Valence Technology Inc. [184–190] and others [191–193]. The first reports of the IC signature of full cells date from the early 2000s with work by Barker et al. [194,195] and the Berkeley National Laboratory [196–200]. However, the analysis of full-cell signature is complex and only little qualitative or quantitative information was decipherable at the time. To circumvent this issue, Bloom et al. introduced another derivative method, differential voltage analysis (DV) or $dV/dQ = f(Q)$ in 2005 [79,166,167]. In the late 2000s, Dubarry et al. proposed a methodology to index IC curves and thus opened the door for the full qualitative and quantitative analysis of ageing on these [81,99,163,164]. Since then, both techniques have been adopted and accepted as valid alternatives to post-mortem techniques to characterise commercial cells [5,201]. The following section introduces the principles and applicability of these EVS.

4.1. EVS principles

Both IC and DV methodologies are based on the study of the changes in the voltage signature of a cell. As mentioned in Section 3, because of differences in chemical composition and/or crystallographic structure, all active electrode materials have a different thermodynamic voltage signature with a different set of voltage plateaus and regions where the voltage varies with composition.

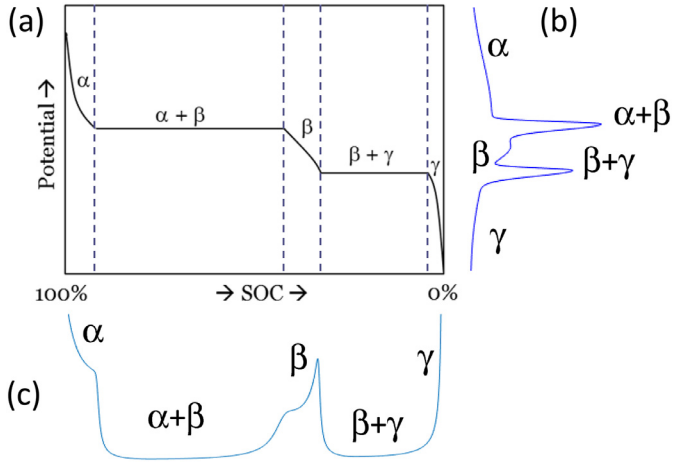

Fig. 7. Relationship between (a) voltage curve and derivative curves (b) IC and (c) DV.

Fig. 7 presents the voltage response of a hypothetical material, M, undergoing a lithiation to LiM and the two derivatives of interest with DV (c) and IC (b). It can be seen that for the IC curve, more focus is given to the phase transformations as the peaks correspond to the voltage plateaus. The DV curves focus on single-phase regions with peaks for solid solutions.

Fig. 8(b) presents the V vs. Q curve, Fig. 8(a) the DV curves and Fig. 8(c) the IC curves associated with a full cell (red curves) and its corresponding positive electrode (PE, blue curves) and negative electrode (NE, black curves). The equations to calculate IC and DV were taken from [79] and are provided in Fig. 8(d). In this representation, it can be seen from Fig. 8(a) that for DV, the signature of the full cell corresponds to the sum of the PE and NE signatures. It can also be seen that the IC curve is much more complex in appearance where no immediate relationship between the full cell, PE, and NE is visible. More details can be found in [202].

In theory, both IC and DV should provide the same information since they are derived from the same voltage curves. The selection of which one to use is, therefore, a matter of preference. There are, however, small differences between the two which could direct a user towards one or the other:

- DV curves offer the advantage of being more visual for identifying the contribution of the PE and NE at first inspection because of the additive nature of their relationship. However, plotting of DV curves is not ideal for several reasons. The curve has to be zoomed into to significantly see the centre peaks, and therefore the information at the two limits is often lost. Moreover, the abscissa is capacity which changes with ageing; therefore, curves either need to be normalised or be aligned with one end of the capacity scale. This could create confusion when comparing studies using different plotting conventions. To alleviate this issue, Bloom et al. [79] suggested shifting the data relative to the data from the anode half-cell. The active area should also be decreased to ensure consistency. Adopting such a procedure aligns the voltage vs. capacity discharge curves; once these adjustments are made, they should not change. IC curves, however, require in-depth knowledge to derive valuable information from first glance, but the abscissa is voltage and thus a reference.
- When composite electrodes are used, i.e. electrodes with several active materials, IC curves might be the better alternative because the signature of both contributions is additive. This is not the case for DV curves, and modelling (next section) will be necessary to analyse the different contributions.

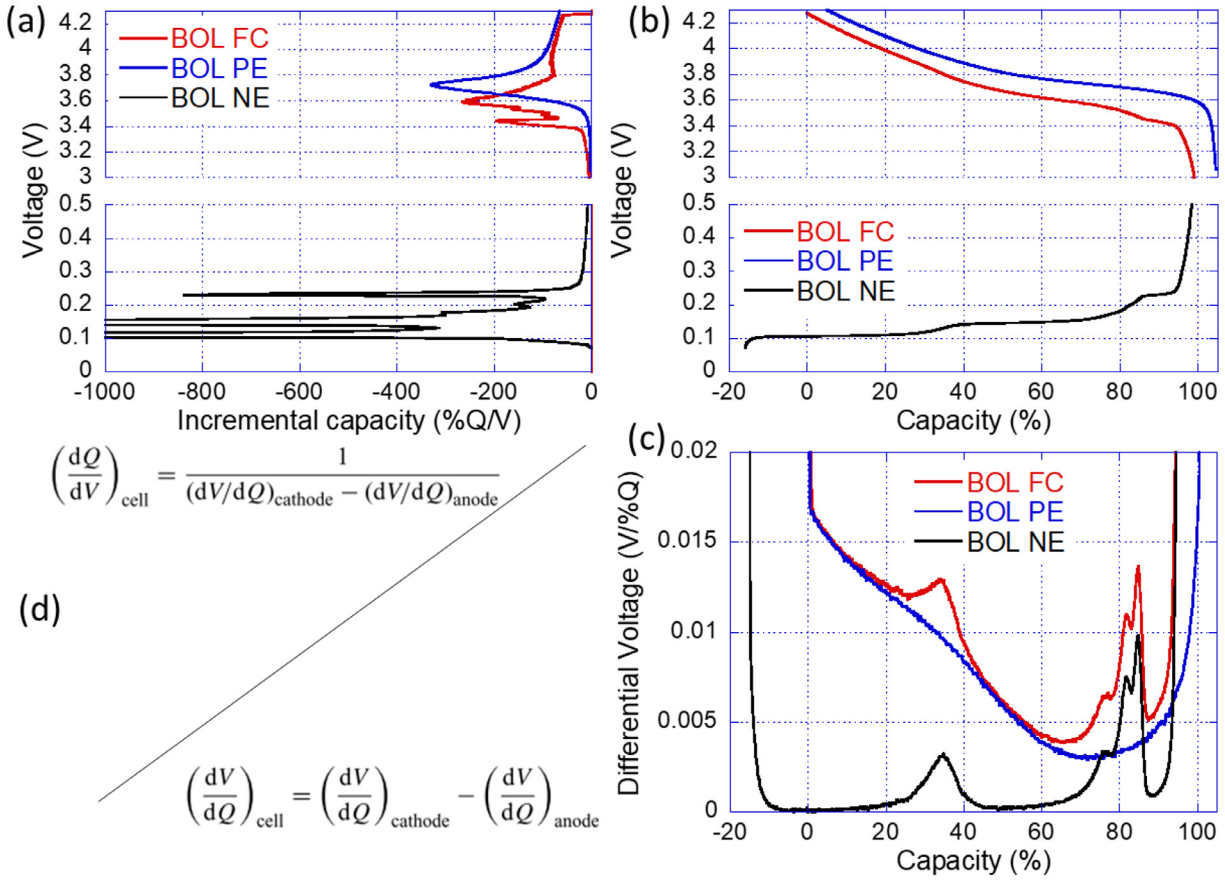

Fig. 8. Half-cell/full-cell relationship under representations (a) IC, (b) V vs. Q and (c) DV and (d) associated equations. BOL stands for beginning of life. Individual electrode data were measured versus metallic Li. The capacity differences between the FC, NE and PE were induced by the usual excess of NE in Li-ion batteries as well as the capacity loss associated with the solid electrolyte interphase formation.

– When analysing data far from equilibrium, i.e. at medium to high rates, IC curves may be a better alternative because the changes of resistance can be visualised and quantified. This is not the case for the DV curves. Indeed, a change of resistance will induce a dV but no dQ. Therefore, for IC, the associated dQ/dV will effectively shift the cell response towards lower/higher potentials during a discharge/charge regime. For DV curves, the dV/dQ for that capacity will be 0; therefore, no changes will be induced and some other characterisation tests will be necessary to quantify the changes in ohmic resistance.

4.2. Application of EVS for qualitative degradation characterisation

Analysing the variations of IC and DV curves with ageing can be a daunting task and might not be necessary for all studies. Some relevant qualitative information can be gathered by simply plotting the curves. From the literature, there are two examples where it proves especially useful and where the IC or DV curves shall be reported; they are summarised in Fig. 9. The first example concerns studies where several hypothetic different duty cycles are compared (e.g. A, B, and C on Fig. 9(a)). Duty cycles could differ in term of temperature, intensity, depth of discharge or any other parameter. In most cases, authors would conclude that A and B degraded the cell at the same rate and that C accelerated the aging by a factor of 2. This conclusion cannot be made from the capacity vs. cycle curve alone because that only shows that the rate of capacity loss is similar or accelerated. The rate of capacity loss and degradation are two different things and should not be confused. Different degradation mechanisms can lead to the same apparent capacity loss, and degradation can also occur without capacity loss [170,203]. IC curves can be plotted and compared to reach a stronger conclusion (Fig. 9(b) and (c)). If these curves are similar, then the degradation is the same; if not, the degradation is different. The second example is often seen in the literature and concerns modelling. In many studies, authors compare the experimental and simulated data on a voltage vs. capacity curve while claiming that they are overlapping quite well, and thus that the electrochemical behaviour of the cell was replicated (Fig. 9(d)). As discussed above, the V vs. Q curves lack the resolution needed to make these claims, and the IC or DV curves must be plotted to provide a better comparison of the modelled and experimental curves. If all peaks match, the electrochemical behaviour has indeed been replicated. If not, the model cannot claim replication (Fig. 9(e)). A good example of how an IC curve can help validate a model is provided in [204].

4.3. Application of EVS for quantitative degradation characterisation

In the above section, EVS was used as a qualitative tool to compare results. Some additional analysis is necessary to gather more quantitative information, and the different degradation modes need to be assessed. It is well known that Li-ion cell degradation is complex and that many degradation mechanisms can occur throughout the life of a cell depending on the operating conditions. An abundance of literature describes these mechanisms [32,42,63–65,67–69]. Quantifying all of these degradation mechanisms individually requires a plethora of tests and likely some significant post-mortem analyses [9]. EVS methods cannot deliver such accu-

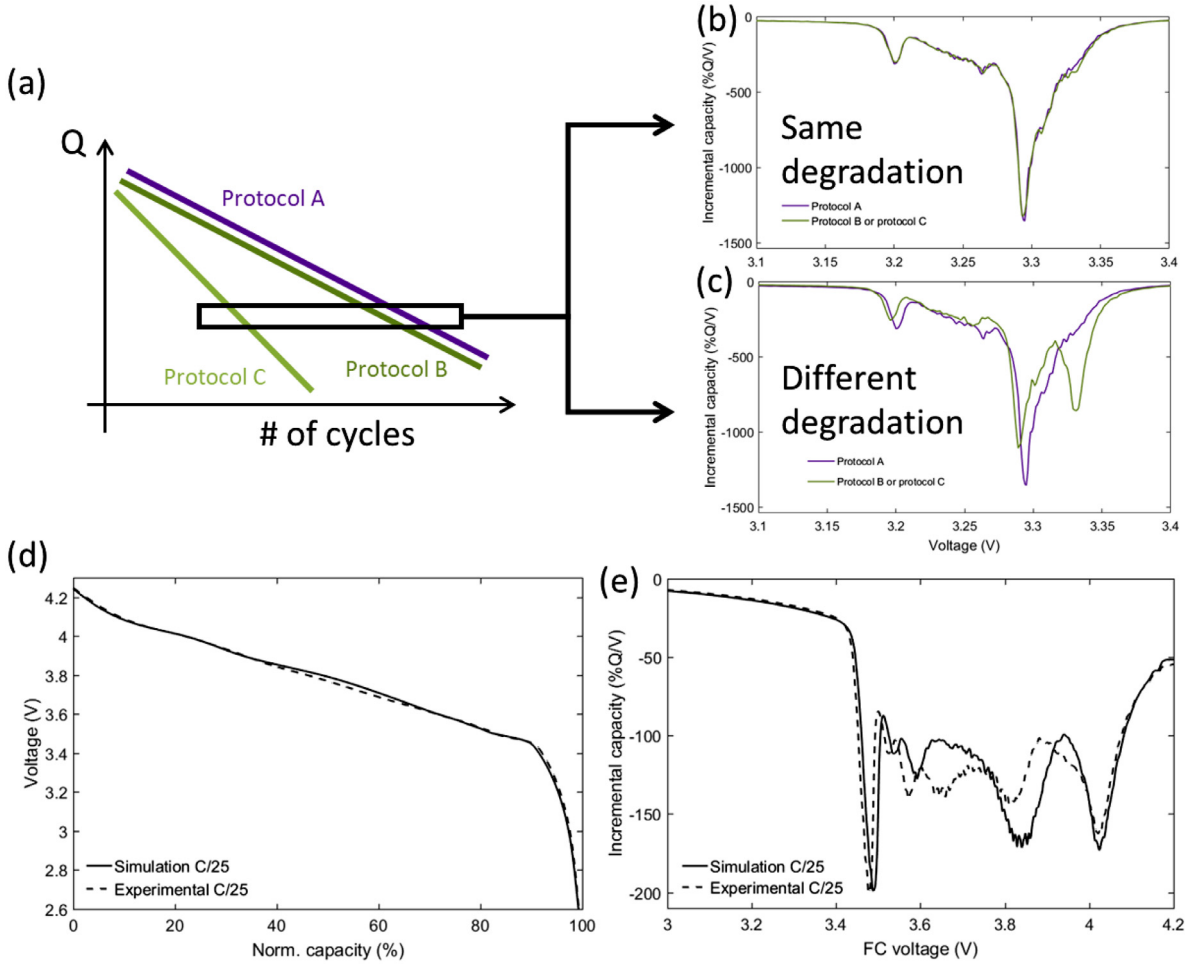

Fig. 9. Example of qualitative application of EVS for (a) accelerated aging and (d) modeling. Protocols A, B, and C are different hypothetic protocols (i.e. different currents, temperatures, SoC ranges…). Voltage curves were simulated using the 'Alawa model [96] with graphite NEs and LFP PEs for (a–c) and $LiMn_2O_4$ PEs for (d–e).

racy and details to compare with these tests, but they can be used to gather information on degradation modes. As Dubarry et al. explained in [96,170], all degradation mechanisms can be classified into one or several of three categories or degradation modes depending on how they affect cell electrochemical behaviour. Some degradation mechanisms affect the amount of active material available for reaction (e.g. dissolution or grain isolation) and thus can be classified as LAM. Some degradation mechanisms consume Li ions from parasitic reactions (e.g. SEI layer growth and inactive species precipitation) and thus can be classified as LLI. Lastly, some degradation mechanisms change the ohmic resistance of a cell (e.g. corrosion of the current collectors) and alter the kinetics of the cell (e.g. growth of passivation layers). These three degradation modes change the balance between the PE and the NE (which may lead to further LAM [205]) and can be quantified using EVS. Bloom et al. [79,166,167] explained how to interpret DV changes and relate them to the different degradation modes. In the DV representation, the signature of the PE and the NE are added to give the FC signature. In the case of LLI, the electrode signatures are not altered but the overall range of usage decreases [206]. In the case of LAM, the affected electrode signature is contracted compared to the other. Changes of resistance are not visible in the DV representation because they do not involve any change of capacity [79,96,207].

Dubarry et al. attempted the same classification for IC curves [81,96,170] by considering a Li-ion cell as a communicating vessel problem (Fig. 10(a)). They realised, with the clepsydra analogy, that the shape of the vessel of a water tank corresponds to the IC curves of the PE and NE and that the voltage of a cell corresponds to the different liquid levels in both vessels. In this analogy, the liquid corresponds to capacity. By changing the size or shape of each vessel or the volume of liquid in each vessel independently, the impact of all three degradation modes can be replicated [96,170]. In the case of a LAM on the PE, the PE vessel becomes smaller than the NE vessel (Fig. 10(b)), but the voltage of all the peaks on the PE IC curves remain the same. This is because the OCV of the PE does not change, and therefore the voltage of all the peaks does not change. Since the volume of the PE becomes smaller, the same amount of liquid (capacity) inside is going to reach a higher level and thus a higher voltage. This will change how the voltage (the difference in liquid level of both vessels) is fluctuating with time. The change of voltage with a LAM can therefore be predicted from the vessel volume change and how it affects its contents. LLI corresponds to a leak in the clepsydra, both NE and PE remain unchanged but some liquid (capacity) is missing. Therefore, for the same starting point, the level of liquid in the NE is lower than it was initially as shown in Fig. 10(c) and will change the voltage as the lower vessel is filled with liquid. Changes in resistance do not influence the balance of the electrodes but do affect their voltage, and thus the vessels become closer in discharge and farther away from each other in charge as shown in Fig. 10(d). The final degradation mode, an increase of the faradaic resistance as shown in Fig. 10(e), can be represented as a stretch of the affected vessel because changes of kinetics are known to broaden the electrochemical peaks while maintaining the same area [208].

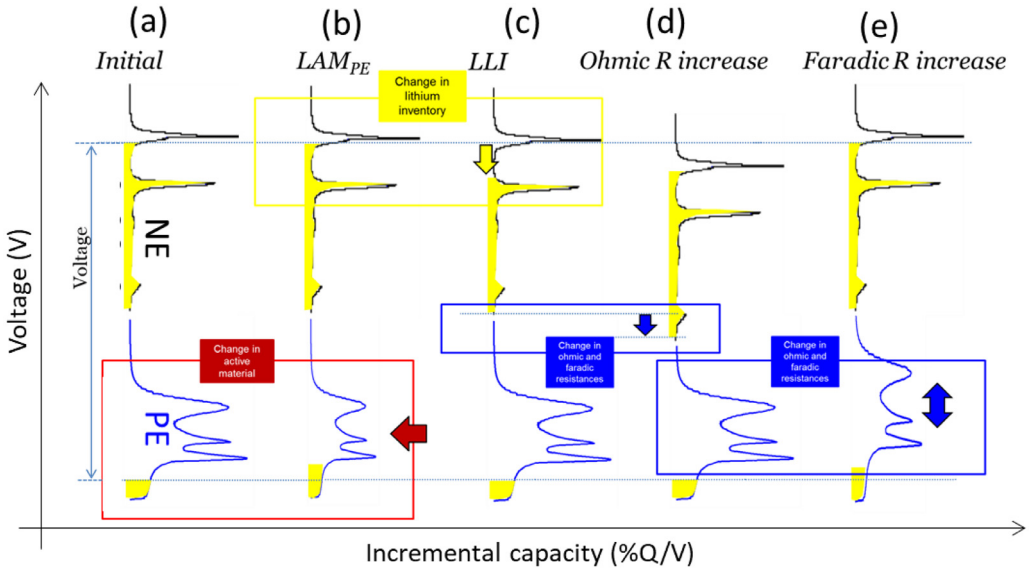

Fig. 10. Illustration of clepsydra analogy for (a) pristine cell, and cells that underwent (b) LAM on PE, (c) LLI, (d) ohmic resistance increase and (e) faradic resistance increase. Arrows exemplify the changes in the electrode IC signature, i.e. compression (horizontal arrow), shift (vertical arrow) or stretch (up-down arrow).

Experimental validation supporting both approaches (DV and IC curves) for quantification of LLI and LAM degradation modes has been reported by several groups [65,209,210]. In some more complex cases [211], the active material can gradually change to another electrochemically active phase with a different OCV. This can be mitigated by considering composite electrodes with both the initial and final phases while gradually changing the composition of the electrodes with cycling.

Based on these observations, the experimental variations of DV and IC curves were analysed and associated with different degradation modes.

4.4. Application of EVS for modelling performance

Although it is possible to analyse the changes in DV and IC curves 'by hand', the quantification is extremely time consuming. To resolve this issue, several groups proposed to use experimental half-cell data and fitting techniques to compose DV curves [79,212–216]. In 2012, both Dahn et al. (DVAP) [207] and Dubarry et al. ('Alawa) [96,217] proposed freeware tool boxes to simplify the analysis. The toolbox of Dahn et al. focused on DV and low-rate curves. The toolbox of Dubarry et al. was more general and calculated DV and IC curves, among others, and could be used at different rates. Following these publications, many noteworthy studies successfully used these concepts [5,15,76,210,218–233] or built new ones upon the proposed framework [5,65,90,234–237].

It is important to the point out that many studies showed that the change in IC and DV peaks were electrode specific and that it is not recommended to extrapolate peak movements and their association with a particular degradation mode from chemistry to chemistry. Examples of degradation tables (i.e. variations of IC or DV curves for individual degradation modes) for graphite intercalation compound (GIC)/LFP (IC and DV) [96], GIC/NCA (IC) [238], GIC/NMC (IC) [219] and $Li_4Ti_5O_{12}$/NMC (IC) [106] cells can be found in the literature.

Pushing towards more automated analysis, some groups proposed methodologies to automatically analyse IC or DV curves for either a large test matrix or BMS applications. Among the proposed methodologies were full fits of the full-cell data [5,232,239–244], partial fits [245,246] and peak tracking [227,232,240,247–252]. Although all of these methods are promising, most authors only considered one degradation path to validate their results. Dubarry et al. [251] showed that peak tracking methods might be far from accurate for all possible degradation modes. They recommended using the information of several features of interest in an nD-space to improve the universality of diagnosis.

4.5. Other EVS techniques

Over the years, other EVS have been proposed in the literature. Smith and Dahn studied the derivatives of IC techniques [253] and Goh at al. [232] the derivatives of DV curves. Some researchers used a distribution function [254,255] or force [256]. More recently, Merla et al. proposed differential thermal voltammetry [257,258] as a new tool to study Li-ion cell degradation. However, these techniques are still in the very early stages and need to be developed further, and more evidence of the advantages offered are required before they can be widely accepted.

4.6. Discussion and future direction

EVS techniques for the analysis of full-cell degradation are only a decade old, but their accuracy and the amount of information which can be deciphered have been demonstrated multiple times. They now appear indispensable for diagnosis studies. They provide nearly analogous information to post-mortem analysis to analyse operando degradation rather than having several cells performing the same function to be able to remove cells periodically for analysis. Moreover, EVS only requires the voltage response of a cell under constant current, so it does not rely on additional equipment or complex protocols and therefore is easy to implement in any study and is potentially embeddable in BMSs.

The analysis of data is still very complex, and more and more studies are trying to automate it. Ultimately, these techniques can be incorporated in BMSs to monitor the SoH of large battery packs. A word of caution from [251] is to ensure that whatever technique is used to automate analysis, a proper sensitivity analysis must be performed beforehand so that all the different degradation paths are tested.

5. Internal impedance/resistance tests

The power capability of a cell is intrinsically related to its impedance characteristics. In simplistic form, the impedance is the voltage drop of a cell under a given current, which depends on the frequency and duration of the applied current. The impedance will depend on the condition of a cell because a cell is an electrochemical system, namely, the SoC through the over-potential of the paired electrode system [259], temperature through electrochemical kinetics highlighted by the Butler–Volmer reaction rate equation [260], current magnitude through diffusion limitation effects [261,262] and ageing history through degradation of the internal cell structure, SEI and parasitic reactions [32,263].

The real part of complex impedance (i.e. the resistive part) is directly responsible for the dissipative heat generation within a cell [38] and thus the temperature rise of a cell while it is being used. The resistive values of impedance have different contributions arising from pure ohmic resistance, charge transfer resistance and entropy change [264–269]. Therefore, the design of a battery pack cooling/heating system is dependent on the cell impedance.

There are three techniques used for measuring cell impedance, two well established and one relatively recent, i.e. pulse power test, EIS test and pulsed multisine signal test. These techniques are discussed in detail in the following section.

5.1. Pulse power tests

5.1.1. Pulse power test procedure

The technique proposed by USABC [270], known as hybrid pulse power characterisation (HPPC) has been widely adopted in the literature [22,24,26,46,111,271] and involves measuring the voltage drop (ΔV) resulting from a square-wave current load (ΔI) applied to a cell. The resistance (R_{pulse}) is then typically defined as the ratio ($\Delta V/\Delta I$) and involves contributions from: (i) ohmic resistance, R_0, which comprises all electronic resistances of the cell [114] and is typically responsible for the steep voltage drop instantaneous of applying the current pulse, (ii) charge transfer resistance, R_{CT}, which is attributed to the charge transfer reaction at the electrode/electrolyte interface and typically occurs within the first few seconds of applying the current pulse [272] and (iii) polarisation resistance, R_p, which accounts for ionic diffusion in the solid phase and is usually considered to be the rate determining step for Li-ion cells [149,273]. These resistances are in fact electrical analogues which enable a simpler intuitive understanding of the complex electrochemical processes involved. The authors want to reiterate that the R_o, R_{CT} and R_p terms are often convoluted; they cannot easily be completely separated in a simple form as shown in Fig. 11. The ratio of R_o, R_{CT} and R_p strongly depends on the cell design. For example, R_o is expected to be lower for high-power capability cell design compared to high-energy capability cell design, even when both designs share the same Li-ion battery chemistry.

In Fig. 11, a general square-wave discharge current load with the associated voltage response is shown. As depicted, the voltage response ΔV, which is the entire voltage drop caused by the current load, does not differentiate between the processes that contributed to it, and therefore, R_{pulse} is a bulk parameter that includes multiple dynamics. Moreover, R_{pulse} is sensitive to the length of the pulse (i.e. time). As reported by Schweiger et al. [274], the resistance $R_{pulse}|_{1C\ 10\ second}$ after 10 s is 11 mΩ, while for the same cell, the resistance after 18 s $R_{pulse}|_{1C\ 18\ second}$ is 14 mΩ. This is because for a pulse magnitude of 1C for 18 s, the cell may have reached its diffusion limitation.

The aim of pulse tests is to estimate the resistance of a cell at a given temperature, SoC and ageing state. For long-duration current pulses, the cell enters a regime of solid-state diffusion where the surface concentration of Li on active mass particles changes.

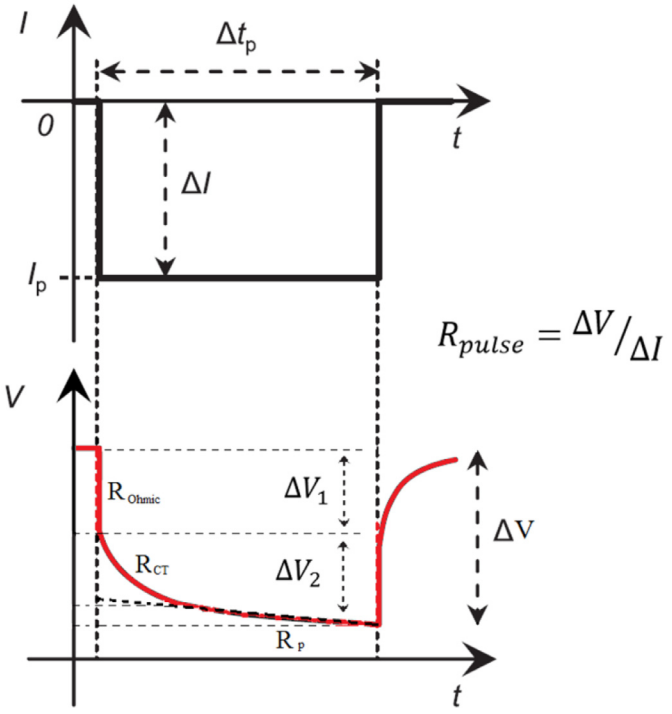

Fig. 11. Schematic of voltage response to current square-wave current load. Portions of the voltage curve resulting from ohmic resistance ($\boldsymbol{R_0}$), charge transfer resistance ($\boldsymbol{R_{CT}}$) and polarisation resistance ($\boldsymbol{R_p}$) are indicated.

This change in surface stoichiometry causes the open circuit potential to change and therefore, in such regimes, it is not possible to strictly attribute R_{pulse} to a single SoC. This was investigated in detail by DuBeshter et al. [275,276] who showed that this effect is much more pronounced for long pulse lengths, high C-rates and low SoCs such as 10% SoC. In line with the results of this work, similar issues are expected at mid-SoC points where a peak in the IC curve exists. However, since the voltage gradient resulting from solid-state diffusion is small, the standard technique of taking the ratio $\Delta V/\Delta I$ [26] is a good approximation, considering that short pulse lengths are used and high C-rates and low SoC points are avoided. For charge current pulse, voltage response will be inverted compared to Fig. 11; however, the above discussion stands, with the exception of a high SoC, e.g. 95% SoC, instead of a low SoC, the R_{pulse} measured from long pulse duration and/or high current cannot be assigned to a single SoC.

Waag et al. [272] attempted to decouple the ohmic and charge transfer contributions to R_{pulse} by linearly interpolating the voltage between 5 and 10 s of a 10 s pulse back to the start of the current pulse. They then defined a direct current voltage drop (ΔV_{DCR}) as the voltage difference between the starting voltage and the voltage interpolated to the start; the direct current resistance was then defined as the ratio $R_{DCR} \equiv \Delta V_{DCR}/\Delta I$. While the predicted resistance between the two methods differed slightly, the choice of interpolation method in the technique of Waag et al. was arbitrary and had little scientific support. Indeed, 10-s [23] and 18-s [23] pulse lengths have little scientific motivation; nevertheless, they are widely adopted in practice [5,26,277].

In general, the resistance in the low SoC region is higher because of the lower number of available Li sites in the cathode as the cell approaches either extremes of SoC as shown in Fig. 12. Resistance also increases at high SoC [278,279], especially when measured with charge current pulse, however, not to the same extent as at a low SoC [279]. Although cell behaviour is typically non-linear in extreme SoC regions, pulse power tests have tradition-

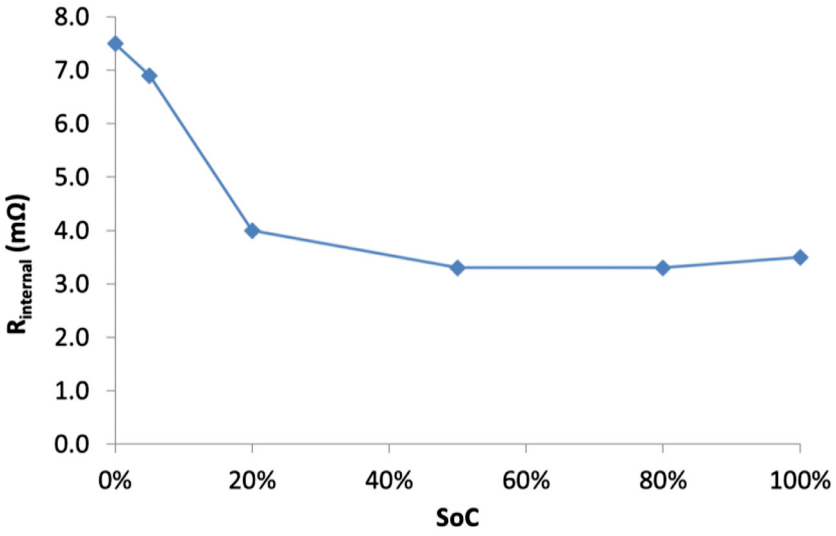

Fig. 12. Internal resistance of 20 Ah NCM pouch cell measured at 25 °C employing discharge pulse current as reported in [19].

ally considered 20%, 50%, and 80% SoC as promoted by the current standards [22,23]. However, valuable information on cell dynamics can be gained by taking pulse measurements at lower and higher SoC points. This is limited at low SoCs and high SoCs by discharge and charge pulses, respectively, which are unable to complete because of the maximum and minimum voltage restrictions on a cell. In those extremes, other techniques such as the tracing of the constant voltage phase during charge as explained by Eddahech et al. [280] can be employed. For the automotive industry investigating these extremes, it is useful for determining the capabilities of cells.

In a system which departs from ohmic behaviour, the resistance R_{pulse} can vary with current load. To account for such non-linearity, testing procedures such as Refs. [22,23,26] suggest multiple pulses spanning various loading currents at the same SoC. The IEC 62,660–1 standard [22] pre-defines pulse magnitudes to be C/3, 1C, 2C, 5C, and maximum C for electric vehicle applications. However, such a method may exceed the operational safety limits of a cell (at a particular SoC and temperature) and therefore provides results that are outside of the usable scope of a cell [274].

5.1.2. Application of pulse power tests for modelling

Internal resistance is a key parameter for various cell models, from simple empirical cell performance models to complex forms of ECMs [17]. The PNGV cooperative research programme, through the Idaho National Engineering and Environmental Laboratory, first popularised the linear lumped parameter equivalent circuit cell model [281] for offline system modelling and analysis. Subsequent publications from the programme presented methods for estimating the parameters of the model from HPPC test data [282]. Extensions of this class of model for real-time and online applications include the work of Sun et al. [283] who employed pulse power tests to parameterise an ECM used to estimate in real time the peak power of a cell. The model achieved an accuracy of 2%. Use of pulse power tests for the development of SoC estimation models is also well documented in the literature; examples include the work of He et al. [277] and Tang et al. [140]. Both studies show how internal resistance values measured from pulse power tests can be utilised to generate SoC and state of energy estimation algorithms. Pulse power tests are also commonly used to validate newly developed performance models [263]. Hu et al. [149] employed HPPC tests at 10 °C, 22 °C and 35 °C to perform a comparative study of 12 different ECMs of Li-ion cells proposed by other researchers. Considering model complexity and accuracy, they suggested a first-order RC model (model with one parallel RC branch) was best suited for an NMC cell and a first-order RC model with one-state hysteresis for an LFP cell.

Pulse power tests have also been used to develop, parameterise and validate cell thermal models [284–287]. Ye et al. [287] parametrised their thermal model via pulse power characterisation test results at various temperatures (0 °C, 10 °C, 25 °C, and 55 °C). Employing the results of pulse power tests, they concluded that reversible (entropic) heat generation is dominant during low-rate discharge, while at high rates, irreversible Joule heating dominates. In control applications, thermal management systems typically couple electrical performance models with thermal models as performed by Nieto et al. [288]. In such cases, the electrical model defines the heat generation which then acts as an input to the thermal model. It is noteworthy that an application boundary exists beyond which pulse power tests are not suitable for model development and parameterisation. In these cases, other internal resistance measurement techniques and dynamic profiles to measure resistance may need to be employed.

5.1.3. Application of pulse power tests for characterising degradation

Degradation is quantified by engineers through capacity loss and resistance rise. This is inherently limited as will be discussed in later sections. Still, in this classical quantification approach, internal resistance is often estimated via pulse power tests [13,14,289,290]. The rise in resistance owing to cycling [13,78] as well as storage [14] was characterised through pulse power tests. These tests combined the effect of various degradation mechanisms and it was next to impossible to de-convolute. As argued in [42], understanding the precise nature of the resistance rise may provide an avenue for avoiding degradation through effective management and control. In [291], the authors showed that prognostics models which were able to accurately estimate battery SoH can be used by intelligent virtual power plants participating in vehicle-to-grid operations to reduce electric vehicle battery degradation by up to 9%.

When employed with other characterisation techniques, pulse power tests can provide complementary data which are useful for the development and validation of ageing models [291,292]. For this, a matrix of tests at various temperatures and SoCs at periodic times is useful.

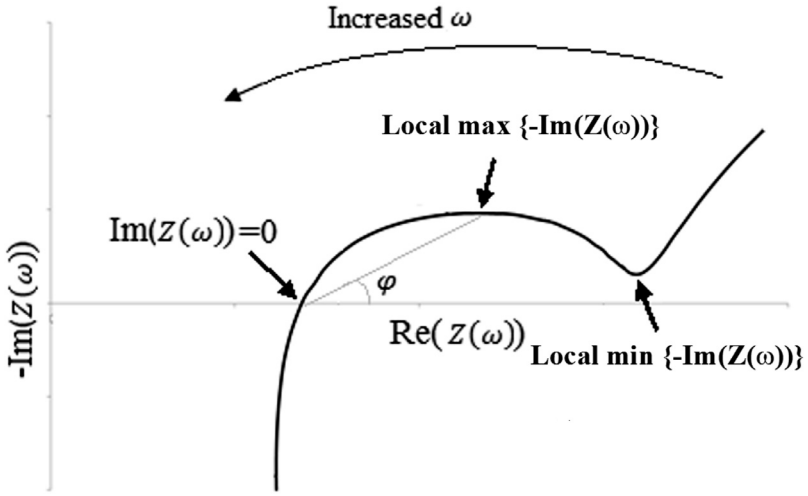

Fig. 13. Typical Nyquist plot representing the impedance spectrum of a Li-ion cell (3 Ah NCA 18,650). Indicated are a number of characteristic points that define the dynamic behaviour of a cell.

5.2. Electrochemical impedance spectroscopy test

5.2.1. Test procedures

EIS is a relatively specialised but widely applied technique employed to investigate the fundamental electrochemical dynamics which occur at various timescales within a cell. A large number of studies have documented static operational conditions and temperature as variables that affect cell impedance.

Electrochemical impedance measurements are usually obtained by applying a small sinusoidal potential to an electrochemical cell and measuring the current response through the cell (potentiostatic measurement). Conversely, a sinusoidal current may be applied and the subsequent potential response measured (galvanostatic measurement). In an ideal case, both yield the same result. In a linear or pseudo-linear system, the current response to a sinusoidal potential is a sinusoid at the same frequency (ω) but shifted in phase (ϕ) and with a different amplitude. In a pseudo-linear system, the impedance of the cell is calculated as

$$V(\omega) = V_o(\omega)e^{j\varphi_2(\omega)} \tag{5}$$

$$I(\omega) = I_o(\omega)e^{j\varphi_1(\omega)} \tag{6}$$

$$Z(\omega) = \frac{V(\omega)}{I(\omega)}\frac{V_o e^{j\varphi_2}}{I_o e^{j\varphi_1}} = Z_0{}^{j(\varphi_2-\varphi_1)}. = Z_0(\cos(\varphi) + i\cdot sin(\varphi)) \tag{7}$$

where $\phi = \phi_2 - \phi_1$. In EIS, $Z(\omega)$ is measured over a range of frequencies, commonly between 10 kHz and 10 MHz [118,270,291], the lower limit being defined by the limits of testing time and the upper limit governed by the capture of inductive behaviour (i.e. $Im(Z(\omega)) > 0$). In addition, lower and upper limits are directly linked to the accuracy of the test equipment. The accuracy of a state-of-the-art EIS system can be in the μV and pA range; however, this accuracy reduces with increases in frequency, especially beyond 1 kHz. For lower frequencies, a different source of error exists; the voltage response needs to be purely owing to the current signal. However, at low frequencies, the battery voltage may change within a measurement cycle even though a small current is used; this is dominated by the length of the cycle. For example, at 1 MHz, the current signal will be applied for 1000 s to measure a full cycle even with a small current because the duration voltage may change; therefore, at a low frequency, the accuracy of the EIS measurement will be reduced. The expression for $|Z(\omega)|$ is composed of real and imaginary parts which can be used to characterise a cell and is typically depicted by a Nyquist plot (see Fig. 13) which plots the real part of $|Z(\omega)|$ on the x-axis against the negative imaginary part of $|Z(\omega)|$ on the y-axis of the chart for all frequency points.

The Nyquist plot as shown in Fig. 13 can be used to characterise the dynamic behaviour of a cell [294,295], develop cell models [296,297], parameterise cell models [298,299] and identify degradation mechanisms [300,301]. This is discussed in the following sections.

5.2.2. Impedance tests for characterising electrochemical dynamics

The impedance spectrum depicted in Fig. 13 has some points which are typically used to characterise a cell. At the point $Im(Z(\omega)) = 0$, the cell changes from a capacitive to an inductive behaviour. At this transition point, both capacitive and inductive behaviours are balanced and an almost pure ohmic resistance (R_0) is observed [272]. As a simple estimation, the difference between $Re(Z(\omega))$ at $\min\{-Im(Z(\omega))\}$ and R_0 is commonly assigned to the charge transfer resistance R_{CT}, which may not be a true representation. The frequency at which $-Im(Z(\omega))$ has a local maximum corresponds to the 1/RC characteristic frequency; the lower this frequency, the slower the voltage will change with fast current changes [272]. According to previous studies [72], cycling a cell at frequencies lower than the 1/RC characteristic frequency will cause the cell to degrade through increased intercalation and de-intercalation reactions, which indicates the importance of cell selection for a particular application.

It has been argued that R_0 and R_{CT} estimated by EIS may differ from that measured using pulse tests. According to current understandings [272,302], this is because under large current loads the cell, which is a complex electrochemical system, exhibits non-linear properties (non-linear Butler–Volmer kinetics). With small current perturbations, however, the system behaves in a linear way, and the linear approximation employed to interpret EIS results hold well. It is worth highlighting that in the recent work of Barai et al. [47], the authors showed that, contrary to the current loads suggested by researchers, the timescales (harmonic content) associated with the applied current govern the apparent difference in measured internal resistance.

In many high-power applications like motorsports and hybrid powertrain battery packs, there are large power demands. In such applications, fast transient response to power demands is crucial. Therefore, R_0 and R_{CT} of the battery cells within the pack are required to be closely matched for optimum performance. In such

cases, EIS testing offers a fast and accurate method for deconvoluting these parameters and can be pivotal.

5.2.2.1. Application of EIS for estimating cell temperature. Recently researchers have attempted to employ EIS to measure the internal temperature of cells. In 2014, Raijmaker et al. [303] proposed that the frequency of the point where the Nyquist plot crosses the x-axis is related to the temperature of a cell. They showed that the frequency changed from 1600 Hz to 250 Hz when the temperature changed from −20 °C to 50 °C. This trend persisted for 20%–100% of SoC. A similar technique was studied earlier by Schmidt et al. [304] and Srinivasan et al. [305]. Adopting a selection of frequency points, Schmidt et al. investigated the internal temperature of a cell and how measurement was affected by the SoC. As reported, the internal temperature was measured with an accuracy of ± 0.17 K when the SoC was known and ± 2.5 K when the SoC was unknown. Srinivasan et al. employed a similar technique but used phase shift as an analogue of temperature change. They studied three types of commercial cells of capacity 53 Ah, 2.3 Ah and 2.5 Ah and reported a 0%–20° shift owing to a temperature change from 50 °C to −20 °C of a 40-Hz sine-wave current signal; the phase shift was affected by 1° with an SoC change from 5% to 95%. Therefore, a very accurate estimation of internal temperature can be achieved when an accurate SoC is known; however, a crude estimation is also possible without knowing the SoC as reported by Schmidt et al. [304]. A more recent study by Zhu et al. [306] and Beelen et al. [307] provided more evidence of measuring internal temperature using EIS. Zhu et al. developed a look-up-table-based methodology where phase shift and impedance changes were both considered at a particular frequency to translate the internal temperature.

However, until now, only the effect of SoC variation on the measurement accuracy has been investigated. There are several other sources which can contribute to the change of frequency point and phase angle such as ageing, cell relaxation. An obvious change of frequency, and thus phase angle, with ageing can be found in the data reported in literature [14,129]. In addition, under load conditions, a temperature gradient across a cell surface exists [28,35], pointing to the fact that the temperature measured in this method might be an average value when the actual temperature might be higher or lower. Further research in this area is essential before this application of EIS can be reliably implemented.

5.2.3. Application of EIS for modelling performance

The Nyquist plot of Fig. 13 depicts a typical new cell at a high SoC. Commercial cells usually go through formation cycles at the end of the manufacturing process and therefore should have an SEI layer formed. For new cells at a high SoC, the semicircles of the SEI and double layer are likely combined as one semicircle. If an EIS test is performed at a low SoC (< 10% SoC), a second semicircle will be more pronounced [308] because the capacitance and resistance related to the SEI are not expected to change as much as the double-layer capacitance and charge transfer resistance with a change in the SoC. In addition, as a cell ages, the SEI layer will grow and become progressively more pronounced at higher SoCs with ageing [158]. Therefore, in a Nyquist plot, the second semicircle at higher frequencies will progressively become more distinct at higher SoCs. In that case, decoupling the contributions of R_0, R_{SEI} and R_{CT} become more convoluted. As proposed by Andre et al. [263], ideally, a second-order ECM as shown in Fig. 14 was fitted to the EIS data to extract the ECM parameters of a cell. The first parallel branches (CPE1, R_{SEI}) are attributed to the SEI, while the second (CPE2, R_{CT}) correspond to the charge transfer and the Warburg impedance W represents the finite diffusion [309]. Complex ECMs have been proposed previously to represent individual physical processes within a cell [310,311]; however, the simplified ECM shown in Fig. 14 is commonly employed. To reiterate, no ECM should be justified by a good fit without direct relation to the physical processes.

The capacitor in an equivalent circuit is often replaced with a constant phase element (CPE) component (as in Fig. 14) as it better describes the inhomogeneity of an electrode surface such as roughness and porosity [312–314]. The electrodes of Li-ion cells are made up of fine microscopic particles of active materials. The thickness of the active material varies and makes the electrode surface rough. Therefore, the intercalation and de-intercalation of Li is not uniform across an electrode surface. This leads to different reaction resistance and capacitance contributions from different sections of the electrode. Overall, a cell's capacitive behaviour deviates from that of a pure capacitive one, which is represented by the CPE. The impedance of a CPE is represented by

$$Z_{CPE} = 1/Q^{o}(j\omega)^{n} \tag{8}$$

where Q^o is the admittance, $\omega = 2\pi f$ and value of n varies from 0 to 1. When $n = 0$, the CPE represents a resistor; for $n = 1$ a capacitor and for $n = 0.5$ a Warburg impedance [312,315].

Higher-order models have been proposed to separate the contribution of individual electrodes [293,296]. However, the reliable separation of these contributions in a commercial cell is still an open question. Nevertheless, a second-order model provides good approximation of the electrochemical mechanisms within the cell and is commonly employed in literature. As an example, Buller et al. [297] developed ECMs based on EIS results for their simulation work. They validated their ECM-based model using a pulse-current profile which showed good agreement between measured data and model estimation. Andre et al. [263] proposed an ideal ECM of a Li-ion cell based on the Nyquist plots generated from EIS test results. They proposed a methodology for ECM parameter estimation from the Nyquist plot of a real battery cell. Based on the results, they proposed models to estimate cell voltage depending on the current, SoC and temperature of a cell. Their models were validated using current profiles to provide evidence that accurate cell voltage prediction can be achieved for highly dynamic automotive applications even at low temperatures.

5.2.3.1. Application of EIS for SoC estimation. As presented in Fig. 12, cell impedance measured by pulse current varies with the SoC, which is also the case for EIS. Therefore, researchers have investigated the use of on-board EIS to estimate the SoC of battery packs. One of the early attempts was made by Rodrigues et al. [312]. They reported that low frequency data from an EIS test is suitable for prediction of the SoC of a cell. In a similar study, Sauvant-Moynot et al. [316] attempted to employ EIS as a diagnostic tool to measure the SoC of a cell. From the measurements on a three-electrode cell, they found that low frequency results could be used for SoC measurement. However, recent studies by Barai et al. [118,317] and Kindermann et al. [119] showed the potential risk of on-board EIS measurement; EIS measurements are not reliable when a minimum relaxation period is applied following a charge/discharge event. For a reliable measurement, ideally, cells need to reach electrochemical equilibrium. Therefore, implementation of EIS for online SoC measurement may not be viable without further research.

5.2.4. Application of EIS for characterising degradation

As a cell ages, its impedance changes. Therefore, researchers employ EIS along with other characterisation techniques to quantify ageing. Compared to other characterisation techniques such as capacity and pulse power tests, EIS can provide some insight on ageing. For example, Waag et al. [272] recently employed EIS to investigate the impedance of Li-ion cells at various ageing states. They reported SEI growth as one of the ageing mechanisms from

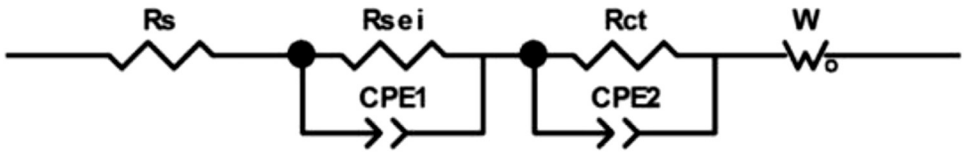

Fig. 14. Example of ECM of full cell recently used by [158,228,308] to fit EIS data originally proposed by Andre et al. [263].

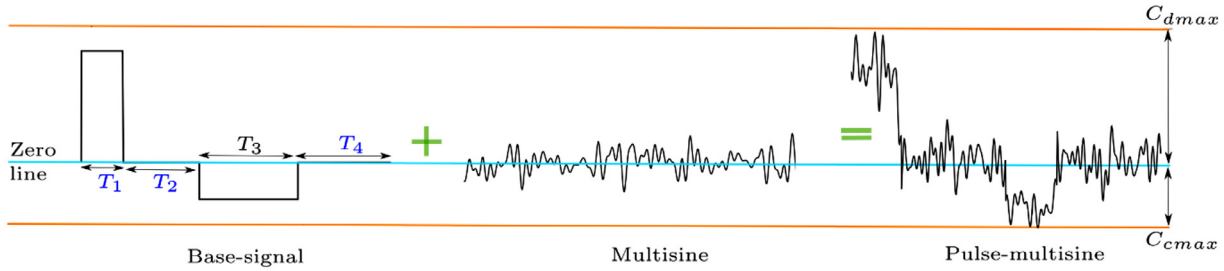

Fig. 15. Design of pulsed multisine current profile. A base signal similar to pulse power test along with multisine signal composed of a frequency of interest are superimposed to produce the final pulsed multisine current profile. Figure adapted from Widanage et al. [320].

their EIS test results. In another ageing study, Shi et al. [129] employed EIS to identify ageing mechanisms owing to the charge–discharge cycling of a cell. From the EIS results, they concluded that Li-ion diffusibility decreases with cycling, which increases the diffusion impedance. Zheng et al. [13] investigated the effect of temperature and charge–discharge rate on cycling ageing using EIS. They identified unstable SEI owing to high current which caused consumption of active Li, impedance rise and capacity fade. Similar mechanisms have been identified by EIS in other ageing studies [13,14,16,75,318]. Vetter et al. [32] reviewed the ageing mechanisms of Li-ion cells and identified EIS as a powerful tool to study cell ageing.

As impedance changes with ageing, the SoH of a cell can be measured by EIS as attempted by Galeotti et al. [308]. They developed an ECM based on a Nyquist plot to generate a model to estimate the SoH of a cell. Their model estimated the SoH of a cell within 3.73% error and within 8.66% for an anomalous cell. However, this was not the first attempt to measure SoH using EIS; previously, Love et al. [300], Kassem et al. [16] and Sauvant-Moynot et al. [316] proposed EIS-based SoH estimation of a battery cell and pack. Love et al. [300,319] showed that single-point EIS measurement is sufficient to identify the SoH of a cell. In their study using a 316-Hz signal, they successfully identified an overcharged cell from a module made of four cells in a series connection.

5.3. Pulsed multisine signal tests

5.3.1. Pulsed multisine test procedure

While EIS offers the advantage of a range of frequencies, pulse power square waves benefit from meaningful current amplitudes with the limitation that, in the frequency domain, they only contain predefined perturbations with odd-integer harmonic frequencies, f, of the form $2\pi(2k-1)f$ where $k \in \mathbb{Z}$. The pulsed multisine procedure aims to combine the advantages of multi-frequency measurements with high pulse currents as applied in pulse tests. Fig. 15 shows the basic design of a pulsed multisine profile which involves a base signal and a multisine profile. The base signal is equivalent to a pulse profile defined by maximum charge/discharge currents and pulse lengths. Superpositioned with this base signal is a multisine wave whose bandwidth and harmonic content are determined by the application. The superimposition of these two signals produced a final pulsed multisine current profile. Although the idea of multi-frequency measurements existed before the publication of [320,321], its application to characterising Li-ion cell models was novel [320,321]. In real-world automotive duty cycles, most of the harmonic content lies in the low (< 10 Hz) to mid (< 1 kHz) frequency regime, although high frequency content is present during charging and regenerative braking because of power electronics switching [66]. Therefore, the pulsed multisine method can better represent both the frequency bandwidth and the current load in applications.

The method involves two key steps: capturing a cell's voltage response to a pulsed multisine current profile, and fitting the data with an ECM to obtain the model parameters and thus the resistance parameters. The method for parameter estimation is outlined in [112].

The frequency content of a multisine current profile varies depending on the application requirement. One way to select the frequency content is by analysing the frequency content of a representative duty cycle. The discrete Fourier transform of the representative duty cycle enables the identification of the frequencies carrying most of the current. In a typical automotive duty cycle, most of the current is delivered at frequencies below 10 Hz. Further details of the design of pulsed multisine signals can be found in [320].

Like pulse and EIS tests, pulsed multisine tests are also typically performed at different SoCs and temperatures. From the voltage response, resistance (as a function of frequency) is estimated by employing an ECM. The resistance $Z(\omega)$ at a given angular frequency ω is related to the complex current and voltage signal as

$$V(\omega) = Z(\omega)I(\omega) + Measurement\ error. \tag{9}$$

The error can arise owing to the measurement error of the equipment and/or nonlinear response of the cell. To estimate the resistance $Z(\omega)$ in Eq. (9) from a known $I(\omega)$ and $V(\omega)$ requires minimising the measurement error in a least-squares sense. A method known as the local polynomial method [321] is employed to estimate the resistance $Z(\omega)$ along with its standard deviation $\sigma_Z(\omega)$. Once $Z(\omega)$ is estimated, an ECM model is fitted to obtain the internal resistance along with other dynamical parameters. A general m^{th}-order ECM can be employed to calculate the series resistance R_0 and remaining RC parameters. The resistance of this general m^{th}-order ECM is given as

$$Z_m(\omega) = R_0 + \sum_{i=1}^{m} \frac{R_i}{j\omega\tau_i + 1}. \tag{10}$$

The first term R_0 is the pure resistive resistance, and the remaining m-terms correspond to the resistance of the m RC pairs

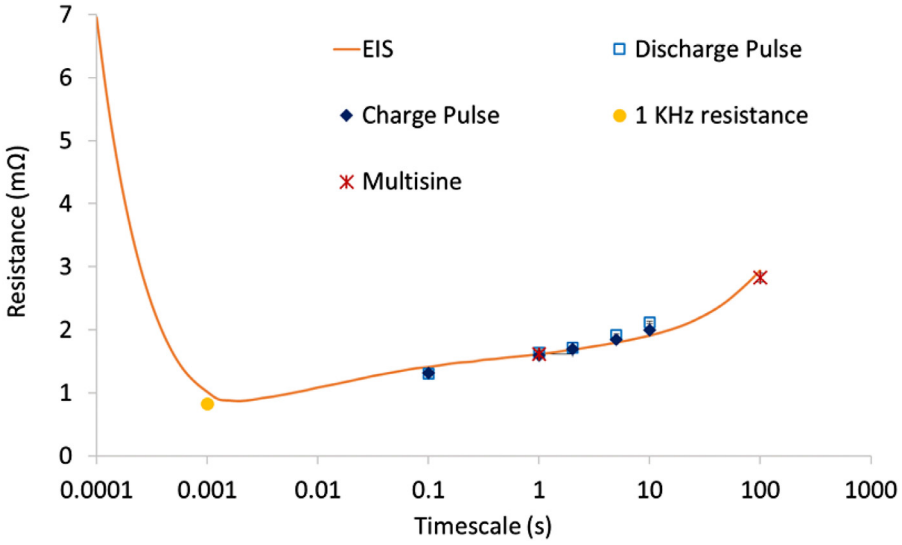

Fig. 16. Internal resistance measured by different techniques vs. measurement timescales (1/frequency) as reported in [47].

with the product R_iC_i denoting the time constant τ_i of the i^{th} RC pair. However, a second-order model as shown in Fig. 14 is usually a good trade-off between computational complexity and accuracy of the parameter estimation.

The first- and second-order ECM parameters estimated from a pulsed multisine test may not be as accurate as those of EIS; however, when an EIS test setup is not available, the multisine test provides more information than performing only a pulse power test, requires no additional equipment and only takes minutes to perform. Even, considering the complex post-processing of data involved for parameter extraction in a pulsed multisine test, the multisine technique offers better separation of the R_o, R_{CT}, and R_p components than that of a pulse test.

5.3.2. Application of pulsed multisine tests for characterisation, modelling and degradation studies

The work of Widanalage et al. [320,321] in which the pulsed multisine technique was first described is relatively new, and thus the implementation of this technique for characterisation and degradation studies is still under development. Allafi et al. [112] used pulse multisine data to validate an online scheme for parameter estimation of a nonlinear Li-ion cell EDM. The authors identified a major drawback of the pulsed multisine approach, namely, that R_0 was no longer well defined. The principal component of the driving multisine current load is $f = 1$ Hz. Thus, the analogy of the ECM components with physico-chemical subprocesses are undermined. Although the authors contend that this issue is not unique to the multisine technique, it is persistent in pulse power experiments (typically $f \leq 0.1$ Hz).

5.4. Discussion and future direction

It is often model parametrisation requirements that drive the exhaustive testing of impedance. However, as is seen with existing testing standards, the proposed test environments often avoid extremities—whether an extreme in temperature such as $T < -20\,^{\circ}C$ or an extreme in SoC such as SoC < 5% or SoC > 95%—where the behaviour of Li-ion cells are most nonlinear. This can be attributed to the assumption that such conditions do not reflect a true representation of application, specifically because BMSs are designed to avoid such extremes. With the growth of Li-ion battery adoption in grid applications, battery operations in extreme temperatures and SoCs are more readily encountered. As such, for improved model performance, more data points are required at extremities to capture the precise nature of the nonlinear behaviour.

The most widely adopted technique for estimating cell resistance is pulse power testing; the key advantage of this technique is its simplicity which promotes accessibility and the use of high currents which mimic real-world scenarios. The pulsed multisine approach is similar to pulse testing in the sense that it employs high currents; in addition, the technique attempts to capture the harmonic content of real-world usage. The motivation being, if the data used for parametrisation are more representative of real-world applications, model accuracy in real-world simulations will be more accurate. However, this technique causes the analogy of the ECM components with physico-chemical subprocesses to be undermined and as a consequence R_0 is no longer well defined. In addition, the multiple RC pairs employed in the technique lead to a problem of unique identifiability, which means that there will be an ambiguity between the model parameters identified and their actual physical values. The latter is a symptom which is persistent in any model, phenomenological, fundamental or otherwise, which employs optimisation for parameter estimation and has multiple unknown parameters.

When using the pulsed multisine technique, it is worth noting that unless researchers have access to expensive and bespoke testing equipment (such as that employed in [66]), the bandwidth will be restricted by the capability of commercial battery cyclers (EIS equipment cannot be used to generate high-current pulsed multisine signals). Current cycler capabilities are limited by their respective signal rise and fall times, and therefore there are limits on current switching (i.e. changes in input current signals). Typically, the shortest step-size varies from 0.1 s to 0.01 s. For a cycler with a 0.01 s step-size, the theoretical maximum frequency that can be achieved is 50 Hz, although the actual frequency is much lower because more than two steps are required to reliably define a single period.

Measurement of internal resistance employing a single sine wave, such as the 1 kHz impedance test, can be a viable technique in high-volume manufacturing environments where a cell's internal impedance is required to be closely matched. In such cases, however, the frequency of the single sine wave should be selected based specifically on the cell type, ideally considering the points of interest on a Nyquist plot such as R_0, R_{CT} or any other point.

EIS can be employed to estimate different cell parameters accurately. To do so, however, necessitates a sophisticated test setup

Table 1
Summary of test methods, test equipment requirements, information generated, application of information and outlook of methods.

Test method	Equipment required	Data generated	Data extracted	Test duration (h)	Factors impacting results	Application of test data	Positive aspects	Drawbacks/cautions
Capacity test ($\geq$ C/3)	Battery cyclers	Voltage drop/rise under given discharge/charge current	➢ Cell capacity (Ah) / Energy (Wh) ➢ Temperature rise	3–8	➢ Charge/discharge rate ➢ Temperature	➢ Cell performance validation ➢ Cell electrical model development and validation ➢ Cell thermal model development and validation	➢ Simplicity ➢ Relatively short test duration ➢ Use of standard battery cyclers	➢ Significant temperature rise during test influences capacity measurement ➢ Cells exposed to high overpotential, leading to degradation
Capacity test ($<$ C/3)	High-precision battery cyclers	Voltage drop/rise under given discharge/charge current	➢ Thermodynamic capacity in Ah and Wh	10–100	➢ Charge/discharge rate ➢ Temperature	➢ Electrochemical modelling ➢ ECM modelling ➢ SoC estimation ➢ Performance degradation ➢ Identification of degradation mechanisms	➢ Wide application of data ➢ $\leq$ C/10 allows EVS analysis and pseudo-OCV depending on cell type	➢ Requires high-precision battery cyclers ➢ Long test duration
GITT	Battery cycler	Voltage relaxation after short charge/discharge pulses	➢ Actual OCV vs. capacity ➢ OCV hysteresis	$>$ 100	➢ Temperature ➢ Relaxation period after charge/discharge ➢ Charge discharge rate (may affect)	➢ Electrochemical modelling ➢ ECM modelling ➢ Performance degradation ➢ Identification of degradation mechanisms	➢ Measurement of actual cell OCV ➢ Actual OCV hysteresis ➢ Use of standard battery cyclers	➢ Long test duration
Pseudo-OCV tests	High-precision battery cycler	Voltage drop/rise with very low (C/25) charge/discharge current	➢ Voltage vs. capacity ➢ Thermodynamic capacity	25–100	➢ Temperature ➢ Charge/discharge rate	➢ SoC estimation ➢ ECM modelling ➢ EVS analysis	➢ Quicker than GITT	➢ Requires high-precision battery cycler ➢ Long test duration
EVS	High-precision battery cycler	Voltage drop/rise with very low (C/25) charge/discharge current	➢ IC and DV curves	25–100	➢ Temperature ➢ Charge/discharge rate	➢ Electrochemical modelling ➢ Performance degradation ➢ Identification of degradation mechanisms	➢ Strong evidence can be generated when used with autopsy techniques ➢ Provides in-situ information of cell degradation ➢ Same data can be used for pseudo-OCV analysis	➢ Requires high-precision battery cycler ➢ Long test duration ➢ Requires specialist knowledge and analysis tools

(*continued on next page*)

Table 1 (*continued*)

Test method	Equipment required	Data generated	Data extracted	Test duration (h)	Factors impacting results	Application of test data	Positive aspects	Drawbacks/cautions
Pulse power test	Battery cycler	DC voltage response	➢ Cell internal resistance	2–12	➢ SoC ➢ Temperature	➢ Cell performance validation ➢ ECM modelling ➢ Power fade definition	➢ Simplicity ➢ Short test duration ➢ Use of standard battery cyclers	➢ Only DC resistance can be measured ➢ No separation of contributions to total resistance
EIS test	Specialised EIS equipment	Impedance as a function of frequency	➢ Cell impedance ➢ ECM model parameters	2–4	➢ SoC ➢ Temperature	➢ Generates cell impedance over a wide spectrum of frequencies ➢ Dynamic modelling ➢ Performance degradation ➢ Identification of some degradation mechanisms	➢ Strong evidence for degradation analysis ➢ Enables development of ECMs	➢ Specialised equipment required ➢ Sophisticated test setup and interconnections required
Pulsed multisine test	Battery cycler	Impedance as a function of frequency	➢ Internal impedance ➢ ECM model parameters	2–4	➢ SoC ➢ Temperature	➢ Electrochemical modelling ➢ ECM modelling ➢ Performance degradation	➢ Use of standard battery cyclers ➢ Current profiles used represent bandwidth of real-world usage	➢ Limited to lower frequency measurements ➢ Accuracy is lower than EIS ➢ Additional data processing involved

to ensure accuracy and reproducibility. It is known that the high-frequency measurements dominated by inductive behaviour can be affected by differences in the arrangement of the signal and sense cables as part of the EIS test setup [309]. The reproducibility of EIS results is also governed by the relaxation period, i.e. open circuit period after cells are charged/discharged [118,119]. In certain cases, EIS measurements can be localised as shown by Osswald et al. [322]. In such cases, rather than measuring the impedance of the entire cell, EIS measures a part of the cell. To avoid such localised measurements, attention must be given to the welding quality used to connect multiple layers (electrodes inside pouch and prismatic cells) or tabs (inside cylindrical cells) and the number of layers/tabs. Nevertheless, when EIS tests are performed correctly, it is a powerful technique for characterising Li-ion cells.

Researchers have reported the dependency of internal resistance measurements on the technique used for characterisation. This dependency is governed by the measurement timescales associated with a technique, i.e. internal resistance values measured by different techniques are different because of the measurement timescales involved [47]. Fig. 16 depicts internal resistance values measured with techniques with a range of associated measurement timescales. The internal resistance values were found to be in close agreement when measurement timescales matched [47]. However, the results reported in [47] were limited by the number of SoCs and test temperatures and therefore need to be validated for a wider range of SoC and temperature.

6. Summary

Test plans are a function of equipment and time availability, data requirements and associated drawbacks. Thus, there is no 'one-size-fits-all' test plan. Practitioners should clearly define their objectives and thus the required data, then identify which characterisation test(s) can best achieve them; this review document facilitates this process. The spectrum of non-destructive test methods which are employed for the characterisation of commercial Li-ion cells is provided below and tabulated in Table 1. This table is a summary of the equipment and time requirements of each test. It includes the types of applications for generated data and provides a cursory overview of the main benefits and drawbacks of each test.

A standard capacity test is one of, if not the most, common method of characterisation. The key driving factor for its popularity is simplicity and repeatability, equipment availability and the speed at which tests can be performed. However, high current rates can create a capacity value which is the convoluted mixture of both kinetic-induced and thermodynamic changes. When high-current tests are unavoidable, active cooling of a cell surface with strict temperature control (better than ± 1 °C) should be employed rather than performing the test within a thermal chamber which only maintains the desired room temperature and does not actively maintain the temperature of the cell. Unfortunately, there is no standard to perform this operation. On the other side of the spectrum, when low currents are used, the signal-to-noise ratio of standard commercial battery cyclers (typical accuracy of 20 mA, 5 mV) is often not sufficient, and therefore the capacity value recorded can be significantly different. Therefore, in such instances, high-precision battery cyclers, e.g. systems capable of accurately measuring current of 1 mA, a voltage of 1 mV, and an input impedance for voltage measurement higher than 100 MΩ should be employed which will subsequently increase the cost of performing this test.

The OCV and subsequent charge–discharge hysteresis measured in the GITT is particularly important to support the development of electrochemical and ECMs. It can also be employed to investigate cell degradation. Although this test can be performed with standard battery cycler equipment, the long duration (200 + hours) limits wide adoption. This leads to the use of pseudo-OCV tests which are comparatively shorter (50 + hours) and provide a larger number of data points throughout the SoC window. However, this method relies on very small currents with high accuracy, and thus the equipment costs rise considerably. In addition, even at very low currents, the voltage/SoC profiles contain a much larger charge–discharge dependency and introduce false higher levels of OCV hysteresis than those of a pure GITT test. This can introduce errors into the SoC calculations which the BMS or human analysis might make. One major advantage of the pseudo-OCV test is that the same data can be used for EVS analysis to produce IC/DV curves. In contrast, because of the limited number of data points from a GITT test, any IC/DV curve must be calculated separately and thus would increase test time and facility utilisation. As explained in Section 4, IC/DV curves are powerful non-destructive techniques to identify degradation sources and mechanisms. They provide nearly analogous information to post-mortem analysis and identify LAM and LLI.

Pulse power tests can be used to determine the DC resistance of cells. This is a relatively simple short-duration test that can be performed with standard battery cycling equipment. Although previously pure Ohmic resistance was separated from dynamic parts, typical commercial cell cyclers are usually limited to 10-Hz data acquisition, whereas much faster (> 100 Hz) data acquisition is required to capture pure Ohmic resistance. Therefore, this separation includes a high level of inaccuracy. Accurate separation can be achieved from EIS test results. EIS allows the separation of capacitive and inductive behaviour and allows for the development of an ECM and parameterisation of the model. This separation also identifies the degradation sources and the contribution of degradation from each source. This makes EIS a powerful technique; however, EIS requires specialised, high-accuracy equipment. In addition, it needs a sophisticated test setup to generate accurate test data with high reliability and reproducibility. If not performed to a high standard, EIS can produce misleading datasets. Every test engineer/researcher may not have access to the equipment and test setup required for an EIS test; therefore, the pulsed multisine test is proposed. This technique can measure impedance with low frequency and high current, and the test can be performed with standard commercial battery cyclers offering the advantages of both the EIS and pulse power technique. Compared to the pulse power technique, pulsed multisine offers an additional dataset at a cost of additional complexity of the test process and data processing. However, when compared to EIS, the accuracy is much lower and, being limited to lower frequency only, pulsed multisine cannot offer separation of all the dynamic parts of internal resistance/impedance.

From the increasing demand and use of Li-ion cells, it is expected that application-specific characterisation tests will progressively become more important for future development. We consider the test procedures reviewed in this review will be of value to the reader to develop their ideal set of characterisation tests.

Acknowledgement

The research presented within this paper is supported by the Innovate UK (https://hvm.catapult.org.uk/https://hvm.catapult.org.uk/wmg) through the WMG Centre High Value Manufacturing (HVM) Catapult in collaboration with Jaguar Land Rover. This work forms part of *A. Barai*'s PhD research programme (Improvement of consistency, accuracy and interpretation of characterisation test techniques for Li-ion battery cells for automotive application, October 2012 to November 2015) at WMG and PhD scholarship provided by the WMG, University of Warwick. K. Uddin was supported by EPSRC grants (EP/M507143/1), (EP/N001745/1), and currently by OVO Energy. M. Dubarry is

thankful for funding from the state of Hawaii as well as ONR Asia Pacific Research Initiative for Sustainable Energy Systems (APRISES), award number N00014-17-1-2206. I. Bloom gratefully acknowledges support from the U. S. Department of Energy (DOE), Office of Energy Efficiency and Renewable Energy, Vehicle Technologies Office. Argonne National Laboratory is operated for DOE Office of Science by UChicago Argonne, LLC, under contract number DE-AC02-06CH11357.

Supplementary material

Supplementary material associated with this article can be found, in the online version, at doi:10.1016/j.pecs.2019.01.001.

References

[1] Dunn B, Kamath H, Tarascon J-M. Electrical energy storage for the grid: a battery of choices. *Science* 2011;**334**(6058):928.
[2] Kalhammer FR, Kopf BM, Swan DH, Roan VP, Walsh MP. *Status and prospects for zero emissions vehicle technology*. Sacramento, California: State of California Air Resources Board; 2007.
[3] Thackeray MM, Wolverton C, Isaacs ED. Electrical energy storage for transportation-approaching the limits of, and going beyond, lithium-ion batteries. *Energy Environ Sci* 2012;**5**(7):7854–63.
[4] Manzetti S, Mariasiu F. Electric vehicle battery technologies: from present state to future systems. *Renewable Sustainable Energy Rev* 2015;**51**:1004–12.
[5] Han X, Ouyang M, Lu L, Li J, Zheng Y, Li Z. A comparative study of commercial lithium ion battery cycle life in electrical vehicle: aging mechanism identification. *J Power Sources* 2014;**251**:38–54.
[6] Mikolajczak C, Kahn M, White K, Long RT. *Lithium-ion batteries hazard and use assessment*. Massachusetts, USA: Fire Protection Research Foundation; 2011.
[7] Chung D, Elgqvist E, Santhanagopalan S. Automotive lithium-ion battery (lib) supply chain and U.S. competitiveness considerations. *U.S.D.o. Energy*. A.N. Laboratory, and N.R.E. Laboratory; 2015. Editors.
[8] Mulder G, Omar N, Pauwels S, Leemans F, Verbrugge B, De Nijs W, Van den Bossche P, Six D, Van Mierlo J. Enhanced test methods to characterise automotive battery cells. *J Power Sources* 2011;**196**(23):10079–87.
[9] Waldmann T, Iturrondobeitia A, Kasper M, Ghanbari N, Aguesse F, E B, Daniel L, Genies S, Jimenez Gordon I, Loble M, De Vito E, Wohlfahrt-Mehrens M. Review—post-mortem analysis of aged lithium-ion batteries: disassembly methodology and physico-chemical analysis techniques. *J Electrochem Soc* 2016;**163**(10):A2149–64.
[10] Lu J, Wu T, Amine K. State-of-the-art characterization techniques for advanced lithium-ion batteries. *Nature Energy* 2017;**2**(3):17011.
[11] Harks PPRML, Mulder FM, Notten PHL. In situ methods for Li-ion battery research: a review of recent developments. *J Power Sources* 2015;**288**:92–105.
[12] Tarascon JM, Armand M. Issues and challenges facing rechargeable lithium batteries. *Nature* 2001;**414**(6861):359–67.
[13] Zhang Y, Wang C-Y, Tang X. Cycling degradation of an automotive $LiFePO_4$ lithium-ion battery. *J Power Sources* 2011;**196**(3):1513–20.
[14] Ecker M, Gerschler JB, Vogel J, Käbitz S, Hust F, Dechent P, Sauer DU. Development of a lifetime prediction model for lithium-ion batteries based on extended accelerated aging test data. *J Power Sources* 2012;**215**:248–57.
[15] Han X, Ouyang M, Lu L, Li J. Cycle life of commercial lithium-ion batteries with lithium titanium oxide anodes in electric vehicles. *Energies* 2014;**7**(8):4895–909.
[16] Kassem M, Bernard J, Revel R, Pélissier S, Duclaud F, Delacourt C. Calendar aging of a graphite/$LiFePO_4$ cell. *J Power Sources* 2012;**208**:296–305.
[17] Chan HL, D S. A new battery model for use with battery energy storage systems and electric vehicles power systems. In: Power Engineering Society Winter Meeting, 2000. IEEE; 2000.
[18] Barai A. Improvement of consistency, accuracy and interpretation of characterisation test techniques for Li-ion battery cells for automotive application. In: WMG. UK: University of Warwick; 2015.
[19] Barai A, Uddin K, Widanalage WD, McGordon A, Jennings P. The effect of average cycling current on total energy of lithium-ion batteries for electric vehicles. *J Power Sources* 2016;**303**:81–5.
[20] Liaw BY, Roth EP, Jungst RG, Nagasubramanian G, Case HL, Doughty DH. Correlation of Arrhenius behaviors in power and capacity fades with cell impedance and heat generation in cylindrical lithium-ion cells. *J Power Sources* 2003;**119–121**:874–86.
[21] Ji Y, Zhang Y, Wang C-Y. Li-ion cell operation at low temperatures. *J Electrochem Soc* 2013;**160**(4):A636–49.
[22] 62660-1 I. *Secondary lithium-ion cells for the propulsion of electric road vehicles – Part 1: performance testing*. Geneva, Switzerland: International Electrotechnical Commission; 2012.
[23] ISO. Electrically propelled road vehicles - test specification for lithium-ion traction battery packs and systems. *Part 1: High-power applications*. Geneva, Switzerland: International Organization for Standardization; 2011.
[24] ISO. Electrically propelled road vehicles - test specification for lithium-ion traction battery packs and systems. *Part 2: High-energy applications*. British Standards Institution; 2012.
[25] INEEL, FreedomCAR battery test manual for power-assist hybrid electric vehicles. 2003.
[26] Energy, U.S.D.o.. Battery test manual for plug in hybrid electric vehicles. *V.T.P. energy efficiency and renewable energy*. Idaho Operations Office; 2014. Editor.
[27] Commission, N.D.a.R., Lithium-ion batteries for electric vehicles. 2006.
[28] Hosseinzadeh E, Genieser R, Worwood D, Barai A, Marco J, Jennings P. A systematic approach for electrochemical-thermal modelling of a large format lithium-ion battery for electric vehicle application. *J Power Sources* 2018;**382**:77–94.
[29] Jaguemont J, Boulon L, Dubé Y. A comprehensive review of lithium-ion batteries used in hybrid and electric vehicles at cold temperatures. *Appl Energy* 2016;**164**:99–114.
[30] Waldmann T, Wilka M, Kasper M, Fleischhammer M, Wohlfahrt-Mehrens M. Temperature dependent ageing mechanisms in Lithium-ion batteries – a post-mortem study. *J Power Sources* 2014;**262**:129–35.
[31] Zhang SS, Xu K, Jow TR. Low temperature performance of graphite electrode in Li-ion cells. *Electrochim Acta* 2002;**48**(3):241–6.
[32] Vetter J, Novák P, Wagner MR, Veit C, Möller KC, Besenhard JO, Winter M, Wohlfahrt-Mehrens M, Vogler C, Hammouche A. Ageing mechanisms in lithium-ion batteries. *J Power Sources* 2005;**147**(1–2):269–81.
[33] Fan J, Tan S. Studies on charging lithium-ion cells at low temperatures. *J Electrochem Soc* 2006;**153**(6):A1081–92.
[34] Petzl M, Kasper M, Danzer MA. Lithium plating in a commercial lithium-ion battery – a low-temperature aging study. *J Power Sources* 2015;**275**:799–807.
[35] Grandjean T, Barai A, McGordon A, Guo Y, Marco J. Large format lithium ion pouch cell thermal gradient characterisation at different ambient temperatures and current discharge rates. *J Power Sources* 2017;**359**:215–25.
[36] Doyle M, Newman J. The use of mathematical modeling in the design of lithium/polymer battery systems. *Electrochim Acta* 1995;**40**(13):2191–6.
[37] Firouz Y, Relan R, Timmermans JM, Omar N, Van den Bossche P, Van Mierlo J. Advanced lithium ion battery modeling and nonlinear analysis based on robust method in frequency domain: nonlinear characterization and non-parametric modeling. *Energy* 2016;**106**:602–17.
[38] Uddin K, Somerville L, Barai A, Lain M, Ashwin TR, Jennings P, Marco J. The impact of high-frequency-high-current perturbations on film formation at the negative electrode-electrolyte interface. *Electrochim Acta* 2017;**233**:1–12.
[39] Fotouhi A, Auger DJ, Propp K, Longo S, Wild M. A review on electric vehicle battery modelling: from lithium-ion toward lithium–sulphur. *Renewable Sustainable Energy Rev* 2016;**56**:1008–21.
[40] Ashwin TR, Chung YM, Wang J. Capacity fade modelling of lithium-ion battery under cyclic loading conditions. *J Power Sources* 2016;**328**:586–98.
[41] Ashwin TR, McGordon A, Widanage WD, Jennings PA. Modified electrochemical parameter estimation of NCR18650BD battery using implicit finite volume method. *J Power Sources* 2017;**341**:387–95.
[42] Uddin K, Perera S, Widanage W, Somerville L, Marco J. Characterising lithium-ion battery degradation through the identification and tracking of electrochemical battery model parameters. *Batteries* 2016;**2**(2):13.
[43] Forman JC, Moura SJ, Stein JL, Fathy HK. Genetic identification and fisher identifiability analysis of the Doyle–Fuller–Newman model from experimental cycling of a $LiFePO_4$ cell. *J Power Sources* 2012;**210**:263–75.
[44] Grandjean T, McGordon A, Jennings P. Structural identifiability of equivalent circuit models for Li-ion batteries. *Energies* 2017;**10**(1).
[45] Osswald PJ, Erhard SV, Rheinfeld A, Rieger B, Hoster HE, Jossen A. Temperature dependency of state of charge inhomogeneities and their equalization in cylindrical lithium-ion cells. *J Power Sources* 2016;**329**:546–52.
[46] He H, Xiong R, Fan J. Evaluation of lithium-ion battery equivalent circuit models for state of charge estimation by an experimental approach. *Energies* 2011;**4**(4):582.
[47] Barai A, Uddin K, Widanage WD, McGordon A, Jennings P. A study of the influence of measurement timescale on internal resistance characterisation methodologies for lithium-ion cells. *Sci Rep* 2018;**8**(1).
[48] Wang Y, Zhang C, Chen Z. A method for joint estimation of state-of-charge and available energy of $LiFePO_4$ batteries. *Appl Energy* 2014;**135**:81–7.
[49] Truchot C, Dubarry M, Liaw BY. State-of-charge estimation and uncertainty for lithium-ion battery strings. *Appl Energy* 2014;**119**(0):218–27.
[50] Liu X, Wu J, Zhang C, Chen Z. A method for state of energy estimation of lithium-ion batteries at dynamic currents and temperatures. *J Power Sources* 2014;**270**(0):151–7.
[51] Williams, T. Real World Test: *2013* Nissan LEAF Range vs 2012 Nissan LEAF Range (w/Viideo). 2013 01/06/2015]; Available from: http://insideevs.com/real-world-test-2013-nissan-leaf-range-vs-2012-nissan-leaf-range/.
[52] Gordon-Bloomfield, N. StaffCar update: after 73,100 miles, our Nissan LEAF loses its second capacity bar. 2015 01/06/2015]; Available from: https://transportevolved.com/2015/04/14/staffcar-update-after-73100-miles-our-nissan-leaf-loses-its-second-capacity-bar/.
[53] Birrell SA, McGordon A, Jennings PA. Defining the accuracy of real-world range estimations of an electric vehicle. In: Intelligent Transportation Systems (ITSC), 2014 IEEE 17th International Conference on; 2014.
[54] Charkhgard M, Farrokhi M. State-of-charge estimation for lithium-ion batteries using neural networks and EKF. *IEEE Trans Indust Electron* 2010;**57**(12):4178–87.
[55] Zhang Y, Xiong R, He H, Pecht MG. Long short-term memory recurrent neural network for remaining useful life prediction of lithium-ion batteries. *IEEE Trans Veh Technol* 2018;**67**(7):5695–705.

[56] Hu X, Jiang J, Cao D, Egardt B. Battery health prognosis for electric vehicles using sample entropy and sparse bayesian predictive modeling. *IEEE Trans Indust Electron* 2015 p. 1-1.

[57] Wang D, Miao Q, Pecht M. Prognostics of lithium-ion batteries based on relevance vectors and a conditional three-parameter capacity degradation model. *J Power Sources* 2013;**239**:253–64.

[58] Patil MA, Tagade P, Hariharan KS, Kolake SM, Song T, Yeo T, Doo S. A novel multistage support vector machine based approach for Li ion battery remaining useful life estimation. *Appl Energy* 2015;**159**:285–97.

[59] Sepasi S, Ghorbani R, Liaw BY. A novel on-board state-of-charge estimation method for aged Li-ion batteries based on model adaptive extended Kalman filter. *J Power Sources* 2014;**245**:337–44.

[60] Singleton RK, Strangas EG, Aviyente S. Extended Kalman filtering for remaining-useful-life estimation of bearings. *IEEE Trans Indust Electron* 2015;**62**(3):1781–90.

[61] Richardson RR, Osborne MA, Howey DA. Gaussian process regression for forecasting battery state of health. *J Power Sources* 2017;**357**:209–19.

[62] Broussely M, Biensan P, Bonhomme F, Blanchard P, Herreyre S, Nechev K, Staniewicz RJ. Main aging mechanisms in Li ion batteries. *J Power Sources* 2005;**146**(1–2):90–6.

[63] Sarre G, Blanchard P, Broussely M. Aging of lithium-ion batteries. *J Power Sources* 2004;**127**(1-2):65–71.

[64] Kanevskii LS, Dubasova VS. Degradation of lithium-ion batteries and how to fight it: a review. *Russ J Electrochem* 2005;**41**(1):1–16.

[65] Birkl CR, Roberts MR, McTurk E, Bruce PG, Howey DA. Degradation diagnostics for lithium ion cells. *J Power Sources* 2017;**341**:373–86.

[66] Uddin K, Moore AD, Barai A, Marco J. The effects of high frequency current ripple on electric vehicle battery performance. *Appl Energy* 2016;**178**:142–54.

[67] Groot J. State of health estimation of Li ion batteries cycle life test methods. *Division of electric power Engineering, department of energy and environment*. Chalmers Bibliotek: Chalmers University of Technology; 2012.

[68] Kabir MM, Demirocak DE. Degradation mechanisms in Li-ion batteries: a state-of-the-art review. *Int J Energy Res* 2017.

[69] Lin C, Tang A, Mu H, Wang W, Wang C. Aging mechanisms of electrode materials in lithium-ion batteries for electric vehicles. *J Chem* 2015;**2015**:1–11.

[70] Zhang Y, Wang C-Y. Cycle-life characterization of automotive lithium-ion batteries with $LiNiO_2$ cathode. *J Electrochem Soc* 2009;**156**(7):A527–35.

[71] Bourlot S, Blanchard P, Robert S. Investigation of aging mechanisms of high power Li-ion cells used for hybrid electric vehicles. *J Power Sources* 2011;**196**(16):6841–6.

[72] Uno M, Tanaka K. Influence of high-frequency charge-discharge cycling induced by cell voltage equalizers on the life performance of lithium-ion cells. *Vehic Technol IEEE Trans* 2011;**60**(4):1505–15.

[73] Chen Z, He Y, Chengbin M. Quantitative evaluation of $LiFePO_4$ battery cycle life improvement using ultracapacitors. *Power Electron IEEE Trans* 2016;**31**(6):3989–93.

[74] Friesen A, Mönnighoff X, Börner M, Haetge J, Schappacher FM, Winter M. Influence of temperature on the aging behavior of 18650-type lithium ion cells: a comprehensive approach combining electrochemical characterization and post-mortem analysis. *J Power Sources* 2017;**342**:88–97.

[75] Zhang Q, White RE. Calendar life study of Li-ion pouch cells. *J Power Sources* 2007;**173**(2):990–7.

[76] Li D, Danilov DL, Xie J, Raijmakers L, Gao L, Yang Y, Notten PHL. Degradation mechanisms of C6/$LiFePO_4$ batteries: experimental analyses of calendar aging. *Electrochim Acta* 2016;**190**:1124–33.

[77] Sarasketa-Zabala E, Gandiaga I, Rodriguez-Martinez LM, Villarreal I. Calendar ageing analysis of a $LiFePO_4$/graphite cell with dynamic model validations: towards realistic lifetime predictions. *J Power Sources* 2014;**272**:45–57.

[78] Wang J, Purewal J, Liu P, Hicks-Garner J, Soukazian S, Sherman E, Sorenson A, Vu L, Tataria H, Verbrugge MW. Degradation of lithium ion batteries employing graphite negatives and nickel–cobalt–manganese oxide + spinel manganese oxide positives: part 1, aging mechanisms and life estimation. *J Power Sources* 2014;**269**:937–48.

[79] Bloom I, Jansen AN, Abraham DP, Knuth J, Jones SA, Battaglia VS, Henriksen GL. Differential voltage analyses of high-power, lithium-ion cells. 1. Technique and applications.. *J Power Sources* 2005;**139**(1-2):295–303.

[80] Dubarry M, Svoboda V, Hwu R, Liaw BY. A roadmap to understand battery performance in electric and hybrid vehicle operation. *J Power Sources* 2007;**174**(2):366–72.

[81] Dubarry M, Truchot C, Cugnet M, Liaw BY, Gering K, Sazhin S, Jamison D, Michelbacher C. Evaluation of commercial lithium-ion cells based on composite positive electrode for plug-in hybrid electric vehicle applications. Part I: initial characterizations.. *J Power Sources* 2011;**196**(23):10328–35.

[82] Dahn JR, Burns JC, Stevens DA. Importance of coulombic efficiency measurements in R&D efforts to obtain long-lived Li-ion batteries. *Electrochem Soc Interface* 2016;**25**(3):75–8.

[83] Smith AJ, Burns JC, Xiong D, Dahn JR. Interpreting high precision coulometry results on Li-ion cells. *J Electrochem Soc* 2011;**158**(10).

[84] Burns JC, Kassam A, Sinha NN, Downie LE, Solnickova L, Way BM, Dahn JR. Predicting and extending the lifetime of Li-ion batteries. *J Electrochem Soc* 2013;**160**(9):A1451–6.

[85] Taylor J, Ball R, McGordon A, Uddin K, Marco J. Sizing tool for rapid optimisation of pack configuration at early-stage automotive product development. In: EVS28. Goyang, Korea: KINTEX; 2015.

[86] Barlow, T.J., S. Latham, I.S. McCrae, and P.G. Boulter, A reference book of driving cycles for use in the measurement of road vehicle emissions. 2009.

[87] Keszei E. *Chemical thermodynamics - an introduction*. Berlin Heidelberg: Springer; 2012.

[88] Pletcher D. *A first course in electrode processes*. Cambridge, UK: Royal Society of Chemistry; 2009.

[89] Marincic N. Lithium batteries with liquid depolarizers. *Modern Aspect Electrochem* 1983.

[90] Birkl CR, McTurk E, Roberts MR, Bruce PG, Howey DA. A parametric open circuit voltage model for lithium ion batteries. *J Electrochem Soc* 2015;**162**(12):A2271–80.

[91] Huggins RA. *Advanced batteries, materials science aspects*. Springer; 2009. ed.

[92] Fergus JW. Recent developments in cathode materials for lithium ion batteries. *J Power Sources* 2010;**195**(4):939–54.

[93] Xu B, Qian D, Wang Z, Meng YS. Recent progress in cathode materials research for advanced lithium ion batteries. *Mater Sci Eng* 2012;**73**(5-6):51–65.

[94] Launay M, Boucher F, Gressier P, Ouvrard G. A DFT study of lithium battery materials: application to the β-$VOXO_4$ systems (X=P, As, S). *J Solid State Chem* 2003;**176**(2):556–66.

[95] Deniard P, Dulac AM, Rocquefelte X, Grigorova V, Lebacq O, Pasturel A, Jobic S. High potential positive materials for lithium-ion batteries: transition metal phosphates. *J Phys Chem Solids* 2004;**65**(2-3):229–33.

[96] Dubarry M, Truchot C, Liaw BY. Synthesize battery degradation modes via a diagnostic and prognostic model. *J Power Sources* 2012;**219**:204–16.

[97] Farmann A, Sauer DU. A study on the dependency of the open-circuit voltage on temperature and actual aging state of lithium-ion batteries. *J Power Sources* 2017;**347**:1–13.

[98] Dubarry M, Truchot C, Liaw BY, Gering K, Sazhin S, Jamison D, Michelbacher C. Evaluation of commercial lithium-ion cells based on composite positive electrode for plug-in hybrid electric vehicle applications: III. Effect of thermal excursions without prolonged thermal aging.. *J Electrochem Soc* 2013;**160**(1):A191–9.

[99] Dubarry M, Truchot C, Liaw BY, Gering K, Sazhin S, Jamison D, Michelbacher C. Evaluation of commercial lithium-ion cells based on composite positive electrode for plug-in hybrid electric vehicle applications. Part II. Degradation mechanism under 2C cycle aging.. *J Power Sources* 2011;**196**(23):10336–43.

[100] Pattipati B, Balasingam B, Avvari GV, Pattipati KR, Bar-Shalom Y. Open circuit voltage characterization of lithium-ion batteries. *J Power Sources* 2014;**269**:317–33.

[101] Bloom I, Trahey L, Abouimrane A, Belharouak I, Zhang X, Wu Q, Lu W, Abraham DP, Bettge M, Elam JW, Meng X, Burrell AK, Ban C, Tenent R, Nanda J, Dudney N. Effect of interface modifications on voltage fade in $0.5Li_2MnO_3$•$0.5LiNi0.375Mn0.375Co0.25O_2$ cathode materials. *J Power Sources* 2014;**249**:509–14.

[102] *USABC electric vehicle battery test procedures manual*. 1996. p. 1-129.

[103] Dubarry M, Svoboda V, Hwu R, Liaw BY. Capacity loss in rechargeable lithium cells during cycle life testing: the importance of determining state-of-charge. *J Power Sources* 2007;**174**(2):1121–5.

[104] Li Z, Huang J, Liaw BY, Zhang J. On state-of-charge determination for lithium-ion batteries. *J Power Sources* 2017;**348**:281–301.

[105] Devie A, Dubarry M, Wu H-P, Wu T-H, Liaw BY. Overcharge study in $Li_4Ti_5O_{12}$ based lithium-ion pouch cell II. Experimental investigation of the degradation mechanism. *J Electrochem Soc* 2016;**163**(13):A2611–17.

[106] Devie A, Dubarry M, Liaw BY. Overcharge study in $Li_4Ti_5O_{12}$ based lithium-ion pouch cell: I. Quantitative diagnosis of degradation modes.. *J Electrochem Soc* 2015;**162**(6):A1033–40.

[107] Thompson AH. Instrumentation for incremental voltage step electrochemical measurements. *Rev Sci Instrum* 1983;**54**(2):229–37.

[108] Wen CJ, Boukamp BA, Huggins RA, Weppner W. Thermodynamic and mass transport properties of "l.iAl". *J Electrochem Soc* 1979;**126**(12):2258–66.

[109] Thompson AH. Electrochemical potential spectroscopy: a new electrochemical measurement. *J Electrochem Soc* 1979;**126**(4):608–16.

[110] Weppner W, Huggins R. Electrochemical methods for determining kinetic properties of solids. *Am Rev Mater Sci* 1978;**8**:269–311.

[111] Energy, U.S.D.o.. Battery test manual for plug in hybrid electric vehicles. *V.T.P. energy efficiency and renewable energy*. Idaho Operations Office; 2010. Editor.

[112] Allafi W, Uddin K, Zhang C, Mazuir Raja Ahsan Sha R, Marco J. On-line scheme for parameter estimation of nonlinear lithium ion battery equivalent circuit models using the simplified refined instrumental variable method for a modified Wiener continuous-time model. *Appl Energy* 2017;**204**:497–508.

[113] Nikolian A, Firouz Y, Gopalakrishnan R, Timmermans J-M, Omar N, van den Bossche P, van Mierlo J. Lithium ion batteries—development of advanced electrical equivalent circuit models for nickel manganese cobalt lithium-ion. *Energies* 2016;**9**(5).

[114] Uddin K, Picarelli A, Lyness C, Taylor N, Marco J. An Acausal electro-thermal Li-ion battery models for automotive applications. *Energies* 2014;**7**(9):5675–700.

[115] Huria T, Ludovici G, Lutzemberger G. State of charge estimation of high power lithium iron phosphate cells. *J Power Sources* 2014;**249**:92–102.

[116] Li A, Pelissier S, Venet P, Gyan P. Fast characterization method for modeling battery relaxation voltage. *Batteries* 2016;**2**(2).

[117] Nyman A, Zavalis TG, Elger R, Behm M, Lindbergh G. Analysis of the polarization in a Li-ion battery cell by numerical simulations. *J Electrochem Soc* 2010;**157**(11):A1236–46.

[118] Barai A, Chouchelamane GH, Guo Y, McGordon A, Jennings P. A study on the impact of lithium-ion cell relaxation on electrochemical impedance spectroscopy. *J Power Sources* 2015;**280**:74–80.

[119] Kindermann FM, Noel A, Erhard SV, Jossen A. Long-term equalization effects in Li-ion batteries due to local state of charge inhomogeneities and their impact on impedance measurements. *Electrochim Acta* 2015;**185**:107–16.
[120] Zhang C, Jiang J, Zhang W, Sharkh SM. Estimation of state of charge of lithium-ion batteries used in HEV using robust extended Kalman filtering. *Energies* 2012;**5**:1098–115.
[121] Baccouche I, Jemmali S, Manai B, Omar N, Amara N. Improved OCV model of a Li-Ion NMC battery for online SOC estimation using the extended Kalman filter. *Energies* 2017;**10**(6).
[122] Nikolian A, Jaguemont J, de Hoog J, Goutam S, Omar N, Van Den Bossche P, Van Mierlo J. Complete cell-level lithium-ion electrical ECM model for different chemistries (NMC, LFP, LTO) and temperatures (-5°C to 45°C) – optimized modelling techniques. *Int J Elect Power Energy Syst* 2018;**98**:133–46.
[123] Choi HU, Jin JS, Park J-Y, Lim H-T. Performance improvement of all-solid-state Li-S batteries with optimizing morphology and structure of sulfur composite electrode. *J Alloys Compd* 2017;**723**:787–94.
[124] Ding J, Lu Z, Wu M, Liu C, Ji H, Yang G. Preparation and performance characterization of AlF 3 as interface stabilizer coated Li 1.24 Ni 0.12 Co 0.12 Mn 0.56 O 2 cathode for lithium-ion batteries. *Appl Surf Sci* 2017;**406**:21–9.
[125] Zhu Y, Gao T, Fan X, Han F, Wang C. Electrochemical techniques for intercalation electrode materials in rechargeable batteries. *Acc Chem Res* 2017;**50**(4):1022–31.
[126] Li H, Wang Y, Huang J, Zhang Y, Zhao J. Microwave-assisted synthesis of CuS/graphene composite for enhanced lithium storage properties. *Electrochim Acta* 2017;**225**(Supplement C):443–51.
[127] Luo M, Lin X, Lan H, Yu H, Yan L, Qian S, Long N, Shui M, Shu J. Lithiation-delithiation kinetics of $BaLi_2Ti_6O_{14}$ anode in high-performance secondary Li-ion batteries. *J Electroanal Chem* 2017;**786**:86–93.
[128] Madej E, Klink S, Schuhmann W, Ventosa E, La Mantia F. Effect of the specific surface area on thermodynamic and kinetic properties of nanoparticle anatase TiO_2 in lithium-ion batteries. *J Power Sources* 2015;**297**:140–8.
[129] Shi W, Hu X, Wang J, Jiang J, Zhang Y, Yip T. Analysis of thermal aging paths for large-format $LiFePO_4$/graphite battery. *Electrochim Acta* 2016;**196**:13–23.
[130] Ma J, Wang C, Wroblewski S. Kinetic characteristics of mixed conductive electrodes for lithium ion batteries. *J Power Sources* 2007;**164**(2):849–56.
[131] Srinivasan V, Newman J. Existence of path-dependence in the $LiFePO_4$ electrode. *Electrochem Solid-State Lett* 2006;**9**(3):A110–14.
[132] Dreyer W, Jamnik J, Guhlke C, Huth R, Moskon J, Gaberscek M. The thermodynamic origin of hysteresis in insertion batteries. *Nat Mater* 2010;**9**(5):448–53.
[133] Thackeray MM. Manganese oxides for lithium batteries. *Prog Solid State Chem* 1997;**25**(1-2):1–71.
[134] Dubarry M, Truchot C, Devie A, Liaw BY, Gering K, Sazhin S, Jamison D, Michelbacher C. Evaluation of commercial lithium-ion cells based on composite positive electrode for plug-in hybrid electric vehicle (PHEV) applications: IV. Over-discharge phenomena. *J Electrochem Soc* 2015;**162**(9):A1787–92.
[135] Dubarry M, Gaubicher J, Guyomard D, Wallez G, Quarton M, Baehtz C. Uncommon potential hysteresis in the $Li/Li_2xVO(H_2-xPO_4)_2$ ($0 \le x \le 2$) system. *Electrochim Acta* 2008;**53**(13):4564–72.
[136] Sethuraman VA, Srinivasan V, Bower AF, Guduru PR. In situ measurements of stress-potential coupling in lithiated silicon. *J Electrochem Soc* 2010;**157**(11):A1253–61.
[137] Jerliu B, Huger E, Dorrer L, Seidlhofer BK, Steitz R, Horisberger M, Schmidt H. Lithium insertion into silicon electrodes studied by cyclic voltammetry and operando neutron reflectometry. *Phys Chem Chem Phys* 2018;**20**(36):23480–91.
[138] Barai A, Widanage WD, Marco J, McGordon A, Jennings P. A study of the open circuit voltage characterization technique and hysteresis assessment of lithium-ion cells. *J Power Sources* 2015;**295**:99–107.
[139] Roscher MA, Bohlen O, Vetter J. OCV hysteresis in Li-ion batteries including two-phase transition materials. *Int J Electrochem* 2011;**2011**.
[140] Tang X, Mao X, Lin J, Koch B. Li-ion battery parameter estimation for state of charge. In: American Control Conference, *San Francisco, CA, USA*; 2011.
[141] Petzl M, Danzer MA. Advancements in OCV measurement and analysis for lithium-ion batteries. *Energy Convers IEEE Trans* 2013;**28**(3):675–81.
[142] Barai A, Widanage WD, McGordon A, Jennings P. The influence of temperature and charge-discharge rate on open circuit voltage hysteresis of an LFP Li-ion battery. In: 2016 IEEE Transportation Electrification Conference and Expo (ITEC); 2016.
[143] Kasavajjula US, Wang C, Arce PE. Discharge model for $LiFePO_4$ accounting for the solid solution range. *J Electrochem Soc* 2008;**155**(11):A866–74.
[144] Meethong N, Huang H-YS, Speakman SA, Carter WC, Chiang Y-M. Strain accommodation during phase transformations in olivine-based cathodes as a materials selection criterion for high-power rechargeable batteries. *Adv Funct Mater* 2007;**17**(7):1115–23.
[145] Bai P, Cogswell DA, Bazant MZ. Suppression of phase separation in LiFePO(4) nanoparticles during battery discharge. *Nano Lett* 2011;**11**(11):4890–6.
[146] Jonghoon K, Gab-Su S, Changyoon C, Bo-Hyung C, Seongjun L. OCV hysteresis effect-based SOC estimation in extended Kalman filter algorithm for a LiFePO<inf>4</inf>/C cell. In: Electric Vehicle Conference (IEVC), 2012 IEEE International; 2012.
[147] Mao Z, Farkhondeh M, Pritzker M, Fowler M, Chen Z. Dynamics of a blended lithium-ion battery electrode during galvanostatic intermittent titration technique. *Electrochim Acta* 2016;**222**:1741–50.
[148] Plett GL. Extended Kalman filtering for battery management systems of LiPB-based HEV battery packs: Part 2. Modeling and identification.. *J Power Sources* 2004;**134**(2):262–76.
[149] Hu X, Li S, Peng H. A comparative study of equivalent circuit models for Li-ion batteries. *J Power Sources* 2012;**198**(0):359–67.
[150] Dees DW, Abraham DP, Lu W, Gallagher KG, Bettge M, Jansen AN. Electrochemical modeling and performance of a lithium- and manganese-rich layered transition-metal oxide positive electrode. *J Electrochem Soc* 2015;**162**(4):A559–72.
[151] Dees DW, Kawauchi S, Abraham DP, Prakash J. Analysis of the galvanostatic intermittent titration technique (GITT) as applied to a lithium-ion porous electrode. *J Power Sources* 2009;**189**(1):263–8.
[152] Delacourt C, Ati M, Tarascon JM. Measurement of lithium diffusion coefficient in $LiyFeSO_4F$. *J Electrochem Soc* 2011;**158**(6):A741.
[153] Bohnke C, Fourquet J-L, Randrianantoandro N, Brousse T, Crosnier O. Electrochemical insertion of lithium into the ramsdellite-type oxide Li 2 Ti 3 O 7: influence of the Li 2 Ti 3 O 7 particle size. *J Solid State Electrochem* 2002;**6**(6):403–11.
[154] Shaju KM, Subba Rao GV, Chowdari BVR. Electrochemical kinetic studies of Li-ion in O_2-structured $Li2/3(Ni1/3Mn2/3)O2$ and $Li(2/3;)+x(Ni1/3Mn2/3;)O2$ by EIS and GITT. *J Electrochem Soc* 2003;**150**(1):A1–A13.
[155] Kleiner K, Melke J, Merz M, Jakes P, Nagel P, Schuppler S, Liebau V, Ehrenberg H. Unraveling the degradation process of LiNi0.8Co0.15Al0.05O2 electrodes in commercial lithium ion batteries by electronic structure investigations. *ACS Appl Mater Interfaces* 2015;**7**(35):19589–600.
[156] Yazami R, Ozawa Y. A kinetics study of self-discharge of spinel electrodes in $Li/LixMn_2O_4$ cells. *J Power Sources* 2006;**153**(2):251–7.
[157] Jiang J, Shi W, Zheng J, Zuo P, Xiao J, Chen X, Xu W, Zhang J-G. Optimized operating range for large-format $LiFePO_4$/graphite batteries. *J Electrochem Soc* 2014;**161**(3):A336–41.
[158] Zheng L, Zhang H, Cheng P, Ma Q, Liu J, Nie J, Feng W, Zhou Z. $Li[(FSO_2)(n\text{-}C4F9SO_2)N]$ versus LiPF6 for graphite/$LiCoO_2$ lithium-ion cells at both room and elevated temperatures: a comprehensive understanding with chemical, electrochemical and XPS analysis. *Electrochim Acta* 2016;**196**:169–88.
[159] Xing Y, He W, Pecht M, Tsui KL. State of charge estimation of lithium-ion batteries using the open-circuit voltage at various ambient temperatures. *Appl Energy* 2014;**113**:106–15.
[160] García-Plaza M, Eloy-García Carrasco J, Peña-Asensio A, Alonso-Martínez J, Arnaltes Gómez S. Hysteresis effect influence on electrochemical battery modeling. *Elect Power Syst Res* 2017;**152**:27–35.
[161] Dahn JR, Zheng T, Liu Y, Xue JS. Mechanisms for lithium insertion in carbonaceous materials. *Science* 1995;**270**(5236):590–3.
[162] Sleigh AK, Murray JJ, McKinnon WR. Memory effects due to phase conversion and hysteresis in $Li/LixMnO_2$ cells. *Electrochim Acta* 1991;**36**(9):1469–74.
[163] Dubarry M, Liaw BY. Identify capacity fading mechanism in a commercial $LiFePO_4$ cell. *J Power Sources* 2009;**194**(1):541–9.
[164] Dubarry M, Svoboda V, Hwu R, Liaw BY. Incremental capacity analysis and close-to-equilibrium OCV measurements to quantify capacity fade in commercial rechargeable lithium batteries. *Electrochem Solid-State Lett* 2006;**9**(10):A454–7.
[165] Dubarry M, Liaw BY. Development of a universal modeling tool for rechargeable lithium batteries. *J Power Sources* 2007;**174**(2):856–60.
[166] Bloom I, Christophersen J, Gering K. Differential voltage analyses of high-power, lithium-ion cells. 2. Applications.. *J Power Sources* 2005;**139**(1-2):304–13.
[167] Bloom I, Christophersen JP, Abraham DP, Gering KL. Differential voltage analyses of high-power, lithium-ion cells. 3. Another anode phenomenon.. *J Power Sources* 2006;**157**(1):537–42.
[168] Zhang Q, White RE. Calendar life study of Li-ion pouch cells: Part 2: simulation. *J Power Sources* 2008;**179**(2):785–92.
[169] Devie A, Baure G, Dubarry M. Intrinsic variability in the degradation of a batch of commercial 18650 lithium-ion cells. *Energies* 2018;**11**(5).
[170] Dubarry M, Devie A, Liaw BY. The value of battery diagnostics and prognostics. *J Energy Power Source* 2014;**1**(5):242–9.
[171] Balewski L, Brenet JP. A new method for the study of the electrochemical reactivity of manganese dioxide. *Electrochem Technol* 1967;**5**:527–31.
[172] Schweigart HELG, Clauss CRA. Cathodic reduction mechanisms of manganese dioxide from derivative discharge curves. *J Electrochem Soc* 1976;**123**(8):1124–7.
[173] Clauss CRA, Schweigart HELG. The reduction of manganese dioxide in Leclanche -type dry cells as displayed by derivative discharge functions. *J Electrochem Soc* 1976;**123**(7):951–9.
[174] Thompson AH. Electrochemical studies of lithium intercalation in titanium and tantalum dichalcogenides. *Physica B+C* 1980;**99**(B):100–6.
[175] Thompson AH. Lithium ordering in $LixTiS_2$. *Phys Rev Lett* 1978;**40**(23):1511–14.
[176] Dahn J, Haering RR. The role of kinetic effects in voltametry studies of intercalation systems. *Solid State Ion* 1981;**2**:19–26.
[177] Dahn JR, McKinnon WR. Thermodynamics of lithium intercalation from high resolution electrochemical measurements. *J Electrochem Soc* 1984;**131**(8):1823–8.
[178] Dahn JR, McKinnon WR. Lithium intercalation in 2H-$LixTaS_2$. *J Phys C: Solid State Phys* 1984;**17**:4231–43.
[179] Barker J. An electrochemical investigation of the doping processes in poly(thienylene vinylene). *Synth Met* 1989;**33**:43–50.
[180] Barker J, Baldwin D, Bott DC. Electrochemical voltage spectroscopy: dopant diffusion in Durham polyacetylene. *Synth Met* 1989;**28**:D127–DD34.
[181] Dahn J. Phase diagram of $LixC_6$. *Phys Rev B* 1991;**44**(17):9170–7.

[182] Ohzuku T, Iwakoshi Y, Sawai K. Formation of lithium-graphite intercalation compounds in nonaqueous electrolytes and their application as a negative electrode for a lithium ion (shuttlecock) cell. *J Electrochem Soc* 1993;**140**(9):2490–8.

[183] Aurbach D, Markovsky B, Weissman I, Levi E, Ein-Eli Y. On the correlation between surface chemistry and performance of graphite negative electrodes for Li ion batteries. *Electrochemica acta* 1999;**45**:67–86.

[184] Barker J. Three electrode electrochemical voltage spectroscopy (TEVS) evaluation of a model lithium ion system. *Electrochemica acta* 1995;**40**(11):1603–8.

[185] Barker J, Koksbang R, Saidi MY. An electrochemical investigation into the lithium insertion properties of $LixNiO_2$. *Solid State Ion* 1996;**89**:25–35.

[186] Barker J, Pynenburg R, Koksbang R, Saidi MY. An electrochemical investigation into the lithium insertion properties of $LixCoO_2$. *Electrochemica acta* 1996;**41**(15):2481–8.

[187] Barker J, Saidi MY, Koksbang R. Diffential capacity as spectroscopic probe for the investigation of alkali metal insertion reactions. *Electrochemica acta* 1996;**41**(16):2639–46.

[188] Koksbang R, Barker J, Saidi MY. Cathode materials for lithium rocking chair batteries. *Solid State Ion* 1996;**84**:1–21.

[189] Koksbang R, JB HSHi, Saidi MY. Cathode materials for lithium rocking chair batteries. *Solid State Ion* 1995;**84**:1–21.

[190] Saidi MY, Barker J, Koksbang R. Structural and electrochemical investigation of lithium insertion in the $Li1- xMn_2O_4$ spinel phase. *Electrochemica acta* 1996;**41**(2):199–204.

[191] Carlier D, Saadoune I, Meńeťrier M, Delmas C. Lithium Electrochemical Deintercalation from O_2-LiCoO[*sub* 2]. *J Electrochem Soc* 2002;**149**(10):A1310.

[192] Gao Y, Dahn JR. Synthesis and characterization of $Li1+Mn_2O_4$ for Li-ion battery applications. *J Electrochem Soc* 1996;**143**(1):100–14.

[193] Paulsen JM, Mueller-Neuhaus JR, Dahn JR. Layered $LiCoO_2$ with a different oxygen stacking (o_2 structure) as a cathode material for rechargeable lithium batteries. *J Electrochem Soc* 2000;**147**(2):508–16.

[194] Barker J, Saidi MY, Swoyer JL. Performance evaluation of the electroactive material, γ-LiV_2O_5, made by a carbothermal reduction method. *J Electrochem Soc* 2003;**150**(9):A1267.

[195] Barker J, Saidi MY, Swoyer JL. A sodium-ion cell based on the fluorophosphate compound $NaVPO_4F$. *Electrochem Solid-State Lett* 2003;**6**(1):A1.

[196] Shim J, Kostecki R, Richardson T, Song X, Striebel KA. Electrochemical analysis for cycle performance and capacity fading of a lithium-ion battery cycled at elevated temperature. *J Power Sources* 2002;**112**(1):222–30.

[197] Shim J, Striebel KA. Cycling performance of low-cost lithium ion batteries with natural graphite and $LiFePO_4$. *J Power Sources* 2003;**119-121**:955–8.

[198] Shim J, Striebel KA. Characterization of high-power lithium-ion cells during constant current cycling. *J Power Sources* 2003;**122**(2):188–94.

[199] Striebel K, Guerfi A, Shim J, Armand M, Gauthier M, Zaghib K. $LiFePO_4$/gel/natural graphite cells for the BATT program. *J Power Sources* 2003;**119-121**:951–4.

[200] Shim J, Striebel KA. The dependence of natural graphite anode performance on electrode density. *J Power Sources* 2004;**130**(1-2):247–53.

[201] Keil P. Aging of lithium-ion batteries in electric vehicles. *Faculty of electrical engineering and information technology*. Technical University of Munich; 2017.

[202] Julien C, Mauger A, Vijh A, Zaghib K. Experimental techniques. *Lithium batteries*. Springer International Publishing; 2016. p. 499–548.

[203] Anseán D, Dubarry M, Devie A, Liaw BY, García VM, Viera JC, González M. Operando lithium plating quantification and early detection of a commercial LiFePO 4 cell cycled under dynamic driving schedule. *J Power Sources* 2017;**356**:36–46.

[204] von Srbik M-T, Marinescu M, Martinez-Botas RF, Offer GJ. A physically meaningful equivalent circuit network model of a lithium-ion battery accounting for local electrochemical and thermal behaviour, variable double layer capacitance and degradation. *J Power Sources* 2016;**325**:171–84.

[205] Franco AA, Doublet ML, Bessler WG. Fuel cells and batteries in silico experimentation through integrative multiscale modeling. In: Franco AA, editor. Physical Multiscale Modeling and Numerical Simulation of Electrochemical Devices for Energy Conversion and Storage. London: Springer-Verlag; 2016 Editor.

[206] Krueger S, Kloepsch R, Li J, Nowak S, Passerini S, Winter M. How do reactions at the anode/electrolyte interface determine the cathode performance in lithium-ion batteries? *J Electrochem Soc* 2013;**160**(4):A542–8.

[207] Dahn HM, Smith AJ, Burns JC, Stevens DA, Dahn JR. User-friendly differential voltage analysis freeware for the analysis of degradation mechanisms in Li-ion batteries. *J Electrochem Soc* 2012;**159**(9):A1405–9.

[208] Li J, Harlow J, Stakheiko N, Zhang N, Paulsen J, Dahn J. Dependence of cell failure on cut-off voltage ranges and observation of kinetic hindrance in $LiNi0.8Co0.15Al0.05O_2$. *J Electrochem Soc* 2018;**165**(11):A2682–95.

[209] Kassem M, Delacourt C. Postmortem analysis of calendar-aged graphite/$LiFePO_4$ cells. *J Power Sources* 2013;**235**:159–71.

[210] Schmidt JP, Tran HY, Richter J, Ivers-Tiffée E, Wohlfahrt-Mehrens M. Analysis and prediction of the open circuit potential of lithium-ion cells. *J Power Sources* 2013;**239**:696–704.

[211] Singer A, Zhang M, Hy S, Cela D, Fang C, Wynn TA, Qiu B, Xia Y, Liu Z, Ulvestad A, Hua N, Wingert J, Liu H, Sprung M, Zozulya AV, Maxey E, Harder R, Meng YS, Shpyrko OG. Nucleation of dislocations and their dynamics in layered oxide cathode materials during battery charging. *Nature Energy* 2018;**3**(8):641–7.

[212] Honkura K, Honbo H, Koishikawa Y, Horiba T. State analysis of lithium-ion batteries using discharge curves. *ECS Trans* 2008;**13**(19):61–73.

[213] Smith AJ, Burns JC, Dahn JR. High-precision differential capacity analysis of $LiMn_2O_4$/graphite cells. *Electrochem Solid-State Lett* 2011;**14**(4):A39.

[214] Honkura K, Takahashi K, Horiba T. Capacity-fading prediction of lithium-ion batteries based on discharge curves analysis. *J Power Sources* 2011;**196**(23):10141–7.

[215] Liu P, Wang J, Hicks-Garner J, Sherman E, Soukiazian S, Verbrugge M, Tataria H, Musser J, Finamore P. Aging mechanisms of LiFePO[sub 4] batteries deduced by electrochemical and structural analyses. *J Electrochem Soc* 2010;**157**(4):A499.

[216] Kumaresan K, Guo Q, Ramadass P, White RE. Cycle life performance of lithium-ion pouch cells. *J Power Sources* 2006;**158**(1):679–88.

[217] HNEI. Alawa central. [cited 2017 March]; Available from: https://www.soest.hawaii.edu/HNEI/alawa/.

[218] Fathi R, Burns JC, Stevens DA, Ye H, Hu C, Jain G, Scott E, Schmidt C, Dahn JR. Ultra high-precision studies of degradation mechanisms in aged $LiCoO_2$/graphite Li-ion cells. *J Electrochem Soc* 2014;**161**(10):A1572–9.

[219] Feng X, Sun J, Ouyang M, He X, Lu L, Han X, Fang M, Peng H. Characterization of large format lithium ion battery exposed to extremely high temperature. *J Power Sources* 2014;**272**:457–67.

[220] Kobayashi T, Kawasaki N, Kobayashi Y, Shono K, Mita Y, Miyashiro H. A method of separating the capacities of layer and spinel compounds in blended cathode. *J Power Sources* 2014;**245**:1–6.

[221] Svens P, Eriksson R, Hansson J, Behm M, Gustafsson T, Lindbergh G. Analysis of aging of commercial composite metal oxide – $Li_4Ti_5O_{12}$ battery cells. *J Power Sources* 2014;**270**:131–41.

[222] Kim C-S, Jeong KM, Kim K, Yi C-W. Effects of capacity ratios between anode and cathode on electrochemical properties for lithium polymer batteries. *Electrochim Acta* 2015;**155**:431–6.

[223] Mao Z, Farkhondeh M, Pritzker M, Fowler M, Chen Z, Safari M. Model-based prediction of composition of an unknown blended lithium-ion battery cathode. *J Electrochem Soc* 2015;**162**(4):A716–21.

[224] Ouyang M, Ren D, Lu L, Li J, Feng X, Han X, Liu G. Overcharge-induced capacity fading analysis for large format lithium-ion batteries with $LiyNi1/3Co1/3Mn1/3O_2+LiyMn_2O_4$ composite cathode. *J Power Sources* 2015;**279**:626–35.

[225] Keil P, Schuster SF, Wilhelm J, Travi J, Hauser A, Karl RC, Jossen A. Calendar aging of lithium-ion batteries. *J Electrochem Soc* 2016;**163**(9):A1872–80.

[226] Li D, Danilov DL, Gao L, Yang Y, Notten PHL. Degradation mechanisms of the graphite electrode in C6 /LiFePO 4 batteries unraveled by a non-destructive approach. *J Electrochem Soc* 2016;**163**(14):A3016–21.

[227] Torai S, Nakagomi M, Yoshitake S, Yamaguchi S, Oyama N. State-of-health estimation of $LiFePO_4$/graphite batteries based on a model using differential capacity. *J Power Sources* 2016;**306**:62–9.

[228] Zhang C, Jiang J, Gao Y, Zhang W, Liu Q, Hu X. Charging optimization in lithium-ion batteries based on temperature rise and charge time. *Appl Energy* 2016.

[229] Keil P, Jossen A. Calendar aging of NCA lithium-ion batteries investigated by differential voltage analysis and coulomb tracking. *J Electrochem Soc* 2017;**164**(1):A6066–74.

[230] Lu T, Luo Y, Zhang Y, Luo W, Yan L, Xie J. Degradation analysis of commercial lithium-ion battery in long-term storage. *J Electrochem Soc* 2017;**164**(4):A775–84.

[231] Lu T, Luo Y, Zhang Y, Luo W, Yan L, Xie J. Degradation analysis of a lithium-ion battery with a blended electrode. *J Electrochem Soc* 2016;**164**(2):A295–303.

[232] Goh T, Park M, Seo M, Kim JG, Kim SW. Capacity estimation algorithm with a second-order differential voltage curve for Li-ion batteries with NMC cathodes. *Energy* 2017;**135**:257–68.

[233] Mussa AS, Klett M, Behm M, Lindbergh G, Lindström RW. Fast-charging to a partial state of charge in lithium-ion batteries: A comparative ageing study. *J Energy Storage* 2017;**13**:325–33.

[234] Marongiu A, Sauer DU. On-board aging estimation using half-cell voltage curves for $LiFePO_4$ cathode-based lithium-ion battery for electric vehicle application. In: EVS28 KINTEX, *Korea*; 2015.

[235] Kleiner K, Jakes P, Scharner S, Liebau V, Ehrenberg H. Changes of the balancing between anode and cathode due to fatigue in commercial lithium-ion cells. *J Power Sources* 2016;**317**:25–34.

[236] Ouyang M, Feng X, Han X, Lu L, Li Z, He X. A dynamic capacity degradation model and its applications considering varying load for a large format Li-ion battery. *Appl Energy* 2016;**165**:48–59.

[237] Schindler S, Danzer MA. A novel mechanistic modeling framework for analysis of electrode balancing and degradation modes in commercial lithium-ion cells. *J Power Sources* 2017;**343**:226–36.

[238] Devie A, Dubarry M. Durability and reliability of electric vehicle batteries under electric utility grid operations. Part 1: Cell-to-cell variations and preliminary testing. *Batteries* 2016;**2**(3):28.

[239] Wang S, Wang J, Vu L, Purewal J, Soukiazian S, Graetz J. On line battery capacity estimation based on half-cell open circuit voltages. *J Electrochem Soc* 2014;**161**(12):A1788–93.

[240] Weng C, Feng X, Sun J, Ouyang M, Peng H. Battery SOH management research in the US-China clean energy research center-clean vehicle consortium. In: IFAC-PapersOnline; 2015.

[241] Li X, Jiang J, Ju Q, Chen Z, Zhanhai C, Zhang Z, Zhang C. Analytical charged capacity expression of Lithium-ion battery for SOH estimation based on constant current charging curves. *ECS Trans* 2016;**73**(1):305–18.

[242] Li X, Jiang J, Wang LY, Chen D, Zhang Y, Zhang C. A capacity model based on charging process for state of health estimation of lithium ion batteries. *Appl Energy* 2016;**177**:537–43.
[243] Wang L, Pan C, Liu L, Cheng Y, Zhao X. On-board state of health estimation of $LiFePO_4$ battery pack through differential voltage analysis. *Appl Energy* 2016;**168**:465–72.
[244] Marongiu A, Sauer DU. On board aging estimation using half-cell voltage curves for $LiFePO_4$ cathode-based Lithuim ion batteries for EV applications. *Int J Automot Technol* 2016;**17**(3):465–72.
[245] Liu G, Ouyang M, Lu L, Li J, Hua J. A highly accurate predictive-adaptive method for lithium-ion battery remaining discharge energy prediction in electric vehicle applications. *Appl Energy* 2015;**149**:297–314.
[246] Liu G, Ouyang M, Lu L, Li J, Han X. Online estimation of lithium-ion battery remaining discharge capacity through differential voltage analysis. *J Power Sources* 2015;**274**:971–89.
[247] Berecibar M, Devriendt F, Dubarry M, Villarreal I, Omar N, Verbeke W, Van Mierlo J. Online state of health estimation on NMC cells based on predictive analytics. *J Power Sources* 2016;**320**:239–50.
[248] Berecibar M, Garmendia M, Gandiaga I, Crego J, Villarreal I. State of health estimation algorithm of $LiFePO_4$ battery packs based on differential voltage curves for battery management system application. *Energy* 2016;**103**:784–96.
[249] Riviere E, Venet P, Sari A, Meniere F, Bultel Y. $LiFePO_4$ battery state of health online estimation using electric vehicle embedeed incremental capacity analysis. In: VPPC; 2016.
[250] Weng C, Feng X, Sun J, Peng H. State-of-health monitoring of lithium-ion battery modules and packs via incremental capacity peak tracking. *Appl Energy* 2016;**180**:360–8.
[251] Dubarry M, Berecibar M, Devie A, Anseán D, Omar N, Villarreal I. State of health battery estimator enabling degradation diagnosis: model and algorithm description. *J Power Sources* 2017;**360**:59–69.
[252] Li Y, Abdel-Monem M, Gopalakrishnan R, Berecibar M, Nanini-Maury E, Omar N, van den Bossche P, Van Mierlo J. A quick on-line state of health estimation method for Li-ion battery with incremental capacity curves processed by Gaussian filter. *J Power Sources* 2018;**373**:40–53.
[253] Smith AJ, Dahn JR. Delta differential capacity analysis. *J Electrochem Soc* 2012;**159**(3):A290–3.
[254] Schönleber M, Ivers-Tiffée E. The distribution function of differential capacity as a new tool for analyzing the capacitive properties of lithium-ion batteries. *Electrochem Commun* 2015;**61**:45–8.
[255] Feng X, Li J, Ouyang M, Lu L, Li J, He X. Using probability density function to evaluate the state of health of lithium-ion batteries. *J Power Sources* 2013;**232**:209–18.
[256] Samad NA, Kim Y, Siegel JB, Stefanopoulou AG. Battery capacity fading estimation using a force-based incremental capacity analysis. *J Electrochem Soc* 2016;**163**(8):A1584–94.
[257] Merla Y, Wu B, Yufit V, Brandon NP, Martinez-Botas RF, Offer GJ. Extending battery life: a low-cost practical diagnostic technique for lithium-ion batteries. *J Power Sources* 2016;**331**:224–31.
[258] Merla Y, Wu B, Yufit V, Brandon NP, Martinez-Botas RF, Offer GJ. Novel application of differential thermal voltammetry as an in-depth state-of-health diagnosis method for lithium-ion batteries. *J Power Sources* 2016;**307**:308–19.
[259] Mizushima K, Jones PC, Wiseman PJ, Goodenough JB. $LixCoO_2$ (0<x<-1): a new cathode material for batteries of high energy density. *Mater Res Bull* 1980;**15**(6):783–9.
[260] Cho H-M, Choi W-S, Go J-Y, Bae S-E, Shin H-C. A study on time-dependent low temperature power performance of a lithium-ion battery. *J Power Sources* 2012;**198**:273–80.
[261] Smith K, Wang C-Y. Solid-state diffusion limitations on pulse operation of a lithium ion cell for hybrid electric vehicles. *J Power Sources* 2006;**161**(1):628–39.
[262] Ratnakumar BV, Smart MC, Whitcanack LD, Ewell RC. The impedance characteristics of Mars Exploration Rover Li-ion batteries. *J Power Sources* 2006;**159**(2):1428–39.
[263] Andre D, Meiler M, Steiner K, Walz H, Soczka-Guth T, Sauer DU. Characterization of high-power lithium-ion batteries by electrochemical impedance spectroscopy. II: Modelling.. *J Power Sources* 2011;**196**(12):5349–56.
[264] Eddahech A, Briat O, Vinassa J-M. Thermal characterization of a high-power lithium-ion battery: potentiometric and calorimetric measurement of entropy changes. *Energy* 2013;**61**:432–9.
[265] Xiao M, Choe S-Y. Theoretical and experimental analysis of heat generations of a pouch type $LiMn_2O_4$/carbon high power Li-polymer battery. *J Power Sources* 2013;**241**:46–55.
[266] Chen K, Unsworth G, Li X. Measurements of heat generation in prismatic Li-ion batteries. *J Power Sources* 2014;**261**:28–37.
[267] Vertiz G, Oyarbide M, Macicior H, Miguel O, Cantero I, Fernandez de Arroiabe P, Ulacia I. Thermal characterization of large size lithium-ion pouch cell based on 1d electro-thermal model. *J Power Sources* 2014;**272**:476–84.
[268] Schuster E, Ziebert C, Melcher A, Rohde M, Seifert HJ. Thermal behavior and electrochemical heat generation in a commercial 40 Ah lithium ion pouch cell. *J Power Sources* 2015;**286**:580–9.
[269] Smith K, Wang C-Y. Power and thermal characterization of a lithium-ion battery pack for hybrid-electric vehicles. *J Power Sources* 2006;**160**(1):662–73.
[270] USABC, A., INEL, SNL, Electric vehicle battery test procedures manual. 1996.
[271] Johnson VH. Battery performance models in ADVISOR. *J Power Sources* 2002;**110**(2):321–9.
[272] Waag W, Käbitz S, Sauer DU. Experimental investigation of the lithium-ion battery impedance characteristic at various conditions and aging states and its influence on the application. *Appl Energy* 2013;**102**:885–97.
[273] Tiwari A, Mishra AK, Kobayashi H, Turner APF. *Intelligent nanomaterials*. John Wiley & Sons; 2012.
[274] Schweiger H-G, Obeidi O, Komesker O, Raschke A, Schiemann M, Zehner C, Gehnen M, Keller M, Birke P. Comparison of several methods for determining the internal resistance of lithium ion cells. *Sensors* 2010;**10**(6).
[275] DuBeshter T, Jorne J. Pulse polarization for Li-ion battery under constant state of charge: Part I. Pulse discharge experiments. *J Electrochem Soc* 2017;**164**(11):E3539–46.
[276] DuBeshter T, Jorne J. Pulse polarization for Li-ion battery under constant state-of-charge: Part II. Modeling of individual voltage losses and SOC prediction. *J Electrochem Soc* 2017;**164**(11):E3395–405.
[277] He H, Zhang Y, Xiong R, Wang C. A novel Gaussian model based battery state estimation approach: state-of-energy. *Appl Energy* 2015;**151**(0):41–8.
[278] Yang S, Deng C, Zhang Y, He Y. State of charge estimation for lithium-ion battery with a temperature-compensated model. *Energies* 2017;**10**(10).
[279] Anseán D, García VM, González M, Viera JC, Blanco C, Antuña JL. DC internal resistance during charge: analysis and study of $LiFePO_4$ batteries. In: EVS27, *Barcelona, Spain*; 2013.
[280] Eddahech A, Briat O, Vinassa J-M. Determination of lithium-ion battery state-of-health based on constant-voltage charge phase. *J Power Sources* 2014;**258**:218–27.
[281] Energy, U.S.D.o., PNGV battery test manual. 2001.
[282] Nelson P, Bloom I, Amine K, Henriksen G. Design modeling of lithium-ion battery performance. *J Power Sources* 2002;**110**(2):437–44.
[283] Sun F, Xiong R, He H, Li W, Aussems JEE. Model-based dynamic multi-parameter method for peak power estimation of lithium–ion batteries. *Appl Energy* 2012;**96**:378–86.
[284] Huang J, Qin D, Peng Z. Effect of energy-regenerative braking on electric vehicle battery thermal management and control method based on simulation investigation. *Energy Convers Manage* 2015;**105**:1157–65.
[285] Gambhire P, Ganesan N, Basu S, Hariharan KS, Kolake SM, Song T, Oh D, Yeo T, Doo S. A reduced order electrochemical thermal model for lithium ion cells. *J Power Sources* 2015;**290**:87–101.
[286] Yi J, Lee J, Shin CB, Han T, Park S. Modeling of the transient behaviors of a lithium-ion battery during dynamic cycling. *J Power Sources* 2015;**277**:379–86.
[287] Ye Y, Shi Y, Cai N, Lee J, He X. Electro-thermal modeling and experimental validation for lithium ion battery. *J Power Sources* 2012;**199**:227–38.
[288] Nieto N, Díaz L, Gastelurrutia J, Alava I, Blanco F, Carlos Ramos J, Rivas A. Thermal modeling of large format lithium-ion cells. *J Electrochem Soc* 2013;**160**(2):A212–17.
[289] Grolleau S, Delaille A, Gualous H, Gyan P, Revel R, Bernard J, Redondo-Iglesias E, Peter J. Calendar aging of commercial graphite/$LiFePO_4$ cell – predicting capacity fade under time dependent storage conditions. *J Power Sources* 2014;**255**:450–8.
[290] Ecker M, Nieto N, Käbitz S, Schmalstieg J, Blanke H, Warnecke A, Sauer DU. Calendar and cycle life study of Li(NiMnCo)O_2-based 18650 lithium-ion batteries. *J Power Sources* 2014;**248**:839–51.
[291] Uddin K, Jackson T, Widanage WD, Chouchelamane G, Jennings PA, Marco J. On the possibility of extending the lifetime of lithium-ion batteries through optimal V2G facilitated by an integrated vehicle and smart-grid system. *Energy* 2017;**133**:710–22.
[292] Uddin K, Gough R, Radcliffe J, Marco J, Jennings P. Techno-economic analysis of the viability of residential photovoltaic systems using lithium-ion batteries for energy storage in the United Kingdom. *Appl Energy* 2017;**206**:12–21.
[293] Momma T, Matsunaga M, Mukoyama D, Osaka T. Ac impedance analysis of lithium ion battery under temperature control. *J Power Sources* 2012;**216**:304–7.
[294] Seki S, Kihira N, Mita Y, Kobayashi T, Takei K, Ikeya T, Miyashiro H, Terada N. AC impedance study of high-power lithium-ion secondary batteries—effect of battery size. *J Electrochem Soc* 2011;**158**(2):A163–6.
[295] Zhuang Q-C, Wei T, Du L-L, Cui Y-L, Fang L, Sun S-G. An electrochemical impedance spectroscopic study of the electronic and ionic transport properties of spinel $LiMn_2O_4$. *J Phys Chem C* 2010;**114**(18):8614–21.
[296] Osaka T, Momma T, Mukoyama D, Nara H. Proposal of novel equivalent circuit for electrochemical impedance analysis of commercially available lithium ion battery. *J Power Sources* 2012;**205**:483–6.
[297] Buller S, Thele M, De Doncker RWAA, Karden E. Impedance-based simulation models of supercapacitors and Li-ion batteries for power electronic applications. *Indust Appl IEEE Trans* 2005;**41**(3):742–7.
[298] Gomez J, Nelson R, Kalu EE, Weatherspoon MH, Zheng JP. Equivalent circuit model parameters of a high-power Li-ion battery: thermal and state of charge effects. *J Power Sources* 2011;**196**(10):4826–31.
[299] Alavi SMM, Birkl CR, Howey DA. Time-domain fitting of battery electrochemical impedance models. *J Power Sources* 2015;**288**:345–52.
[300] Love CT, Virji MBV, Rocheleau RE, Swider-Lyons KE. State-of-health monitoring of 18650 4S packs with a single-point impedance diagnostic. *J Power Sources* 2014;**266**:512–19.
[301] Zheng Y, He Y-B, Qian K, Li B, Wang X, Li J, Chiang SW, Miao C, Kang F, Zhang J. Deterioration of lithium iron phosphate/graphite power batteries under high-rate discharge cycling. *Electrochim Acta* 2015;**176**:270–9.
[302] Kowal J. Spatially-resolved impedance of nonlinear inhomogeneous devices - using the example of lead-acid batteries. *Electrical engineering and information technology*. RWTH Aachen; 2010.

[303] Raijmakers LHJ, Danilov DL, van Lammeren JPM, Lammers MJG, Notten PHL. Sensorless battery temperature measurements based on electrochemical impedance spectroscopy. *J Power Sources* 2014;**247**:539–44.
[304] Schmidt JP, Arnold S, Loges A, Werner D, Wetzel T, Ivers-Tiffée E. Measurement of the internal cell temperature via impedance: evaluation and application of a new method. *J Power Sources* 2013;**243**:110–17.
[305] Srinivasan R. Monitoring dynamic thermal behavior of the carbon anode in a lithium-ion cell using a four-probe technique. *J Power Sources* 2012;**198**:351–8.
[306] Zhu JG, Sun ZC, Wei XZ, Dai HF. A new lithium-ion battery internal temperature on-line estimate method based on electrochemical impedance spectroscopy measurement. *J Power Sources* 2015;**274**:990–1004.
[307] Beelen HPGJ, Raijmakers LHJ, Donkers MCF, Notten PHL, Bergveld HJ. A comparison and accuracy analysis of impedance-based temperature estimation methods for Li-ion batteries. *Appl Energy* 2016;**175**:128–40.
[308] Galeotti M, Cinà L, Giammanco C, Cordiner S, Di Carlo A. Performance analysis and SOH (state of health) evaluation of lithium polymer batteries through electrochemical impedance spectroscopy. *Energy* 2015;**89**:678–86.
[309] Barsoukov E, Macdonald JR. *Impedance spectroscopy, theory, experiment, and applications*. 2 ed. New Jersey: John Wiley & Sons; 2005.
[310] Momma T, Matsunaga M, Mukoyama D, Osaka T. Ac impedance analysis of lithium ion battery under temperature control. *J Power Sources* 2012;**216**(0):304–7.
[311] Osaka T, Momma T, Mukoyama D, Nara H. Proposal of novel equivalent circuit for electrochemical impedance analysis of commercially available lithium ion battery. *J Power Sources* 2012;**205**(0):483–6.
[312] Rodrigues S, Munichandraiah N, Shukla AK. AC impedance and state-of-charge analysis of a sealed lithium-ion rechargeable battery. *J Solid State Electrochem* 1999;**3**(7-8):397–405.
[313] Kochowski S, Nitsch K. Description of the frequency behaviour of metal–SiO_2–GaAs structure characteristics by electrical equivalent circuit with constant phase element. *Thin Solid Films* 2002;**415**(1–2):133–7.
[314] Shoar Abouzari MR, Berkemeier F, Schmitz G, Wilmer D. On the physical interpretation of constant phase elements. *Solid State Ion* 2009;**180**(14–16):922–7.
[315] Zhang J, Ge H, Li Z, Ding Z. Internal heating of lithium-ion batteries using alternating current based on the heat generation model in frequency domain. *J Power Sources* 2015;**273**:1030–7.
[316] Sauvant-Moynot V, Bernard J, Mingant R, Delaille A, Mattera F, Mailley S, Hognon J-L, Huet F. ALIDISSI, a research program to evaluate electrochemical impedance spectroscopy as a SoC and SoH diagnosis tool for Li-ion batteries. *Oil Gas Sci. Technol. – Rev. IFP* 2010;**65**(1):79–89.
[317] Barai A, McGordon A, Jennings P. A study of the effect of short-term relaxation on the EIS test technique for EV battery cells. In: 8th International Workshop on Impedance Spectroscopy, *Chemnitz, Germany*; 2015.
[318] Eddahech A, Briat O, Vinassa J-M. Performance comparison of four lithium–ion battery technologies under calendar aging. *Energy* 2015;**84**:542–50.
[319] Love C, Dubarry M, Reshetenko T, Devie A, Spinner N, Swider-Lyons K, Rocheleau R. Lithium-ion cell fault detection by single-point impedance diagnostic and degradation mechanism validation for series-wired batteries cycled at 0°C. *Energies* 2018;**11**(4).
[320] Widanage WD, Barai A, Chouchelamane GH, Uddin K, McGordon A, Marco J, Jennings P. Design and use of multisine signals for Li-ion battery equivalent circuit modelling. Part 1: signal design.. *J Power Sources* 2016;**324**:70–8.
[321] Widanage WD, Barai A, Chouchelamane GH, Uddin K, McGordon A, Marco J, Jennings P. Design and use of multisine signals for Li-ion battery equivalent circuit modelling. Part 2: model estimation.. *J Power Sources* 2016;**324**:61–9.
[322] Osswald PJ, Erhard SV, Noel A, Keil P, Kindermann FM, Hoster H, Jossen A. Current density distribution in cylindrical Li-ion cells during impedance measurements. *J Power Sources* 2016;**314**:93–101.

Dr Anup Barai (PhD, Energy Storage System, University of Warwick), is an energy storage system test and characterisation expert, with specializing in automotive and grid linked energy storage systems. Since joining WMG in 2011, Dr Barai have established a successful research theme in the area of developing methodologies for next generation characterisation of energy storage system for transport and stationary applications. Dr Barai deliver research, which has tangible impact on industrial and academic researcher's success, making fundamental changes in the way energy storage systems are characterised. Dr Barai as PI and Co-I previously led research projects funded by the 'Research Development Fund' at the University of Warwick and the UK Department of Transport. In the past, he delivered multiple commercial research packages and authored high impact journal articles in the area of lithium-ion battery characterisation. Dr Barai currently lead energy storage characterisation related research within the energy innovation centre (EIC) at WMG, University of Warwick.

Kotub Uddin is Head of Research at OVO Energy. He leads the identification and integration of exploratory academic research into the development of commercial products. He also leads OVO Energy's electrochemical energy storage strategy and guides the development of smart control strategies for energy storage devices. Kotub joined OVO Energy in February 2018, previously leading research on energy storage technologies at WMG, University of Warwick. He has nearly 10 years' experience in collaborative research specialising in the application of electrochemical energy storage technologies for low carbon transport and power-grid decarbonisation which ranges from mathematical modelling and fundamental science to systems engineering and experimental validation. He has published over 20 peer-reviewed articles and led a wide portfolio of collaborative research projects funded by EPSRC, Innovate UK and Industry. These projects have been underpinned by significant industrial and academic collaboration with leading UK and International organisations (e.g. JLR, ATKearney, Honda, AVL, Peel Group, eCar Club, Arrival, Cenex). Before the University of Warwick, Kotub held a Visiting Research Fellow position at the Department of Mechanical Engineering, Imperial College (2013–2016). In industry, he was a Senior Research Engineer at Jaguar Land Rover (2009–2012) and Principal Technical Consultant in alternative fuels at Ricardo Energy and Environment (2015–2016).

Matthieu Dubarry (PhD, Electrochemistry & Solid State Science, University of Nantes), has over 15 years of experience in renewable energy, with an emphasis in the area of lithium ion batteries. Following his PhD on the synthesis and characterization of materials for lithium batteries, Dr. Dubarry joined the Hawaii Natural Energy Institute at the University of Hawaii at Mānoa as a post-doctoral fellow in 2005 to work on the analysis of the usage of a fleet of electric vehicles. He was later appointed a faculty position in 2010 with a focus on battery testing, modeling and simulation. While working for HNEI, Dr. Dubarry pioneered the use of new techniques for the analysis of the degradation of Li-ion cells and developed numerous software tools facilitating the prognosis of Li-ion battery degradation both at the single cell and the battery pack level. Current projects include the evaluation of grid scale Li-ion battery energy storage systems; the evaluation of the impact of vehicle-to-grid strategies on electric vehicle battery pack degradation; and the testing of emerging battery technologies for grid-connected and transportation applications.

Dr Limhi Somerville is currently the Advanced Cell Design Manager at Jaguar Land Rover, having also worked as a lithium-ion cell specialist. He previously worked at Argonne National Laboratory looking into methods of materials and electrical characterisation of lithium-ion cells for lifetime determination. His doctorate, completed at The University of Warwick was on the same topic and he also holds a Masters of Science degree in Innovation from The University of Warwick and a Bachelors of Science degree in Chemistry from Bangor University.

Andrew McGordon Andrew joined WMG in May 2005 working on the Premium Automotive Research and Development Hybrid Vehicle projects and developed the hybrid powertrain simulation tool, WARPSTAR. Andrew is currently a Principal Engineer in the Energy Storage and Management group at WMG, working on energy storage, vehicle modelling and battery ageing. He currently supervises research students working on vehicle energy management strategies, autonomous vehicle path planning techniques and battery performance in different duty cycles.

Paul Jennings received a BA degree in physics from the University of Oxford in 1985 and an Engineering Doctorate from the University of Warwick in 1996. Since 1988 he has worked on industry-focused research for WMG at the University of Warwick. His current interests include: vehicle electrification, in particular energy management and storage; connected and autonomous vehicles, in particular the evaluation of their dependability; and user engagement in product and environment design, with a particular focus on automotive applications.

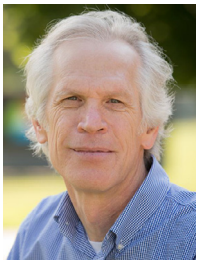

Ira Bloom (PhD, Inorganic Chemistry, University of Chicago) has over 30 years of experience in electrochemical energy conversion devices, with an emphasis lately on lithium-ion batteries. Following his doctoral work on the synthesis and characterization of organometallic compounds, Dr. Bloom join Argonne National Laboratory as a post-doctoral fellow to work on homogeneous catalysis. He later joined the Argonne faculty in 1984 with an emphasis on glass electrolytes for high-temperature, sodium-ion batteries. While at Argonne, Dr. Bloom developed new techniques and software for the characterization of battery degradation. These methods were transparent to battery technology and to battery scale (cell and pack). His current interests are the investigation of battery degradation mechanisms, battery testing, and post-test analysis of aged battery materials.